UNIVERSITÀ
DEGLI STUDI
DI PADOVA

Università degli Studi di Padova

Dipartimento di Scienze Biomediche

PhD course in Biomedical Sciences, XXXV cycle

ACTIVATION OF MUSCLE-SPECIFIC AKT1 REVERTS CANCER-DEPENDENT SKELETAL MUSCLE WASTING

Coordinator: Ch.mo Prof. Fabio Di Lisa

Supervisor: Ch.mo Prof. Bert Blaauw

Co-supervisor: Dr. Martina Baraldo, PhD

Ph.D. Student: Alessia Geremia

Academic Year 2021-2022

INDEX

ABSTRACT ..... *VI*

LIST OF ABBREVIATIONS ..... *VII*

LIST OF FIGURES AND TABLES ..... *IX*

LIST OF SUPPLEMENTARY FIGURES ..... *XI*

1. INTRODUCTION *1*

1.1. Cancer cachexia **1**

1.1.1. Mechanisms and pathophysiology of cancer cachexia 2

1.2. Skeletal muscle structure and function **4**

1.3. Mechanisms of cancer-associated skeletal muscle wasting **7**

Protein degradation processes 7

The IGF1/Akt/mTOR pathway 10

Myostatin and Activin A 13

2. AIM OF THE WORK *15*

3. MATERIAL AND METHODS *16*

3.1. Animal Experiments and treatments **16**

Genotyping of transgenic animals 17

3.2. In vivo muscle force measurement **17**

3.3. Colchicine treatment **18**

3.4. Measurement of in vivo protein synthesis **18**

3.5. Antibodies and western blotting **18**

Protein gel electrophoresis 18

Transfer of the protein to the nitrocellulose membrane 19

Incubation with antibodies 19

Quantification of Immunoblotting 20

3.6. Gene expression analysis **20**

RNA extraction and qRT-PCR reaction 20

Quantification of the PCR products 21

Primer pair design 22

3.7. Mito-Keima experiment **23**

3.8. Histological analysis and immunofluorescence staining **23**

Haematoxylin and Eosin staining (H&E) 23
Periodic Acid-Schiff staining (PAS) 24
Succinate Dehydrogenase staining (SDH) 24
Neural Cell Adhesion Molecule 1 (NCAM-1) staining 24
3.9. PAS quantification 25
3.10. RNAseq 25
3.11. CIBERSORTx analysis 25
3.12. Statistical analysis 26
4. RESULTS 27
4.1. Characterization of muscle wasting during cancer cachexia 27
4.2. Cancer cachexia is associated with reduced Akt-mTORC1 signaling and protein synthesis rates in the C26 mouse model 29
4.3. Inducible muscle-specific deletion of mTOR or Raptor does not increase skeletal muscle atrophy in cachectic mice 31
4.4. Loss of mTORC1 during cancer cachexia increases autophagic flux 35
4.5. Loss of mTOR or Raptor does not alter skeletal muscle innervation during cancer cachexia 39
4.6. Muscle-specific Akt activation is sufficient to rescue skeletal muscle mass in tumor-bearing mice 40
4.7. Akt overexpressing mice show a restoration of muscle function and denervation markers 42
4.8. Muscle-specific Akt activation does not affect tumor or spleen mass. 43
4.9. Activation of Akt rescues skeletal muscle transcriptome 44
4.10. Differentially expressed genes revealed a normalization in the autophagy and ubiquitin proteasome systems in Akt tumor-bearing mice. 45
4.11. CIBERSORTx analysis suggests a decrease inflammatory state in muscle of Akt tumor-bearing mice. 48
5. DISCUSSION AND CONCLUSION 51
SUPPLEMENTARY FIGURES 56
REFERENCES 61

ABSTRACT

Cancer-related muscle wasting occurs in most cancer patients. An important regulator of adult muscle mass and function is the Akt-mTORC1 pathway (1). While Akt-mTORC1 signaling is important for adult muscle homeostasis, it is also a major target of numerous cancer treatments and its inhibition induces a worsening in muscle wasting in cancer patients (2). Which role Akt-mTORC1 signaling plays during cancer cachexia in muscle is currently not known. Here we aimed to determine how activation or inactivation of this pathway affects skeletal muscle during cancer cachexia. We used inducible, muscle-specific Raptor (mTORC1) and mTOR (mTORC1 and mTORC2) ko mice to determine the effect of reduced mTOR signaling during cancer cachexia. On the contrary, to understand if skeletal muscle maintains its anabolic capacity and if activation of Akt-mTORC1 signaling can reverse cancer cachexia, we generated mice in which we can inducibly activate Akt specifically in skeletal muscle. We found that mTORC1 signaling is impaired during cancer cachexia, using the Lewis-Lung Carcinoma (LLC) and C26 colon cancer model, and is accompanied by a reduction in protein synthesis rate. Further reduction of mTOR signaling, as seen in Raptor ko animals, leads to a 1.5-fold increase in autophagic flux, but does not further increase muscle wasting. On the other hand, activation of Akt-mTORC1 signaling in already cachectic animals completely reverses the loss in muscle mass and force. Interestingly, Akt activation only in skeletal muscle completely normalizes the transcriptional deregulation observed in cachectic muscle, despite having no effect on tumor size or spleen mass. In addition to stimulating muscle growth, it is also sufficient to prevent the increase in protein degradation normally observed in muscles from tumor-bearing animals. Our results demonstrate that activation of muscle-specific Akt is sufficient to completely revert cancer-dependent muscle wasting. Intriguingly, these results show that skeletal muscle maintains its anabolic capacities also during cancer cachexia, possibly giving a rationale behind some of the beneficial effects observed in exercise in cancer patients.

LIST OF ABBREVIATIONS

4EBP1: Eukaryotic translation initiation factor 4E-binding protein 1

AchRγ: Acetylcholine Receptor isoform γ

ActRIIB: Activin receptor type IIB

AKT: Ak strain transforming

AMP: Adenosine monophosphate

AMPK: Adenosine monophosphate-activated protein kinase

ATG7: Autophagy related 7

ATP: Adenosine triphosphate

BAT: Brown Adipose Tissue

C26: C26 colon carcinoma

DAPI: 4′,6-diamidino-2-phenylindole

DEG: Differentially expressed genes

DNA: Deoxyribonucleic acid

E1: Ubiquitin-activating enzyme

E2: Ubiquitin-conjugating enzyme

E3: Ubiquitin-ligase enzyme

eIF2B: Eukaryotic initiation factor 2 B

eIF3-f: Eukaryotic Translation Initiation Factor 3 subunit F

ER: Estrogen Receptor

ERK: Extracellular signaling-regulated kinase

FDB: Flexor Distal Brevis

FF: Fast-fatigable

FR: Fast-resistance

GAPDH: Glyceraldehyde 3-phosphate dehydrogenase

GC: Gastrocnemius

GS: Glycogen synthase

GSK3: Glycogen synthase kinase 3

HPRT: Hypoxanthine-guanine phosphoribosyltransferase

HRP: Horse radish peroxidase

HSA: Human Skeletal Actin

IGF1: Insulin growth factor 1

IL-1: Interleukin 1

IL-6: Interleukin 6

IRS1: insulin receptor substrate 1

LC3: Microtubule-associated protein 1A/1B-light chain 3

LLC: Lewis Lung Carcinoma

MAPK: Mitogen-activated protein kinases

mTOR: Mammalian target of rapamycin

MuRF1: Muscle Ring Finger protein 1

MuSK: Muscle specific kinase

MyHC: Myosin heavy chain

NCAM-1 : Neural Cell Adhesion Molecule 1 (protein)

Ncam1 : Neural Cell Adhesion Molecule 1 (gene)

NMJ: Neuronal muscular junction

P70S6K: Ribosomal protein S6 kinase beta-1

PAS: Periodic Acid Schiff

PCR: Polymerase Chain Reaction

PDK1: Phosphoinositide-Dependent Kinase-1

PI3K: Phospho-Inositol 3 Kinase

PKB: Protein Kinase B

PTEN: Phosphatase and TENsin homolog deleted on chromosome 10

REE: Resting Energy Expenditure

RNA: Ribonucleic acid

RUNX1: Runt-related transcription factor 1

S6: Ribosomal protein S6

SDH: Succinate Dehydrogenase

SEM: Standard Error of Mean

TA: Tibialis Anterior

TGF-β: Transforming growth factor beta

TNFα: Tumor necrosis factor α

TORC1: mTOR complex 1

TORC2: mTOR complex 2

TRAF6: Tumor necrosis factor receptor associated factor 6

ULK1: Autophagy activating kinase

UPS: Ubiquitin Proteasome System

LIST OF FIGURES AND TABLES

Figure 1. Cancer cachexia as a multi-organ syndrome (2). 4
Figure 2. Skeletal muscle structure. 5
Figure 3. Actin-myosin interaction. 6
Figure 4. IGF1/Akt/mTOR signaling 12
Figure 5. Schematic representation of signaling pathways leading to cancer cachexia (89) 14
Figure 6. Characterization of Raptor ko and mTOR ko tumor-bearing mice. 32
Figure 7. Deletion of Raptor or mTOR does not increase muscle atrophy in tumor-bearing mice. 33
Figure 8. Muscle force measurements in Raptor ko tumor-bearing mice. 33
Figure 9. Akt-mTOR signaling in Raptor ko tumor-bearing mice. 34
Figure 10. Increased in autophagy markers in Raptor ko and mTOR ko tumor-bearing mice. 35
Figure 11. Raptor deletion leads to an increase in autophagic flux during cancer cachexia. 37
Figure 12. Mitophagy is increased in Raptor ko tumor-bearing mice. 38
Figure 13. Analysis of NMJ markers in Raptor ko and mTOR ko mice during cancer cachexia. 39
Figure 14. Activation of Akt-mTORC1 signaling restores body weight loss 41
Figure 15. Analysis of muscle histology in Akt tumor-bearing mice. 42
Figure 16. Akt activation in tumor-bearing mice restores muscle function. 42
Figure 17. Restoration of denervation markers in Akt tumor-bearing mice. 43
Figure 18. Tumor and spleen weight in Akt tumor-bearing mice 44
Figure 19. Activation of Akt recovers muscle transcriptome. 45
Figure 20. Gene ontology analysis of muscle transcriptome revealed normalization in the autophagy and UPS in Akt tumor-bearing mice. 46
Figure 21. Akt activation reverts muscle transcriptome during cancer cachexia. 46
Figure 22. Protein expression of autophagy and UPS markers. 47
Figure 23. Akt activation rescues the increase in the translational repressor 4E-BP1. 48
Figure 24. RNA deconvolution analysis with CIBERSORTx estimates member cell types in skeletal muscle. 49
Figure 25. Inflammatory cell populations are differently expressed in Akt tumor-bearing mice. 50

Table 1. Antibodies used for western blotting. 20
Table 2. Primers used for quantitative RT-PCR 23

LIST OF SUPPLEMENTARY FIGURES

Supplementary Figure 1. Timeline representation of mice treatments 56
Supplementary Figure 2. Characterization of Lewis Lung carcinoma as cancer cachexia mouse model..... 57
Supplementary Figure 3. Analysis of mTOR signaling showed a slight decrease in mTOR signaling. 57
Supplementary Figure 4. Fat and muscle analysis in Raptor ko and mTOR ko C26 mice. 58
Supplementary Figure 5. Akt-mTOR signaling western blotting analysis in mTOR ko C26 mice. 59
Supplementary Figure 6. Expression of FoxO-dependent genes are blunted in Akt tumor-bearing mice. 60

1. INTRODUCTION

1.1. Cancer cachexia

Cachexia, etymologically meaning “bad condition”, is characterized by an involuntary loss of body weight normally associated with a loss of homeostatic control of body energy and protein balance. This condition is associated with many malignant diseases, including AIDS, heart failure, kidney disease, chronic obstructive pulmonary disease, neurological disease and rheumatoid arthritis.

Cancer-associated cachexia is defined by an international consensus as a multifactorial syndrome characterized by a strong loss of skeletal muscle and fat mass that cannot be fully reversed by nutritional support (3). Many types of cancers can develop cachexia, such as pancreatic, esophageal, gastric, pulmonary, hepatic, and colorectal cancers and they account approximately for half of all cancer deaths worldwide. The incidence of cachexia in these types of cancers is very high, approximately more than 80% in gastric or pancreatic cancer, and over 50% in lung, prostate or colon cancer (4). This syndrome is usually correlated with the severity of cancer and occurs at the end of life.

The substantial loss in muscle and fat mass during cancer cachexia, are generally driven by an altered protein, carbohydrate and lipid metabolism and are associated with a systemic inflammatory state, leading to a negative energy balance. Contemporarily, the presence of anorexia during this condition exacerbates an already catabolic state, accelerating disease progression. A peculiarity of this syndrome is the inability to fully treat involuntary weight loss with nutritional support therapies, stressing a critical alteration in metabolism and energy homeostasis (3).

Cancer cachexia is classified into three stages: (i) The early stage of the disease is precachexia where early clinical and metabolic signs precede weight loss. (ii) Cachexia stage is defined as body weight loss greater than 5% within 6 months. (iii) The third stage, refractory cachexia, is when life expectancies are dramatically decreased because of advanced cancers or unresponsiveness to therapies. Notably, not all cachectic patients manifest all these stages, the progression depends on factors such as cancer type, food intake, systemic inflammation and personal anamnesis (3).

Cancer-associated cachexia is linked with poor survival, decreased quality of life and response rate to chemotherapy. Hence, cancer cachexia has a major clinical importance considering its incidence in many types of cancers and its involvement with almost 20% of cancer deaths.

1.1.1. Mechanisms and pathophysiology of cancer cachexia

Cancer cachexia is defined as a multifactorial syndrome. One particular and well-established feature that characterized this strong body weight loss is the altered energy balance due to different types of molecular mechanisms. The resting energy expenditure (REE) overcomes the energy intake leading to caloric deficits and weight loss. Mostly, the increased REE is related to an high energy demand of the tumor, inflammation and an increase in the futile cycles activity (4,5). Instead, the decreased energy intake is due to the presence of anorexia.

Adipose tissue wasting that accompanied skeletal muscle loss is another key feature of cancer cachexia. White adipose tissue is characterized by an increase in lipolysis, indeed increased plasma free fatty acids and glycerol levels are often observed in cachectic patients (6).

Even brown adipose tissue, a site of heat production, is involved in this syndrome. Indeed, it was found an increase in BAT activity and in markers of beige adipocytes, which are white adipocytes undergoing a "browning process". These characteristics contribute to an increased energy expenditure during cancer cachexia (7).

Systemic inflammation is a hallmark of cancer patients, and it originates from tumor cells and activated immune cells which release cytokines, chemokines and other inflammatory mediators (8). These mediators have a major role in promoting tumor growth, survival and progression but also in cachexia (6). Several cytokines are implicated in promoting cancer cachexia, among which tumor necrosis factor (TNFα), interleukin-6 and -1 (IL-6/IL-1) and interferon gamma (10). TNFα, also called "cachectin", is released by many types of cells including macrophages, CD4+, neutrophiles and it can be produced by tumor itself. Its expression leads to anorexia, muscle and adipose wasting, and increased energy expenditure in both clinical and experimental model of cancer cachexia (11). IL-6 can be produced by immune cells and from tumor itself and its circulating levels correlates with weight loss in cancer patients and reduced survival (12). IL-6 can directly drive acute phase response in liver and muscle wasting by STAT3 activation (13). The upregulation of pro-inflammatory cytokines co-occurs with decreased expression of anti-inflammatory ones, such as IL-4 -10 and -12.

In addition to skeletal muscle also heart is affected by cancer cachexia leading to fibrosis and functional changes. Cardiac alterations ultimately result in heart failure and arrhythmia and like skeletal muscle, cardiac muscle wasting is mediated by increased protein degradation.

Also liver is affected and participates to cancer cachexia. Liver mass is strongly increased during this condition, and it contributes to the increased REE. Indeed, liver participates to an oncological version of Cori Cycle in which gluconeogenesis is performed using the lactate derived from tumor aerobic glycolysis (the Warburg effect). Another typical feature is the onset of steatosis, both in patients and in murine models of cancer cachexia. Moreover, liver participates to systemic inflammation by secreting acute phase proteins and reducing albumin secretion (14).

The previous section has offered a basic overview of cancer cachexia and has very simply described some of the mechanisms mediating cachexia (Fig. 1). Among all these multi-organ alterations, skeletal muscle wasting is a central player in cancer cachexia. The mechanisms leading to skeletal muscle wasting during cancer cachexia will be discussed after a brief description of skeletal muscle structure and function.

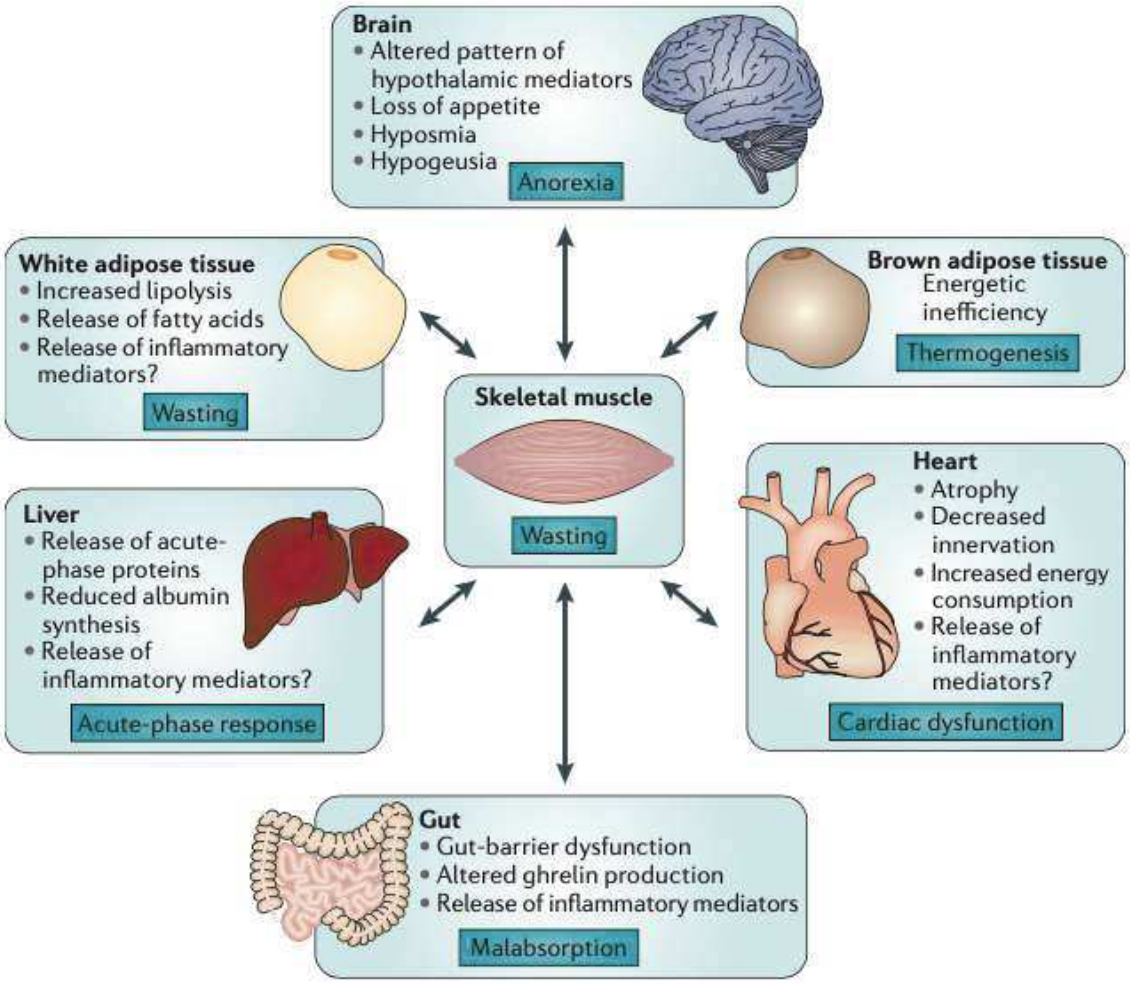

Figure 1. Cancer cachexia as a multi-organ syndrome (4).

1.2. Skeletal muscle structure and function

Skeletal muscle mass accounts for almost 40% of body mass and it is the site of 30-45% of whole-body protein turnover (15). It is responsible for body posture and voluntary movements controlled by the somatic nervous system through the alpha motor neuron innervation.

Skeletal muscle fiber (muscle cell) is an elongated, cylindrical and multinucleated cell surrounded by a sarcolemma, in turn wrapped by a basal lamina. Individual muscle fiber cells are separated from each other by endomysium. Muscle fibers are organized in bundles or fascicles and surrounded by connective tissue, known as perimysium. The last layer is called epimysium (Fig. 2).

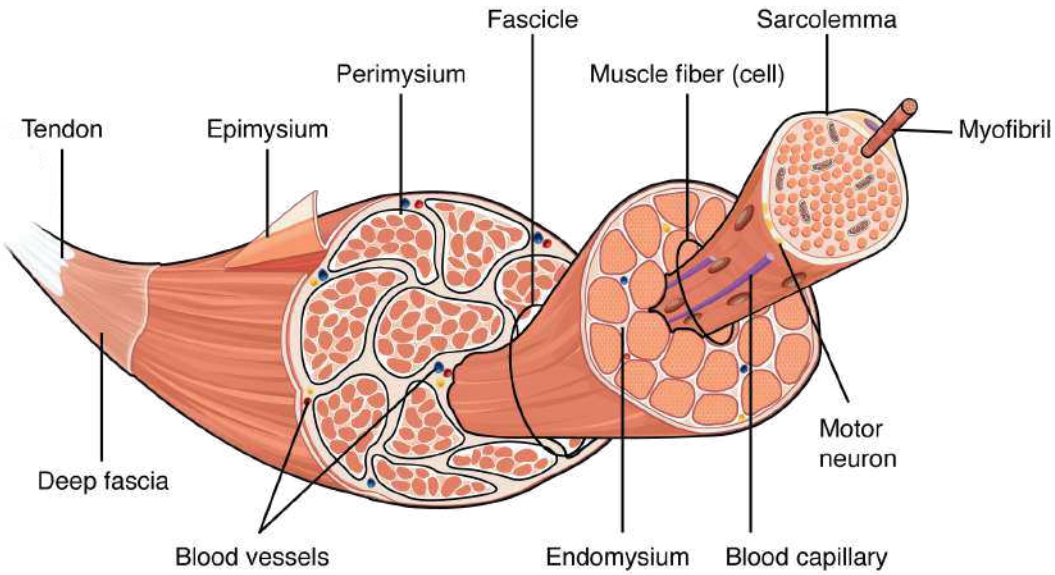

Figure 2. Skeletal muscle structure.

The sarcoplasm, delimited by the sarcolemma, contains thousands of cylindrical structures, called myofibrils, responsible for muscle contraction. Myofibrils are composed of contractile proteins, which are organized in thin and thick filaments. The thick myofilaments contain myosin protein and thin myofilaments contain actin protein. Thin and thick filaments provide contractility to the cell and are spatially arranged in repetitive structures called sarcomeres, the functional unit of skeletal muscle fiber. The myosin molecule is composed by 2 heavy chains and 4 light chains. The heavy chains contain the myosin heads that interact with actin and allow muscle to contract. The myosin heavy chain in the head region contains an adenosine triphosphate (ATP) binding site and allows the enzyme ATPase for hydrolyzing ATP into adenosine diphosphate (ADP) and inorganic phosphate (Pi), which provides the energy for contraction. The thin filament is made of actin and two regulatory proteins, troponin and tropomyosin. The interaction of myosin and actin allows muscles to contract, a process called excitation-contraction coupling (EC Coupling) in which an electrical stimulus is converted into mechanical contraction. The motor neuron, leading the electrical stimulus, is in contact with muscle fiber through a chemical synapse, which is called neuromuscular junction (NMJ).

The electrical stimulus coming from the motor neuron leads to the release of Acetylcholine, a neurotransmitter, into the synaptic cleft which binds to postsynaptic receptors located on the sarcolemma, resulting in muscle fiber depolarization and thus generation of an action potential. Upon stimulus Ca2+ is released by the sarcoplasmic reticulum and binds to troponin and, through tropomyosin, exposes a myosin binding site on the actin molecule (Fig. 3). In the

presence of ATP, the myosin head binds to actin and pulls the thin filament along the thick filament, allowing the sarcomere to shorten. This process is called cross-bridge cycling (16).

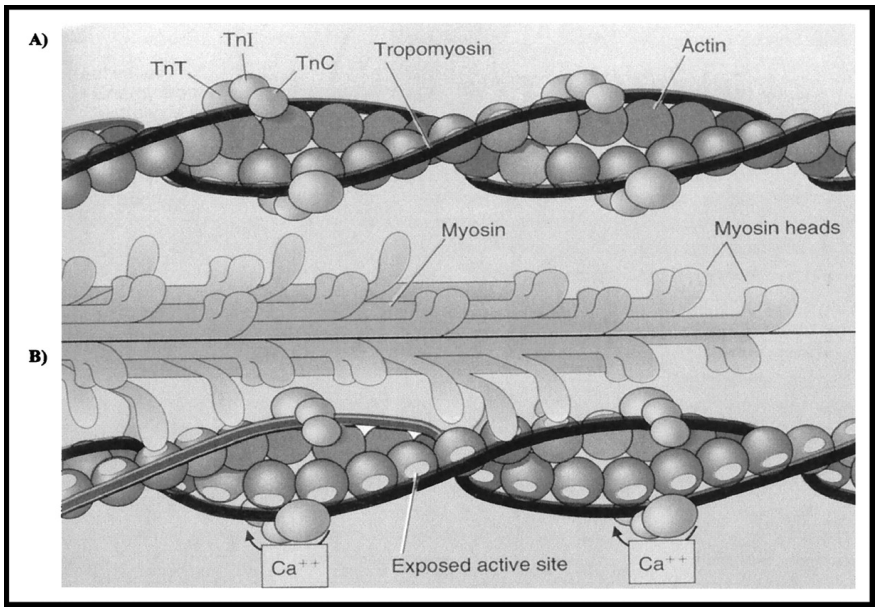

Figure 3. Actin-myosin interaction.

The contractile properties of a muscle depend on fiber type composition based on different myosin isoforms. The four myosin isoforms that were identified in mammals were MyHCI, MyHCIIA, MyHCIIX and MyHCIIB and they corresponded to the isoforms identified by myosin ATPase staining as types I, IIA, IIX, and IIB respectively; notably in humans the fourth and fastest myosin heavy chain isoform (MyHCIIB) is not present. This classification is made by structural proteins, but they differ also in the mechanical properties, such as velocity of contraction and resistance to fatigue, in metabolism (glycolytic or oxidative) and in mitochondrial content. This leads to a broader classification: slow oxidative (type I) fibers contain high amount of myoglobin and mitochondria, and they are specialized in aerobic activity. Fast-twitch oxidative glycolytic (IIA) fibers are rich in mitochondria also and contain high amounts of glycogen, indeed they can do also anaerobic glycolysis and make fast-twitches. Then, the type IIB/X fibers are also called fast glycolytic fibers. They contain fewer mitochondria and high amount of glycogen. This classification can be extended also to the functional unit of the motor system, the motor unit, composed of a motor neuron and a bunch of muscle fibers with similar, if not identical, fiber type. Motor units are classified upon contractile speed and resistance to fatigue. The fast-fatigable (FF) units are composed of IIB fibers, and fatigue-resistant (FR) units are composed of IIA fibers. Motor unit of type IIX fibers

have twitch properties like those of IIA and IIB units and has an intermediate resistance to fatigue. Lasty the slow fatigue resistant motor units (S) are composed of slow type I muscle fibers (17). Here I remarked only a few of the heterogeneities of muscle fibers that allow the same muscle to be used for various tasks, from continuous low-intensity activity (e.g., posture) to fast and maximal contraction (e.g., jumping).

Skeletal muscle is a plastic tissue, this means that its structural and functional properties can vary in response to hormonal and neural influences, or generally in response to external stimuli. These adaptative changes include changes in muscle fiber types (e.g., fast-to-slow fiber type switch) and in fiber size. Changes in fiber size lead to two different conditions, muscle atrophy and muscle hypertrophy. Muscle atrophy, a decrease in muscle fiber size, occurs either in physiological condition, aging, or in pathological conditions, such as AIDS or cancer. On the other hand, muscle hypertrophy is due to growth of pre-existing muscle fibers, thus resulting in an increase in skeletal muscle mass. These two states are defined by a balance between protein synthesis and degradation; when protein synthesis overcomes the degradation process an increase of muscle mass, hypertrophy, occurs, vice versa for muscle atrophy. Considering the clinical importance of atrophy/hypertrophy, several signaling pathways have been identified.

1.3. Mechanisms of cancer-associated skeletal muscle wasting

Cancer-associated skeletal muscle wasting is a condition of muscle atrophy, associated with an imbalance in protein synthesis and protein breakdown, which ultimately leads to skeletal muscle loss (18). Whether a reduction in protein synthesis, an increase in degradation or a combination of both is more relevant is still under debate. Various molecular pathways and mechanisms underlie the altered skeletal muscle protein turnover associated with cancer cachexia (19). Hereby I describe some of the pathways/molecules that are known to be involved in cancer-associated skeletal muscle wasting and are more relevant for the purpose of my thesis.

Protein degradation processes

There is a constant turnover of muscle proteins that require both protein degradation and protein synthesis. The process of protein degradation is mainly carried out by two systems: the autophagy system and the ubiquitin-proteasome system (UPS). These machineries are important to recycle nutrients during starvation, eliminate unnecessary structures and organelles during cell differentiation, to fight against pathogens and to renew tissue

components delaying aging. In skeletal muscle protein breakdown occurs not only during pathologies or ageing but also in physiological conditions to remodel the tissue during development or to remove damaged components (20).

Autophagy is responsible for removing and eliminating unfolded and toxic proteins or abnormal and dysfunctional organelles. This system generates a double membrane vesicle, called autophagosome, that engulfs portion of cytoplasm, organelles and protein aggregates. Autophagosome fuses with the lysosome in which cargo can be degraded by lysosomal hydrolases (21). Alteration of the autophagy system can be evidenced by measuring the increased lipidated form of LC3, in which LC3 is conjugated with phosphatidylethanolamine and bound to the autophagosome. Another marker that indicates an impaired lysosomal clearance is p62, an autophagy cargo protein (22).

Autophagy is a system influenced by the energy status of the cell. A well characterized signaling cascade that senses nutrient status is the mTOR pathway. In particular mTOR complex 1 (mTORC1), activated by the presence of nutrients, inhibits Ulk1, an initiator of the autophagy cascade, hence negatively regulating autophagy (23). Another protein that regulates a special form of autophagy, termed mitophagy, is AMP-activated protein kinase (AMPK), which phosphorylates and activates Ulk1, thus triggering autophagy (24). Contrary to mTOR regulation, AMPK is activated by reduced cellular energy (ATP).

Autophagy is regulated also by hormones and growth factors through pathways different from those of nutrients, but still converge on mTOR. Insulin and insulin-like growth factors regulate mTOR through PI3K and subsequent activation of PKB/Akt. A negatively regulator of this pathway, the phosphatase PTEN, decreases the downstream Akt/PKB and thus positively regulates autophagy (25). When hormones are absent, mTOR is inactivated, releasing the inhibitory effect on autophagy. In general, autophagy is induced by lack of nutrients, hormones, oxidative stress and negative energy balance (26). Various autophagy-related genes are regulated at transcriptional level by Forkhead box transcription factor class (FoxO). In particular, FoxO isoform 3 (FoxO3) induces the transcription of multiple autophagy genes, including LC3II, Bnip3, Ulk2, Beclin1(27). Among the atrophy-related genes (atrogenes), LC3 and Gabarapl1 are upregulated during catabolic conditions, such as fasting, indicating an activation of autophagy (28). An excessive autophagy causes an exacerbated protein degradation inducing atrophy, on the other hand, also defective autophagy leads to an atrophic condition. This occurs because there is an accumulation of abnormal mitochondria and sarcoplasmic reticulum together with sarcomere disorganization that are toxic for the cell. This

was seen in a muscle-specific ATG7 ko mice where autophagy inhibition resulted in muscle atrophy and age-dependent weakness (29).

Studies in humans and preclinical models suggest that autophagy may be upregulated in cancer cachexia (18,21,22,24). In tumor-bearing mice, stimulation of muscle autophagy worsens muscle atrophy and this is supposed to be related to activation of mitophagy and impairment of mitochondrial function (23). Both IL-6 and activin A, important mediators of cancer cachexia, can drive autophagy in muscle cells (34). In another study instead, it was suggested that a block in the autophagic flux occurs in skeletal muscle of cachectic mice, since its reactivation through rapamycin, a well-known mTOR inhibitor, or an AMPK agonist restores skeletal muscle wasting (35).

The ubiquitin proteasome system regulates the degradation of intracellular short-lived proteins. Briefly this process starts from attaching a chain of multiple ubiquitin molecules to target proteins through a coordinated reaction of three enzymes, the ubiquitin-activating enzyme (E1), the ubiquitin-conjugating enzyme (E2) and the ubiquitin ligases (E3). The E1 is the activating enzyme and is encoded by only one gene. The ubiquitin ligase enzyme, E3, binds the protein substrate and catalyzes the movement of the ubiquitin from the E2 enzyme to the substrate. This is the rate-limiting step of the ubiquitination process. After forming a polyubiquitin chain, the target protein is bound by the proteasome, allowing protein degradation into small peptides and free amino acids (36). Ubiquitin has seven lysine residues, which are all used for polymerization, but polyubiquitin chains formed via lysin at 48 (Lys48) or 63 (Lys63) are the best characterized. A polyubiquitin via Lys48 usually is a marker for proteolysis; on the other hand, Lys63-linked polyubiquitin is related to membrane trafficking processes, playing a role also in regulating autophagy-dependent cargo recognition (37). The ubiquitin-proteasomal pathway is constitutively active in skeletal muscle to sustain protein turnover and guarantee correct homeostasis.

Among the known ubiquitin ligase enzymes (E3), only few of them are expressed specifically in skeletal muscle and upregulated during atrophying condition. The first to be identified were Atrogin-1/MAFbx and MuRF1, which are expressed specifically in smooth and striated muscles (38,39). These two enzymes are found to be strongly upregulated also in animal model of cancer cachexia (40). MuRF1 is implicated in the degradation process of muscle structural proteins, such as myosin heavy chains, actin and troponin I. Instead, Atrogin-1 promotes degradation of MyoD, a muscle transcription factor, and eIF3-f, an activator of protein synthesis.

Their expression is under the control of FoxO transcription factors, playing a central role in regulating catabolic process. Indeed, deletion of three FoxO factors simultaneously protects from muscle atrophy, preventing the induction of many E3 ligases, including Atrogin1 and Murf1 that occurs during starvation or upon denervation (41). It was found that even in a condition of cancer-associated muscle atrophy, inhibition of FoxO prevents skeletal muscle atrophy (42).

The increase in protein degradation and in the ubiquitin proteasome system during cancer cachexia can be attributed to inflammatory cytokines or mediators such as Activin. For example, TNFα (11), Twist1(43), NF-kB signaling pathway (44) and p38 MAPK signaling pathway (45), which were all discovered to be upregulated during cachexia, converge on the E3 ligases MuRF1 and Atrogin1, promoting proteasome hydrolysis in the UPS and leading to skeletal muscle protein degradation.

Highlighting the importance of these pathways during cancer cachexia, it has been found that the use of NF-kB inhibitors results in a decrease in tumor-induced muscle loss, partly through the blocking of MuRF1 upregulation (46). In another study the use of the proteasome inhibitor MG132 ameliorates cachexia through the inhibition of NF-kB pathway and downregulation of MuRF1 and Atrogin1 (47).

Another E3 ligase found having a role in cancer cachexia is Fbox40. It has been suggested that its upregulation leads to ubiquitination of IRS and thus to a decrease in protein synthesis (48). TRAF6, another E3 ligase that mediated the conjugation of Lys63-linked polyubiquitin chains to a target protein, plays a critical role in cancer cachexia and it is induced in muscles of gastric cancer patients (49). Moreover, targeted ablation of TRAF6 inhibits skeletal muscle wasting in a murine model of cancer cachexia (50).

In contrast to pre-clinical studies, the role of UPS during cancer cachexia in humans is not clear. Indeed some studies indicate an increased expression of UPS components (51,52) while others do not detect any changes (53–55).

The IGF1/Akt/mTOR pathway

Beside the above-mentioned increase in protein degradation, cachexia-induced muscle atrophy is also associated with a reduced protein synthesis rate. The IGF1/Akt/mTOR pathway is one of the main anabolic pathways and is activated by the insulin-like growth factor 1 (IGF1). The role of IGF1 pathway has been dissected by a variety of gain- and loss-of-function genetic approaches. It has been demonstrated that inactivation of IGF1 receptor leads to impaired

muscle growth (56) whereas muscle-specific IGF1 overexpression results in muscle hypertrophy (57). IGF1 elicits its function activating both the mitogen-activated protein kinase/extracellular signal-regulated kinase (MAPK/ERK) and the PI3K-Akt pathways. However, it has been shown that selectively activation of ERK pathway does not lead to muscle hypertrophy, whereas activation of PI3K-Akt pathway does (58). Indeed inducible muscle-specific Akt activation leads to a strong fiber hypertrophy (59). Akt promotes protein synthesis, either by activation of mTOR kinase or by inhibition of GSK3β. On the other hand, Akt blocks protein degradation preventing the induction of muscle specific E3 ligases through the phosphorylation and inhibition of FoxO transcription factors. Both these functions of Akt lead to muscle growth upon its activation.

mTOR, one of the main kinases stimulating protein synthesis, exists as two multiprotein complexes: mTORC1, when it is bound to Raptor, and mTORC2, when bound to Rictor. While mTORC2 is responsible for cell survival and cytoskeletal reorganization, and it is implicated in Akt activation, mTORC1 is mainly involved in cell growth and ribosome biogenesis. mTORC1 stimulates protein synthesis modulating two major effectors: the 70-kDa ribosomal protein S6 kinase (p70S6K) and eukaryotic initiation factor 4E binding protein1 (4EBP1). mTORC1 inhibits autophagy through the phosphorylation and inhibition of Ulk1. P70S6K stimulates protein synthesis through the activation of ribosomal protein S6, that is involved in the transport of 5' TOP mRNA to the ribosome. When 4EBP1 is phosphorylated and inhibited by mTORC1, it allows the generation of eIF4F complex, involved in the translational process. Akt stimulates cell growth though inhibition of GSK3β resulting in eIF2B activation and increased protein translation. Moreover, GSK3β inhibits Glycogen Synthase (GS), the enzyme catalyzing the last step of glycogen synthesis.

The IGF1-Akt pathway is regulated by different feedback loops. P70S6K, through a negative feedback loop, phosphorylates IRS1, promoting its degradation. On the other hand, mTORC2, through a positive feedback loop, phosphorylates Akt on its Ser473 residue. This phosphorylation, together with the one on Thr308 residue done by PDK1, results in the complete activation of the kinase. Both these modifications are required for its effect on FoxO transcription factors, but not for its action on p70S6K. Moreover, Akt takes part in other cellular processes, such as cell survival, angiogenesis, metabolism and cell cycle through the phosphorylation of a great variety of downstream targets.

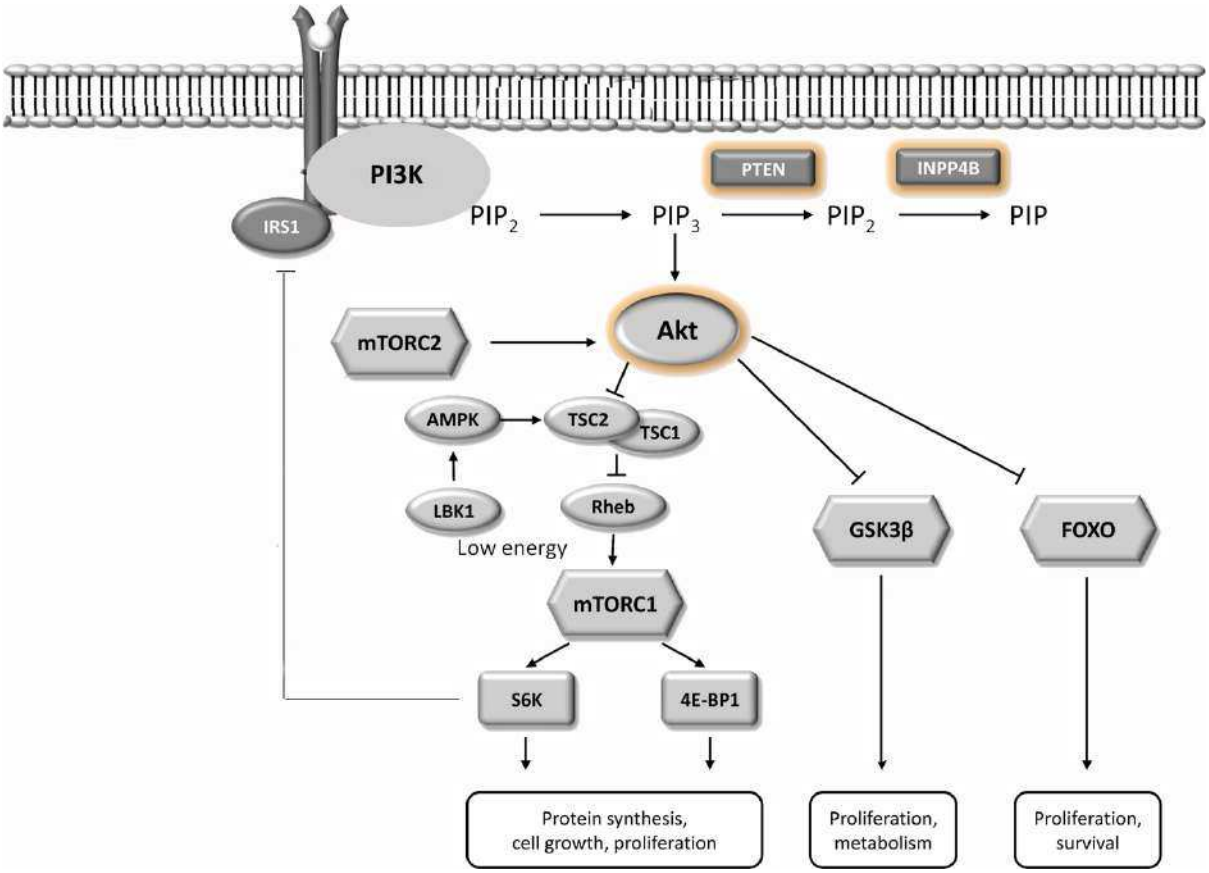

Figure 4. IGF1/Akt/mTOR signaling

Even if mTOR stimulates protein synthesis and cell growth, its sustained activation in skeletal muscle leads to a myopathic phenotype (60). Indeed, it has been shown that an increase in mTOR activity occurs during denervation or ageing, where it plays a key role in promoting muscle atrophy (61,62). At the same time genetic loss-of-function through deletion of mTOR or Raptor (mTORC1) genes leads to muscle atrophy and also to premature death (63,64). This means that an equilibrium in mTOR activation is crucial for maintaining muscle homeostasis.
Akt-mTOR pathway involvement in tumor cachexia was evidenced in cancer patients; indeed, a reduced activation of this pathway has been observed in muscle biopsies of patients with pancreatic carcinoma (65). In another study an increase in the phosphorylation level of Akt was found in muscle biopsies of cachectic patients, even if a significant decrease in Akt protein level was present (66).
In murine models of cancer cachexia, there are contrasting results regarding Akt-mTOR regulation. In ApcMin/+ mice, a model of colorectal cancer, a progressive decrease of mTORC1 activity was found in gastrocnemius muscle, and this inhibition was mediated by an activation of AMPK due to increased level of IL-6 (67,68). Also in Lewis Lung Carcinoma

mouse model showed an inhibition in mTOR activity in skeletal muscle (69). Accordingly, to a downregulation of the Akt-mTOR signaling in skeletal muscle during cancer cachexia, many treatment options lead to activation of this pathway. Aerobic exercise leads to an amelioration of muscle wasting in cachectic mice through an increase in mTORC1 activity (70,71). Also the use of the plant Salidroside prevents cancer cachexia in LLC and C26 model with a restoration in the mTOR protein level (72). In these models prevention of tumor cachexia is associated with restored Akt-mTORC1 activity.

Contrary to these results Penna et al. found an increase in Akt targets, such as GSK3β and p70S6K, in muscle of cachectic mice suggesting an upregulation of this pathway (73). Moreover, mTOR inhibition in some cases demonstrated to be effective in protecting from cancer-associated skeletal muscle wasting. In fact, the use of rapamycin, mTOR inhibitor, in C26 mice prevented cancer cachexia (35). Similarly, everolimus, a specific mTOR inhibitor, alleviates muscle wasting in CT-26 murine model of cancer cachexia (74). Moreover, it was found that a dual inhibition of MEK and Akt/mTOR pathway rescues cancer cachexia in C26 mouse model (75).

Considering these results, the regulation and the role of the Akt-mTOR pathway in skeletal muscle during cancer cachexia is still controversial.

Myostatin and Activin A

Myostatin is a growth factor and is a member of the TGF-β protein family. It is synthetized and secreted mainly form skeletal muscle cells and bind to activin type II receptor (ActIIR), which leads to activation of a Smad2 and Smad3 transcription factor complex (76). Overexpression of myostatin in mice leads to muscle atrophy (77), instead its inhibition results in a strong increase in muscle mass and fiber size (78,79). Studies suggest that myostatin exerts its effects through different pathways. Myostatin through the phosphorylation of SMAD2/3 inhibits mTORC1, thus blunting protein synthesis, and Akt, leading to activation of FoxO that mediates inhibition of genes associated with muscle differentiation (80). Evidences indicate that myostatin levels and associated signaling are activated in animal models and patients with cancer cachexia (81).

In addition to myostatin, Activin A is another TGF-β family member induced by inflammatory cytokines. Activin A has been found to be upregulated in skeletal muscle after activation of the TNFα signaling pathway; moreover tumors can also induce muscle itself to produce Activin A (82). Indeed, elevated circulating levels of Activin A have been found in patients with cancers

(83). Accordingly, inhibition of the activin receptor type IIB (ActRIIB) has been shown to spare skeletal muscle wasting and prolong lifespan in different mouse models of cancer cachexia (84,85).

As can be seen from Figure 4, the signaling pathways that play a role in cancer-associated skeletal muscle wasting converge into a final common pathway centered on Akt-mTOR-FoxO module. These pathways are tightly interconnected and together orchestrate cancer-associated skeletal muscle wasting.

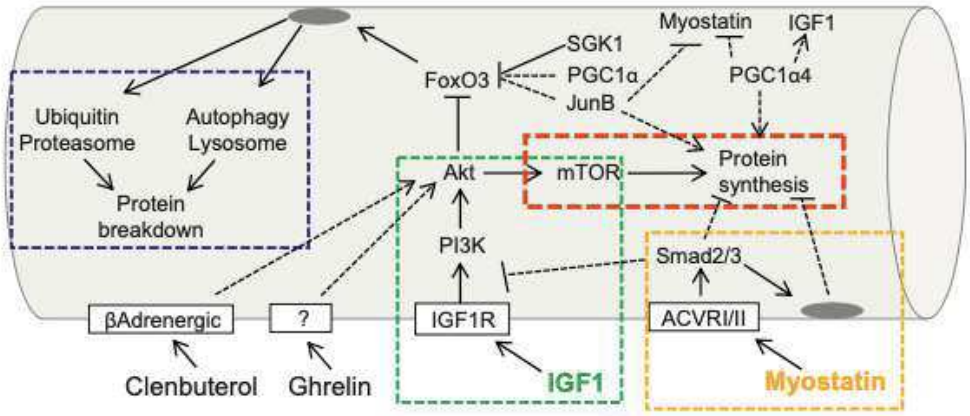

Figure 5. Schematic representation of signaling pathways leading to cancer cachexia (86).

2. AIM OF THE WORK

Cancer cachexia is a multi-organ syndrome which is characterized by a strong loss in body weight. It occurs in 50-80% of cancer patients and is due to a drastic loss in muscle and adipose tissue. One of the major intracellular pathways regulating adult skeletal muscle mass and function is the Akt-mTORC1 pathway (87,88). Studies about the regulation of this pathway in muscle of experimental models of cancer cachexia are controversial. Mice inoculated with Lewis Lung Carcinoma (LLC) or Colon-26 (C26) have shown reductions in mTORC1 signaling (69,72). The same was observed in transgenic mice which spontaneously develop intestinal polyps, leading to a cachectic phenotype between 3 to 6 months of age (67). Interestingly, treatments which show an improvement of the cachectic muscle phenotype, like treadmill running or the natural plant product salidroside, are accompanied by a restoration of mTORC1 signaling (70,72). These results are somewhat in contrast to another study, which showed that treatment of C26 mice with the mTORC1 inhibitor rapamycin is actually able to reduce muscle atrophy, possibly by restoring autophagy to normal levels (35).

In patients the link between mTORC1 signaling and cachexia is not that clear, however, there are reports which suggest that the systemic use of mTOR inhibitors can aggravate cancer cachexia. Indeed, long-term treatment with mTOR inhibitors was accompanied by a loss in muscle mass, while not affecting fat mass or body weight (89). Considering that different results have been obtained when examining the activation levels of Akt-mTORC1 signaling in tumor bearing animals, the aim of this thesis is to better understand the importance of this pathway during cancer cachexia.

Here, we use loss of function and gain of function mouse models to determine the role of Akt-mTORC1 signaling in skeletal muscle during cancer cachexia. In order to investigate the effects of mTOR inhibition in skeletal muscle during cancer cachexia we used inducible muscle-specific mouse models: the Raptor ko model, i.e., mTORC1 deletion, and the mTOR ko, i.e., deletion of mTORC1 and mTORC2. As gain of function model we used the Akt-overexpressing mouse, a well-known model of muscle hypertrophy (59).

3. MATERIAL AND METHODS

3.1. Animal Experiments and treatments

Inducible muscle-specific Raptor or mTOR knock-out mice were generated as described previously (90). Briefly, C57BL/6J strain mice expressing the floxed Raptor or mTOR gene ($Raptor^{fl/fl}$ and $mTOR^{fl/fl}$) were crossed with mice carrying the Cre recombinase fused to a mutated estrogen receptor (ER) domain under the control of human skeletal actin promoter (HSA) (91). In Raptor ko mice tamoxifen-induced Cre LoxP recombination was achieved by intraperitoneal injection of tamoxifen (3mg) once daily for one week in 2-month-old mice. C26 cells were injected 3 weeks after the end of tamoxifen treatment. In mTOR ko mice tamoxifen-induced Cre LoxP recombination was activated by intraperitoneal injection of tamoxifen (3mg) three times a week for one month in 2-month-old mice. C26 cells were injected 1 week after tamoxifen treatment finished. All mice were back-crossed at least for two generations in a BALB/c background. Both male and female mice were used.

Inducible Akt transgenic mice were generated as described previously (59). Briefly, a transgenic line that expresses the Cre recombinase under a muscle-specific (myosin light chain 1 fast) promoter was crossed with a second line that expresses Akt1 only after the deletion of a floxed upstream sequence by the Cre recombinase. The Akt coding sequence is fused to a modified estrogen receptor-binding domain; Akt phosphorylation and activation are induced only by exogenous treatment of tamoxifen, which binds the estrogen receptor.

C26 and LLC cells, a gift from Paola Costelli's lab, were cultured in high glucose DMEM (# 41966 Gibco). All culture media were supplemented with 10% fetal bovine serum (Gibco) and Pen/Strep solution (penicillin 100 U/ml and streptomycin 0.1 mg/ml, Gibco). All cell cultures were maintained at 37°C with a humidified atmosphere of 5% CO_2. Low-passage cell lines were used. C26 and LLC cell suspensions were injected subcutaneously dorsally in 3-month-old mice, BALB/c or C57BL/6J strain respectively. Tumor-bearing mice received $5x10^5$ C26 or LLC cells in physiological solution. Control mice were inoculated with physiological solution. In all experimental models of cancer cachexia mice were treated until they reached the experimental endpoint, determined by ethical criteria (loss of 20% initial body mass). C26 mice were sacrificed when they reached -20% of body weight, generally 14 days after inoculation; LLC mice were sacrificed after 30 days, at -20% of body weight or at reaching of a humane endpoint. In Akt mice C26 cells were injected in 3-month-old mice and when they lost 10-12% of initial body weight, 1mg of tamoxifen was injected intraperitoneally for 5 days in order to activate Akt. Akt mice were sacrificed when they regained body weight after

tamoxifen treatment. Control mice received tamoxifen as well and they were sacrificed when they lost 20% of body weight. A detailed scheme for the mouse models used is provide in Suppl. Fig. 1.

Analysis of body composition in mice was performed by quantitative magnetic resonance using an EchoMRI^{TM}-100 (EchoMRI, LLC., TX, USA) without the use of anesthesia.

Experimental protocols were reviewed and approved by the local Animal Care Committee, University of Padova.

Genotyping of transgenic animals

Mice were identified by analyzing the presence of Cre-recombinase on genomic DNA by PCR. DNA was extracted using a lysis buffer containing Tris-HCL 1M pH 7.5 and Proteinase K 10mg/mL (Life Technologies). The samples were denatured by incubation for 1 hour at 57°C and then proteinase K was inactivated at 99°C for 5 minutes. For the PCR reaction we used the following primers:

Cre Forward - NSP-780: CACCAGCCAGCTATCAACTCG
Cre Reverse - NSP-979: TTACATTGGTCCAGCCACCAG

Akt Forward: ACTATCCCGACCGCCTTACT
Akt Reverse: TAGCGGCTGATGTTGAACTG

Raptor Forward: CTCAGTAGTGGTATGTGCTCAG
Raptor Reverse: GGGTACAGTATGTCAGCACAG

mTOR AC11: GCTCTTGAGGCAAATGCCACTATCACC
mTOR AC14: TCATTACCTTCTCATCAGCCAGCAGTT

3.2. In vivo muscle force measurement

Gastrocnemius muscle force was measured in living mice as previously described (92). Briefly, animals were anesthetized and muscle contractile performance was measured *in vivo* using a 305B muscle lever system (Aurora Scientific Inc.). Contraction was elicited by electrical stimulation of the sciatic nerve. Common peroneal nerve was cut and the torque developed during isometric contractions was measured by stepwise increasing stimulation frequency, with pauses of at least 30 seconds between stimuli to avoid fatigue. Duration of the stimulation trains

were 600ms. Force was normalized to the muscle mass as an estimate of specific force. Animals were then sacrificed by cervical dislocation and muscles were dissected, weighted and frozen.

3.3. Colchicine treatment

Colchicine was used to monitor autophagic flux as described previously (4). Wt and Raptor ko, tumor-bearing mice and sham-treated controls, were treated with 0.4 mg/Kg of colchicine or vehicle by intraperitoneal injection. The treatment was repeated twice, 24 and 12 h prior to muscle collection.

3.4. Measurement of in vivo protein synthesis

0,04µmol/g of puromycin was injected i.p. exactly 30 minutes before removal of muscles as described previously (93).

3.5. Antibodies and western blotting

Cryosections of 20µm of TA muscles were lysed in 100µl of a buffer containing 50mM Tris pH 7.5, 150mM NaCl, 10mM $MgCl_2$, 0.5mM DTT, 1mM EDTA, 10% glycerol, 2% SDS, 1%Triton X-100, Roche Complete Protease Inhibitor Cocktail and Roche Phospho-Stop Phosphatase Inhibitor Cocktail. To detect Lys48 polyubiquitin chain content, samples were also added to two proteasome inhibitors: MG132 (Tocris bioscience) and NEM (Sigma-Aldrich).

Lysates were incubated at 70°C for 10 minutes and centrifuged at 13.300 rpm for 15 minutes at 4°C. Concentration of surnatant protein was measured using BCA protein assay kit (Pierce) following manufacturer's instructions.

Protein gel electrophoresis

Extracted proteins were solubilized in a buffer containing 5µl of 4X NuPAGE® LDS Sample Buffer (Life Technologies), 1µl of 20X DTT (Life Technologies) and water, until reaching 20µl of volume. After 10 minutes of denaturation at 70°C, samples were loaded on SDS 4-12% or SDS 3-8% precast polyacrylamide gels (Life Technologies), according to molecular weight of the protein to be analyzed. The electrophoresis was run in 1x MES/MOPS or 1X Tris-Acetate Running buffer, respectively (Life Technologies), starting from a voltage of 90V until reaching 150V when samples entered the wells.

Transfer of the protein to the nitrocellulose membrane

Proteins were now transferred from gels to nitrocellulose membranes. For the transfer, we used a Semi-dry method (Bio-Rad). Membrane and blotting paper (Bio-Rad) were equilibrated with Transfer Buffer, composed by 20% Methanol and 1X Tris-Glycine (SERVA). Transfer was obtained by applying a current of 2mA/cm^2, according to the dimension of the gel, for 1 hour at RT. To evaluate the efficiency of the transfer, proteins were stained with Red Ponceau 1X (Sigma-Aldrich). The staining was easily reversed by washing with distilled water.

Incubation with antibodies

After the transfer of proteins into nitrocellulose membranes, the membranes were saturated with Blocking Buffer (5% no-fat milk powder or BSA solubilized in TBS 1X with 0,1% TWEEN) for 1 hour at RT and incubated over-night with different primary antibodies at 4°C. Tris-buffer saline (TBS) is composed by 50mM Tris and 150mM NaCl in water, adjusted to pH 7.6.

Membranes were then washed 3 times with TBS 1X with 0,1% TWEEN at RT and incubated with secondary HRP-conjugated antibody for 1 hour at RT. Immunoreaction was revealed by Clarity Chemiluminescent substrate (Bio-Rad) and developed with ImageQuant LAS 4000 Mini (GE Healthcare).

Stripping Solution was made with 25mM glycine and 1% SDS, pH 2.

Antibody	**Costumer**	**Dilution**
Rabbit anti-Raptor	Cell Signaling #2280	1:1000
Rabbit anti-mTOR	Cell Signaling #2983	1:1000
Rabbit anti-phospho-Akt (Ser473)	Cell Signaling #4060	1:1000
Rabbit anti-phospho-Akt (Thr308)	Cell Signaling #9275	1:1000
Rabbit anti-Akt	Cell Signaling #9272	1:1000
Rabbit anti-phospho-S6 (Ser240/244)	Cell Signaling #2215	1:1000
Rabbit anti-S6	Cell Signaling #2217	1:1000
Rabbit anti-phospho-4Ebp1 (Thr37/46)	Cell Signaling #9459	1:1000

Rabbit anti-4Ebp1	Cell Signaling #9452	1:1000
Rabbit anti-LC3	Sigma L7543	1:1000
Rabbit anti-p62	Sigma P0067	1:1000
Mouse anti-puromycin	Millipore MABE343	1:1000
Mouse anti-Lys48	Millipore 04-263	1:5000
Mouse anti-GAPDH	Abcam ab 8245	1:10000
Goat anti-mouse IgG	Bio-Rad 1706516	1:2000
Goat anti-rabbit IgG	Bio-Rad 1706515	1:2000

Table 1. Antibodies used for western blotting.

Quantification of Immunoblotting

Quantification of the signal obtained through immunoreaction was measured with ImageJ software. Signal of interested protein was normalized for levels of a housekeeping protein, representative of gel loading. As housekeeping proteins we used either Actin or GAPDH, since their content did not change during experimental conditions. Results are expressed as mean±SEM.

3.6. Gene expression analysis

RNA extraction and qRT-PCR reaction

Total RNA was extracted from Gastrocnemius muscle by using Trizol (Life Technologies) according to manufacturer's instructions. 400 ng of total RNA was reversely transcribed to obtain cDNA using SuperScript™ IV (Life Technologies) in the following mix:

Random primer hexamers (50ng/µl): 1µl; dNTPs 1mM: 1µl. The volume was brought to 13µl with RNase-free water.

Samples were denatured at 65°C for 5 minutes to avoid secondary structures of RNA. After the denaturation, samples were added to the following components:

DTT 100mM: 1µl

Rnase OUT (Life Technologies): 1µl

SuperScript™ IV (Life Technologies): 1µl

RNase-free water: 0,5µl

The reaction program was: Step 1: 23°C for 10 minutes; Step 2: 50°C for 10 minutes; Step 3: 80°C for 10 minutes. At the end of the reaction, the volume of each sample was brought to 50µl with RNase-free water.

Quantitative real-time PCR was performed using SYBR Green chemistry (Applied Biosystems). SYBR Green is a fluorescent dye used as nucleic acid stain. Indeed, it intercalates into double-strand DNA, producing a fluorescent signal. Real-time PCR products accumulate during PCR cycles, creating an amplification plot, which is the plot of fluorescence signal versus cycle number, and, thus, allowing their detection through real-time PCR machine. At the beginning of PCR, the little change in fluorescent signal defines the baseline for the amplification plot. An increase in fluorescent signal above the baseline indicates the detection of PCR products. A fixed fluorescence threshold can be set above the baseline. Ct (threshold cycle) is defined as the fractional cycle number at which the fluorescence passes the fixed threshold. So, lower Ct value indicates a higher amount of the sample which can be therefore detected earlier through PCR process.
1µl of diluted cDNAs was amplified in 10µl PCR reactions in an ABI Prism 7000 (Applied Biosystem) thermocycler, coupled with an ABI Prism 7000 Sequence Detection System (Applied Biosystems) in 384-wells plates (Micro Amp Optical, Applied Biosystems). In each well 5µl sample mix and 5µl reaction mix were mixed.

Sample mix was prepared as follows:
cDNA: 1µl
RNase-free water: 4µl
SYBR Green was added to primer mix as follows:
SYBR Green qPCR (Applied Biosystems): 4,8µl
Forward/Reverse primer mix (50mM): 0,2µl

The PCR cycle used for the Real-Time PCR was:
Step 1: 95° C for 15 minutes
Step 2: 95° C for 25 seconds
Step 3: 58° C for 1 minute
Step 4: go to step 2 for 40 times

Quantification of the PCR products

Pfaffl in 2001 described a quantification method to evaluate the differences in gene expression, by measuring the ratio between a test sample and a housekeeping gene (94). The relative expression ratio of a target gene is calculated based on the primer efficiency (E) and the

threshold cycle deviation (ΔCt) of unknown sample versus a control and expressed in comparison to a reference gene.

The mathematical model is defined with this equation:

$$\text{Ratio} = \frac{(E_{\text{target}})^{\Delta Ct}}{(E_{\text{reference}})^{\Delta Ct}}$$

The reference gene used in our real-time PCR was HPRT, which did not change under experimental conditions.

Primer pair design

Gene-specific primer pairs were selected with Primer Blast software (http://www.ncbi.nlm.nih.gov/tools/primer-blast/). Primer pairs were selected in a region close to the 3'-end of the transcript, and amplified fragments of 150-250bp in length. To avoid the amplification of contaminant genomic DNA, the target sequences were chosen on distinct exons, separated by a long (more than 1000bp) intron. The melting temperature was chosen to be of about 58-60° C. The sequences of the primer pairs are listed in Table 3.

	Forward primer (5'-3')	**Reverse primer (3'-5')**
Raptor	GCCTGGAGTCACACTGGATT	CAGTTCAGCTCTCCCAGAGG
Mtor	GAGAAGGGTATGAATCGAGATGA	CCCATGAGGTCTTTGCAGTA
Ncam1	GGTGACCCCTGATTCAGAAA	GGATGGAGAAGACGGTGTGT
Runx1	CCGCAGCATGGTGGAGGTA	AGCGATGGGCAGGGTCTTG
Musk	ATCACCACGCCTCTTGAAAC	TGTCTTCCACGCTCAGAATG
Myogenin	CCAACCCAGGAGATCATTTG	TCTGGGAAGGCAACAGACAT
Chrng (Acrg)	AGCCTCCCCAGCCATCCAGG	GGCCCACCAGCAACCACTCC
Fbxo32 (Atrogin1)	GCAAACACTGCCACATTCTCTC	CTTGAGGGGAAAGTGAGACG
Fbxo30	TCGTGGAATGGTAATCTTGC	CCTCCCGTTTCTCTATCACG

(Musa)		
Trim63 (Murf-1)	ACCTGCTGGTGGAAAACATC	ACCTGCTGGTGGAAAACATC
Map1lc3b (LC3)	CACTGCTCTGTCTTGTGTAGGTTG	TCGTTGTGCCTTTATTAGTGCATC
Bnip3	TTCCACTAGCACCTTCTGATGA	GAACACCGCATTTACAGAACAA
p62	CCCAGTGTCTTGGCATTCTT	AGGGAAAGCAGAGGAAGCTC
Hprt	GTTTGTTGTTGGATATGCCCTTG	GGCAACATCAACAGGACTCC

Table 2. Primers used for quantitative RT-PCR

Data were normalized to HPRT expression. Results are expressed as mean±SEM.

3.7. Mito-Keima experiment

Analysis were done as described previously (90). Briefly, electroporation was performed on FDB muscles from wild-type and knockout animals, C26 and shams. FDB muscles were collected in 1% P/S Dulbecco's modified Eagle's medium, dissociated and plated on glass coverslips coated with 10% Matrigel in Tyrode's salt solution (pH 7.4). Mitochondria-targeted mito-Keima plasmid (mito-Keima, MBL International) was used to monitor mitophagy in transfected FDB single fibers. Fluorescence of mito-Keima was imaged in two channels via two sequential excitations (458 nm, green, and 561 nm, red) and using a 570- to 796-nm emission range. The level of mitophagy was defined as the total number of red pixels divided by the total number of all pixels. The ratio indicates the amount of mitochondria inside the lysosome.

3.8. Histological analysis and immunofluorescence staining

Collected muscles were directly frozen in liquid nitrogen. Then, muscles were cut in 10µm thick cryosections (or 2µm for mTOR staining) by using Cryostat (Leica CM 1950) and used for different analysis. Images were collected with an Upright Microscope Leica DM6 B.

Haematoxylin and Eosin staining (H&E)

Haematoxylin is a basic dye which binds to basophilic substrates, such as DNA and RNA contained in ribosomes and nuclei, thus staining them violet. Eosin colors eosinophilic structures, such as intracellular and extracellular proteins, staining them pink. H&E staining was performed using H&E staining ki (Bio-optica code 04-061010) according to the manufacturer's instructions.

Periodic Acid-Schiff staining (PAS)

PAS staining is a method to detect polysaccharides such as glycogen and glycoproteins. Periodic Acid oxidizes vicinal diols of these sugars, breaking up the bond between two adjacent carbons and creating a pair of aldehydes. These aldehydes, then, react with Schiff reagent, giving a purple-magenta color.

Material	**Time**
Carnoy's solution	10 minutes
Wash in distilled water	5-6- times
Periodic Acid 0,5% (Merck)	5 minutes
Wash in distilled water	5-6- times
Schiff reagent (Merck)	15 minutes
Wash in running tap water	5 minutes
Mount with Elvanol	

Carnoy's solution is a fixative composed of 60% ethanol, 30% chloroform and 10% glacial acetic acid.

Elvanol is a saturated solution of polyvinyl alcohol in Phosphate Buffered Saline (PBS), 20% glycerol and 1mM sodium azide.

Succinate Dehydrogenase staining (SDH)

Succinate dehydrogenase is an enzyme which forms complex II of respiratory chain and it is localized in the inner mitochondrial membrane. Colorimetric evaluation of the staining is used either to assess approximately the quantity and the distribution of mitochondria within muscle fibers or to evaluate oxidative activity of the enzyme. The reaction gives a purple coloration in the oxidative fibers, whereas glycolytic ones appear white. The sections were incubated for 30 minutes at 37°C with SDH solution (0.2M sodium succinate) (Sigma-Aldrich), 0.2M phosphate buffer (Sigma) pH 7.4 and 50mg of nitro blue tetrazolium (NBT) (Sigma-Aldrich). After the incubation, sections were washed with distilled water for 5 times and then mounted with Elvanol solution.

Neural Cell Adhesion Molecule 1 (NCAM-1) staining

NCAM-1 is localized at NMJ level in a normal muscle, whereas it diffuses throughout myofibers when an impairment in the communication nerve-muscle occurs. So, NCAM1-1

staining is used as a sign of muscle denervation.

Muscle cryosections were fixed with Methanol -20°C and incubated in blocking solution (10% goat serum in PBS) at room temperature (RT) for 1 hour. Samples were then incubated with the primary antibody against NCAM-1 (Millipore) (dilution 1:100 in 2% goat serum in PBS) at 4°C over-night. Then the sections were washed with PBS three times for 5 minutes and incubated with the anti-rabbit-594-conjugated secondary antibodies (dilution 1:200 in 2% goat serum in PBS) at 37°C for 1 hour (Jackson ImmunoResearch). After the washes and incubation with DAPI, that labels nuclei, slides were mounted with Elvanol solution.

3.9. PAS quantification

For PAS quantification, images of four TA sections per group were acquired using the same exposure settings on a Leica DM6B. Images were acquired using LAS X software and analyzed with Fiji (95). In brief, picture have been converted to 8bit, surrounding background and imperfections have been excluded from the analysis by converting their value to full black. An increasing threshold have been run through the picture and the selected pixel have been measured for mean intensity and area, obtaining a distribution profile for each picture. Measures values are expressed in terms of percentage of area for each section above a common threshold, which has been determined as the mean intensity of the control group pictures (wt sham) (96).

3.10. RNAseq

Total RNA was isolated from gastrocnemius muscle using Trizol reagent (Life Technologies) according to the manufacturer's instructions (n=3 per group). Total RNA was submitted to CRIBI – Biology Department, University of Padova. RNA was checked for purity and integrity in a Bioanalyzer device (Agilent Technologies, Inc., Santa Clara, CA) and Quant Seq 3' mRNA-seq Library Prep kit (Lexogen) is used for library construction. Sequencing is performed on NextSeq500 ILLUMINA instrument to produce 5 million reads (75bp SE) for sample.

3.11. CIBERSORTx analysis

CIBERSORTx is an *in silico* analysis that infers cell-type-specific gene expression profiles without physical cell isolation. To infer the 12 different cell populations RNA deconvolution analysis was done using CIBERSORTx (97) using the signature matrix from muscle scRNA-seq from the Cosgrove lab (98). CIBERSORTx is an online tool (http:// cibersortx.stanford.edu) and

its functionalities are divided into three main parts: the custom signature matrix from scRNA-seq, the estimation of cell type composition in bulk tissue and the imputation of cell type-specific expression profiles from bulk tissue.

3.12. Statistical analysis

Statistical tests (Student t-test and two-way ANOVA) were used as described in the figure legends. For all graphs, data are presented as means ± s.e.m. The p values are reported in the figure legends and p value <0.05 was considered statistically significant. Statistical analyses were performed using GraphPad PRISM 9.0a (GraphPad, La Jolla, CA, USA). For RNAseq data analysis we applied a two-sided t-test as well as a two-way Analysis of Variance (ANOVA) in the Perseus software (99). For pairwise comparisons, a permutation-based approach to correct for multiple testing (100). For visualization, the software InstantClue was utilized (101); hierarchical clustering was performed using the Euclidean distance and complete method. The Principal Component Analysis was performed after scaling the data to unit variance and mean zero.

4. RESULTS

4.1. Characterization of muscle wasting during cancer cachexia

Numerous types of cancers are associated with a loss in body weight due to a reduction in muscle and adipose tissue. Considering the role of mTOR signaling in the regulation of muscle homeostasis, we wondered if this pathway is altered during cancer cachexia.

To investigate cancer-associated muscle atrophy we took advantage of two well-established murine models of cachexia, the C26 colon carcinoma and the Lewis Lung Carcinoma (LLC) (102). We inoculated C26 cells or LLC cells subcutaneously into BALB/c or C57BL/6 strain respectively. Our endpoint is at minus 20% of body weight obtained in 2-3 weeks for the C26 model (Fig. 1A). The LLC model instead is characterized by a milder loss in body weight, usually obtained in 1 month, and by a greater tumor volume compared to the C26 model (Suppl. Fig.2A and B). As can be seen in Figure 1B and Suppl. Fig. 2C, both experimental models lead to the expected loss in body weight. We observed a decrease in lean and fat mass in C26 mice starting around day 10 after inoculation (Fig. 1C and 1D). After the same period C26 tumor-bearing mice significantly decreased food intake (Fig. 1E), indicating the presence of anorexia in this model. Skeletal muscle revealed an atrophic condition, about 20% decrease in muscle mass of gastrocnemius (GC) and tibialis anterior (TA) in C26 and LLC cachectic animals (Fig. 1F and Suppl. Fig. 2D). The smaller loss in body weight occurring in the LLC model can be explained by its greater tumor volume compared to the C26 one, which can lead to the underestimation of the amount of cachexia.

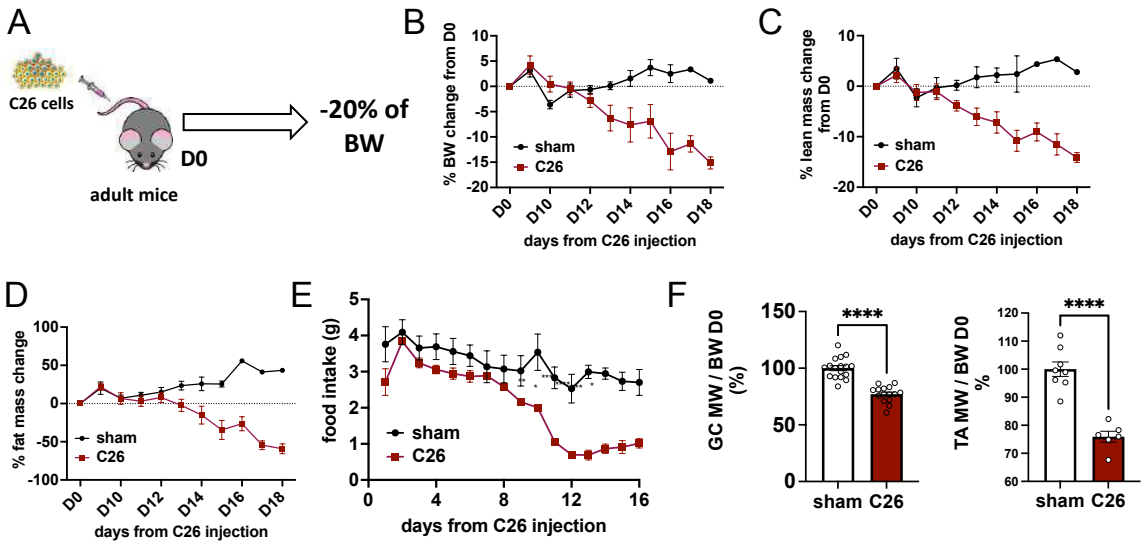

Figure 6. Muscle wasting in the C26 colon carcinoma model.

***A**. Experimental procedure: inoculation of C26 cells in adult BALB/c mice. The established endpoint is at minus 20% of body weight, about 2-3 weeks after inoculation. **B**. Body weight measurements in cachectic and control mice (n=10 per group). **C**. Graph of progressive decline in lean mass measured by Echo-MRI in cachectic mice (n=10 per group). **D**. Fat mass quantification by Echo-MRI in C26 mice and controls (n=10 per group). **E**. Food intake progression in C26 and sham mice (n=8 sham, n=10 C26). **F**. % of gastrocnemius (GC) and tibialis anterior (TA) muscle normalized to body weight in D0 in C26 mice, data shown as expression relative to D0. (GC: n=17 sham; n=15 C26. TA: n=8 sham, n=6 C26). Data presented as mean ± s.e.m. Unpaired two-tailed student's t test. ****p<0.0001.*

To get more insight the molecular mechanisms underlying this muscle wasting, we analyzed muscles in the C26 and LLC model at the endpoint of -20% of body weight and 1 month after inoculation respectively. Basic histological analysis revealed the presence of small fibers in tumor-bearing mice indicating muscle atrophy, also confirmed by cross-sectional area analysis in both C26 and LLC model (Fig. 2A and Suppl. Fig. 2E). Qualitative analysis of mitochondrial distribution observed by succinate dehydrogenase (SDH) staining did not reveal significant changes in the C26 model (Fig. 2A). We did however observe a reduction in glycogen content in the TA and GC muscles of C26 tumor-bearing mice (Fig. 2B). Next, we examined muscle force production *in vivo* in C26 animals, by measuring torque production by gastrocnemius muscle after electrical stimulation of the sciatic nerve. As can be observed in figure 2C and 2D, not only did we observe a reduced absolute force production due to atrophy, but also when force is normalized for muscle mass, a small, yet significant reduction in maximal tension persists.

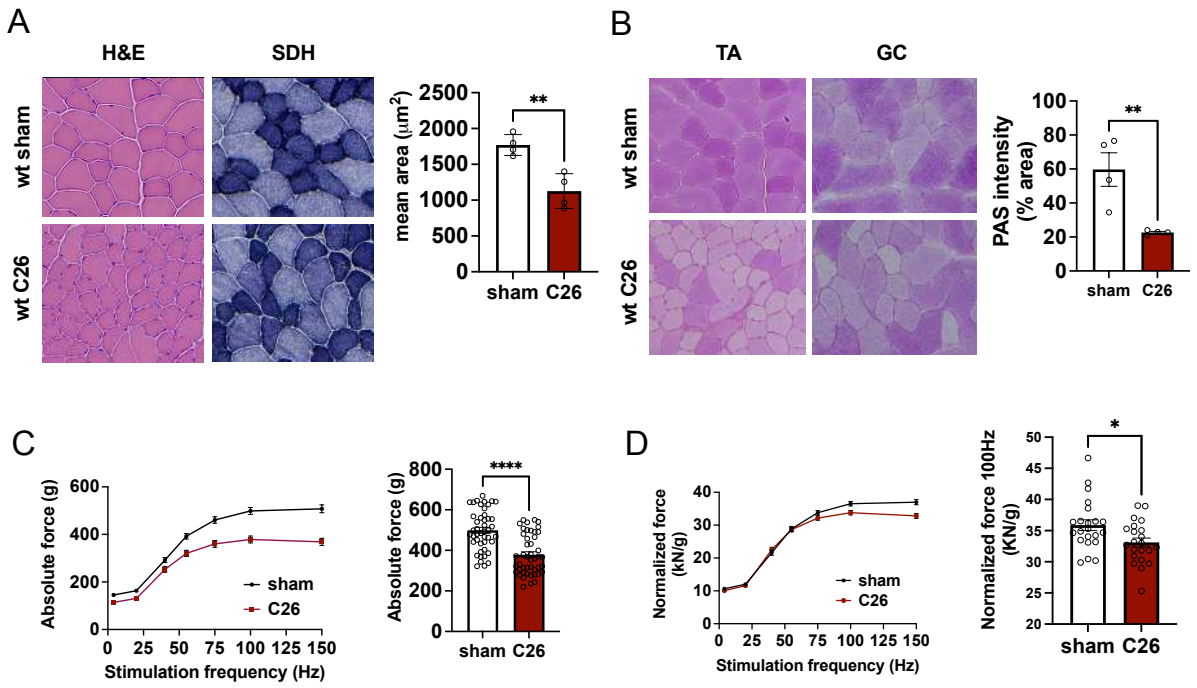

Figure 7. Loss of muscle mass and force in tumor-bearing mice.

A. *Representative Hematoxylin & Eosin (H&E) and Succinate Dehydrogenase (SDH) staining in cryosections of TA from cachectic and control mice; cross sectional area of TA in tumor-bearing mice (n=4 per group).* ***B.*** *Representative Periodic acid-Schiff (PAS) staining of TA and GC muscles in C26 and control mice; graph quantification of PAS staining in TA muscles (n=4 per group).* ***D.*** *In vivo measurement of absolute muscle force of gastrocnemius muscle and graph quantification of tetanic force (100Hz) in C26 tumor-bearing and sham control mice (n=45 muscles per group, taken from 23 animals).* ***E.*** *Normalized muscle force and tetanic force quantification in cachectic mice (n=45 muscles per group, n=23 mice). Data presented as mean ± s.e.m. Unpaired two-tailed student's t test. **p<0.01.*

4.2. Cancer cachexia is associated with reduced Akt-mTORC1 signaling and protein synthesis rates in the C26 mouse model

One of the major regulators of muscle mass and force is the Akt-mTORC1 pathway (103). To determine if the observed loss of muscle mass and force is accompanied by alterations in this signaling pathway, we performed western blotting analysis of principal downstream targets. As can be seen from the representative images of Akt-mTORC1 signaling markers and related quantification, we found a trend to decrease in the phosphorylation of Akt and ribosomal protein S6 (S6) in muscles of C26 tumor-bearing mice (Fig. 3A and B). The total levels of S6 and eukaryotic translation initiation factor 4E binding protein 1 (4E-BP1) are significantly altered in the C26 cachexia model indicating a downregulation of this signaling pathway. In

support of these results, we observed a slight, yet not significant, downregulation of the mTORC1 pathway also in muscles of LLC animals (Suppl. Fig. 3). Next, we examined if this general downregulation of mTORC1 signaling is also accompanied by changes in protein synthesis rate. Taking advantage of puromycin, an antibiotic that blocks the translation process, we observed a decrease in puromycin incorporation of 57% in C26 tumor-bearing animals indicating a decrease in protein synthesis rate (Fig. 3C).

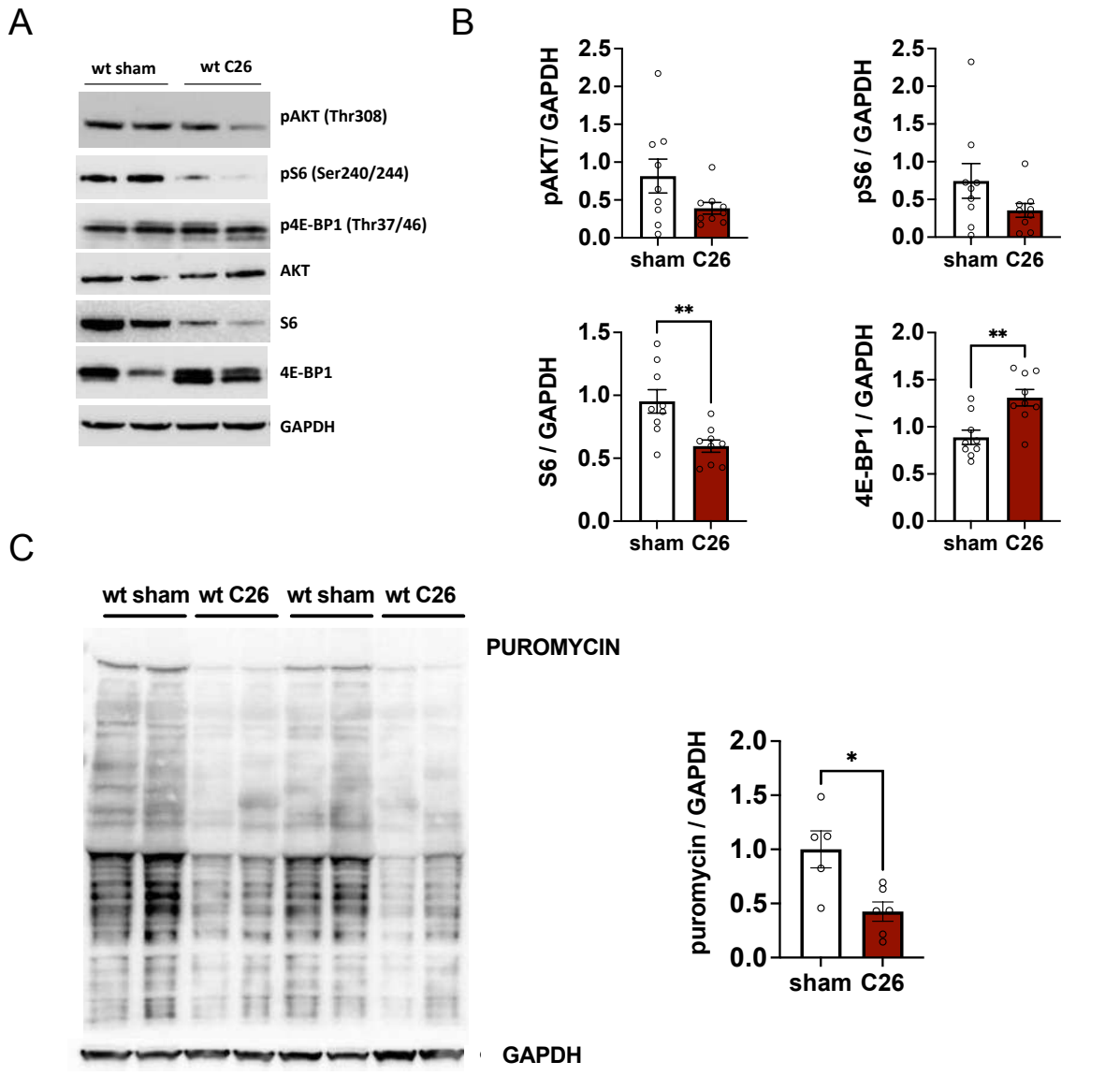

Figure 8. C26 cancer cachexia model is accompanied by a decrease in mTORC1 signaling and protein synthesis rates in skeletal muscle.

A. Western Blot representation of mTOR signaling in C26 tumor-bearing mice. B. Quantification of pAKT and pS6 markers and total level of 4E-BP1 and S6 proteins (n=9 per group). C. Western blot and

*quantification of puromycin in C26 and sham mice. Data presented as mean ± s.e.m. Unpaired two-tailed student's t test. *p<0.05, **p<0.01.*

4.3. Inducible muscle-specific deletion of mTOR or Raptor does not increase skeletal muscle atrophy in cachectic mice

As numerous cancer treatments aim at reducing Akt-mTOR activity in the tumor, we wondered if this reduction in Akt-mTORC1 signaling could have adverse effects on skeletal muscle during cancer cachexia, possibly by reducing mTORC1 signaling even further. Indeed, the use of mTOR inhibitors in the clinic has been linked to increased muscle wasting in patients (2). To address this, we used two different transgenic mouse lines, in which we can inducibly delete either mTOR (i.e., mTORC1 and mTORC2) or Raptor (mTORC1), specifically in skeletal muscle by tamoxifen administration. Since we have previously characterized these mouse lines, we know that the deletion efficiency is different in one line compared to the other; however, both show a similar onset and progression of muscle pathology when deleted from skeletal muscle (90). We deleted mTOR/Raptor in adult mice for one month, a timepoint at which animals do not show a significant phenotype yet, and then we induced cachexia using the C26 colon carcinoma, a more reproducible model compared to LLC (Fig. 4A). As can be seen in Figure 4B, the progression of body weight loss during cachexia is comparable between mTOR ko or Raptor ko mice and controls. Next, we confirmed the deletion of Raptor both at transcriptional level and protein level (Fig. 4C). In the mTOR transgenic line instead, we confirmed the mTOR deletion at transcriptional level but the mTOR protein level was still slightly present in ko animals, even if reduced when compared to wt (Fig. 4D).

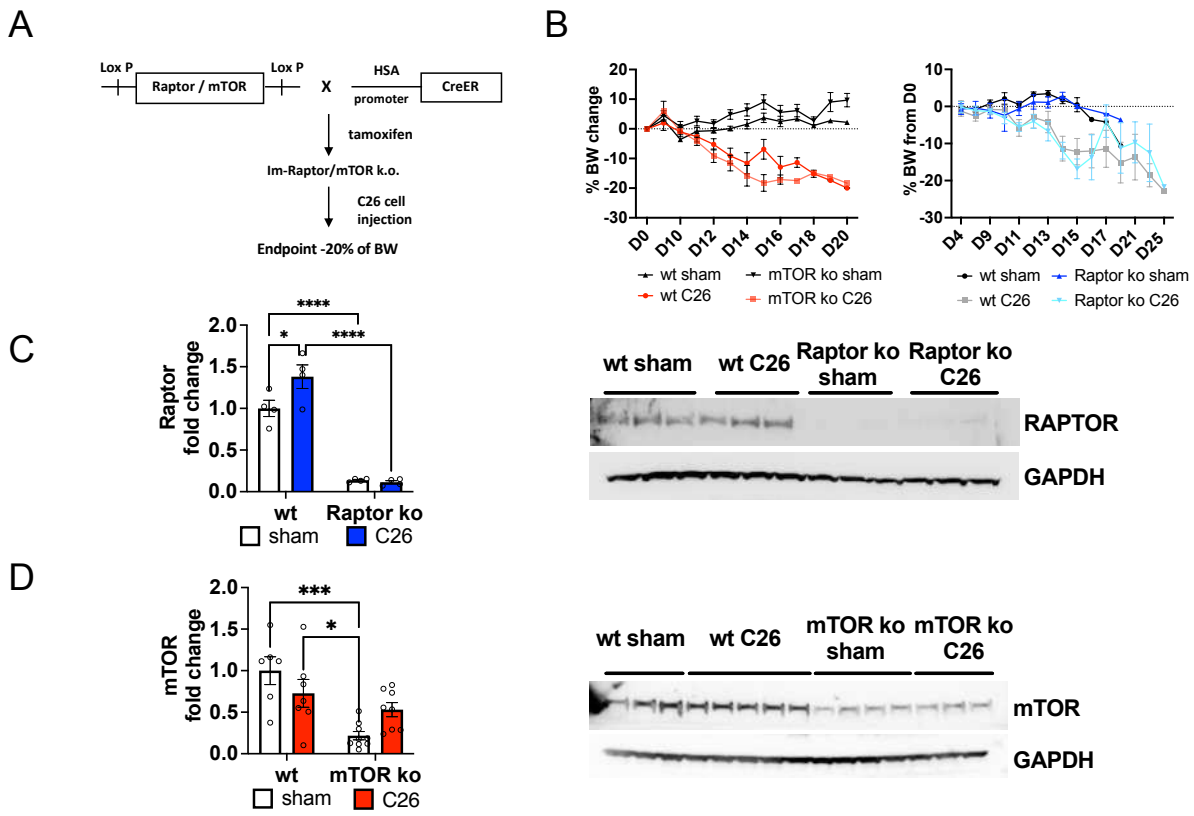

Figure 6. Characterization of Raptor ko and mTOR ko tumor-bearing mice.

A*. Schematic representation of the experimental procedure: after inducible muscle-specific deletion of Raptor or mTOR gene through tamoxifen treatment, C26 cells were injected subcutaneously on the back of mice. Mice were sacrificed when they lose about 20% of body weight.* ***B****. Body weight progression in mTOR ko and Raptor ko tumor-bearing mice (mTOR graph: n=7 wt sham and C26, n= 8 mTOR ko sham and C26, Raptor graph: n=7 each group).* ***C****. Validation of Raptor ko model by qRT-PCR and western blotting analysis (n=4 each group.)* ***D****. Validation of mTOR ko model by qRT-PCR and western blotting analysis (n=6 wt sham, n=7 wt C26, n=8 mTOR ko sham and C26). Data presented as mean ± s.e.m. Two-way ANOVA with Tukey's multiple comparison post-hoc test was performed. *p<0.05, **p<0.01, ***p<0.001, ****p<0.0001.*

As can be seen in Figure 5A and Suppl. Fig. 4A, mice lacking mTOR or Raptor from skeletal muscle, show the same loss in lean and fat mass as wildtype mice after inoculation of C26 cells. Moreover, even when we looked at skeletal muscle, gastrocnemius and tibialis anterior showed the same amount of atrophy in mTOR or Raptor ko tumor-bearing mice compared to controls (Fig. 5B and Suppl. Fig. 4A). By histological analysis of GC muscle, we did not observe any differences between wildtype and transgenic animals during cancer cachexia (Fig. 5C and Suppl. Fig. 4C).

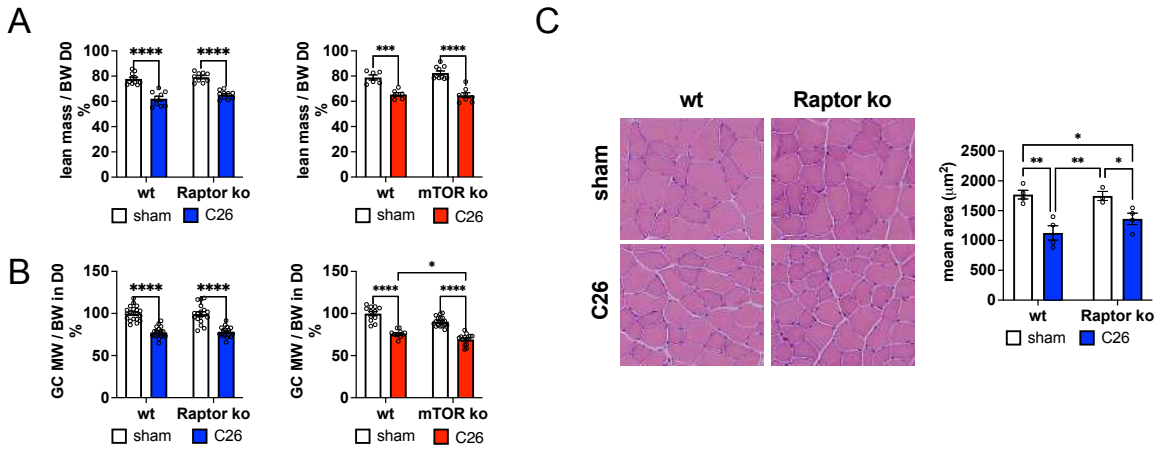

Figure 7. Deletion of Raptor or mTOR does not increase muscle atrophy in tumor-bearing mice.

A*. % of final lean mass normalized to body weight in D0 in Raptor ko and mTOR ko tumor-bearing mice and controls, data shown as expression relative to wt sham (Raptor ko: n= 10 each group, mTOR ko: n=7 each group).* ***B****. % of gastrocnemius weight normalized to body weight in D0 in Raptor ko and mTOR ko tumor-bearing mice and controls, data shown as expression relative to wt sham (Raptor ko: n=18 each group, mTOR ko: n=12 each group).* ***C****. Representative H&E staining of tibialis anterior muscle and quantification of cross-sectional area in Raptor ko tumor bearing mice and controls (n=4 wt sham, wt C26 and Raptor ko C26; n=3 Raptor ko sham). Data presented as mean ± s.e.m. Two-way ANOVA with Tukey's multiple comparison post-hoc test was performed. *p<0.05, **p<0.01, ***p<0.001, ****p<0.0001.*

To assess muscle function, we measured gastrocnemius force using *in vivo* electrical stimulation of the sciatic nerve. The force-frequency graph and tetanus quantification of absolute force (100 Hz) in Figure 6A revealed a comparable decrease in cachectic animals. Instead, deletion of Raptor during cancer cachexia showed a slight, yet significant, reduction in normalized muscle force compared to controls (Fig. 6B).

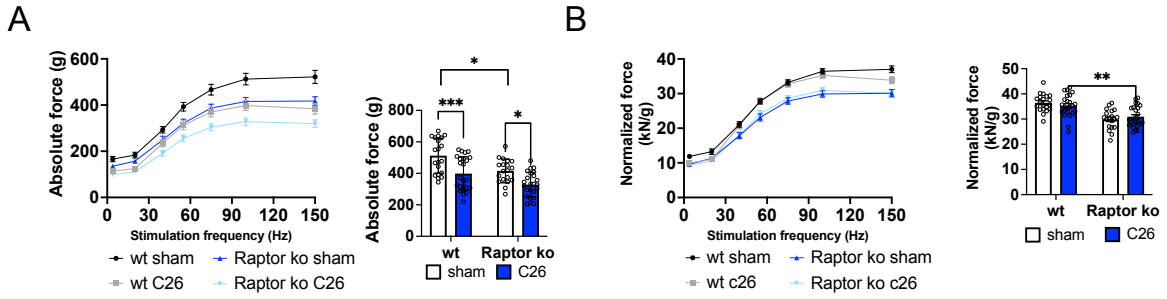

Figure 8. Muscle force measurements in Raptor ko tumor-bearing mice.

A. *Force-frequency curve and histogram of tetanic force at 100Hz of absolute muscle force in GC muscle in Raptor ko C26 and controls.* ***B****. Normalized force of GC muscle in Raptor ko C26 and controls (n=20 wt and Raptor ko sham, n=24 wt and Raptor ko C26). Data presented as mean ± s.e.m. Two-way ANOVA with Tukey's multiple comparison post-hoc test was performed. *p<0.05, **p<0.01, ***p<0.001.*

When we performed analysis of the signaling changes, we observed an increase in phospho-Akt in Raptor ko shams due to the absence of the negative feedback signaling from P70S6K to IRS1 (90), while in Raptor ko tumor-bearing mice phosphorylation of Akt is significantly reduced compared to control levels. This data suggests the presence of a downregulation of Akt activity during cancer cachexia. As expected, the main downstream targets of mTORC1, phospho-S6 and phospho-4E-BP1, are significantly reduced in Raptor ko mice but do not change after cachexia. Moreover, the previously observed increase in the inhibitory protein 4E-BP1 in tumor-bearing mice is not altered by mTORC1 deletion (Fig.7). We performed analysis of Akt-mTORC1 signaling also in mTOR ko mice during cancer cachexia. This transgenic model leads to a milder decrease in mTOR signaling compared to Raptor ko mice, but it remarks the changes observed in Raptor ko mice during cancer cachexia (Suppl. Fig. 5).

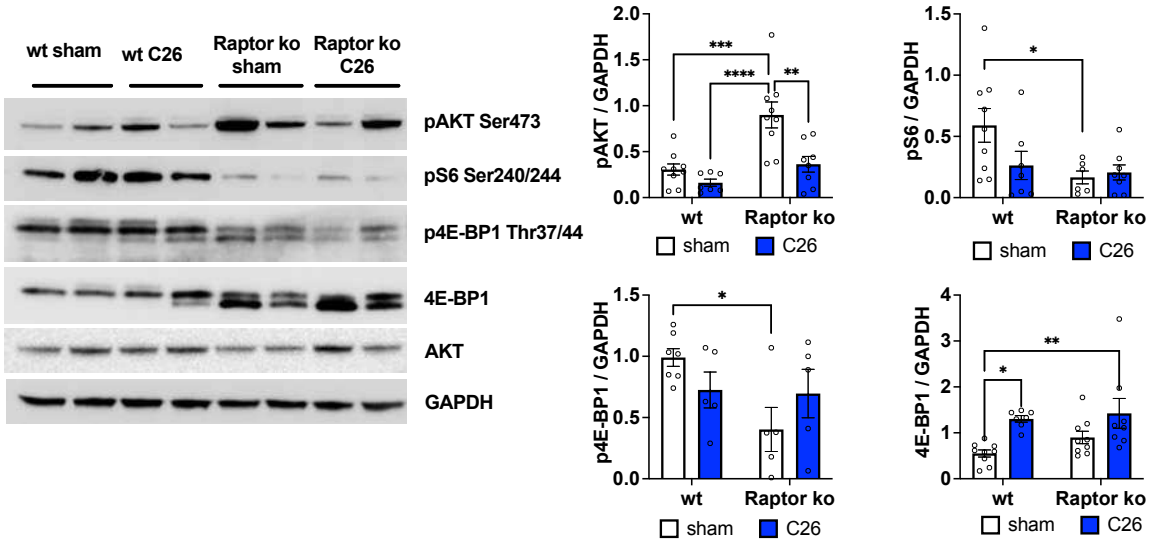

Figure 9. Akt-mTOR signaling in Raptor ko tumor-bearing mice.

*Western blotting representation of Akt-mTORC1 signaling markers in Raptor ko C26 mice and related quantification. Data presented as mean ± s.e.m. Two-way ANOVA with Tukey's multiple comparison post-hoc test was performed. *p<0.05, **p<0.01, ***p<0.001, ****p<0.0001.*

4.4. Loss of mTORC1 during cancer cachexia increases autophagic flux

As autophagy is known to be activated during cancer cachexia and very sensitive to changes in mTORC1 activity levels, we evaluated the regulation of autophagy and the role played by mTORC1 in tumor-bearing mice (31,60). When examining the lipidation of Microtubule-associated protein 1A/1B-light chain 3 (LC3) and the scaffold protein p62 in wildtype mice, we confirmed the previously reported increase in LC3 lipidation (LC3II) in cachectic animals (31), while p62 showed only a trend to increase in C26 wt mice (Fig. 8A and B). Loss of Raptor leads to a slight increase in LC3 lipidation under normal conditions, as we observed previously (90), which is markedly increased during cancer cachexia (Fig. 8A). To understand if this increase in LC3 lipidation during cachexia was due to altered mTOR signaling, we performed a similar analysis in mTOR ko mice. As can be seen in Figure 8B, mTOR ko mice showed that both LC3 lipidation and p62 are increased in C26 model as compared to wildtype cachectic mice (Fig. 8B).

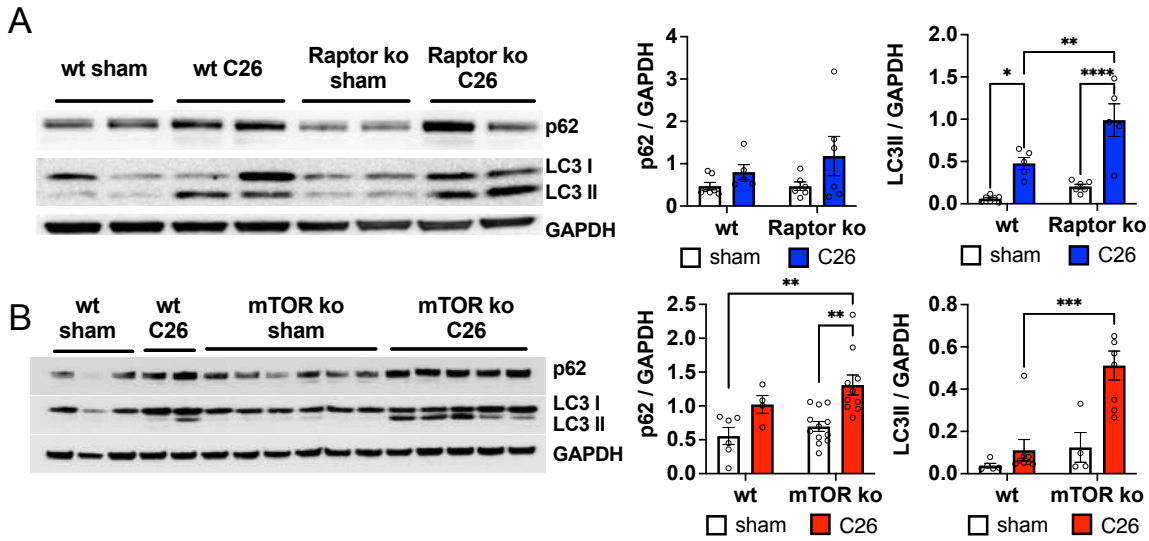

Figure 10. Increased in autophagy markers in Raptor ko and mTOR ko tumor-bearing mice.

A. *Representative western blotting analysis of LC3 and p62 autophagy markers in Raptor ko tumor-bearing mice and controls. Quantification of p62 and LC3 lipidated form (LC3II) (p62 quantification: n=7 wt sham, n=6 Raptor ko sham and C26, n=5 wt C26; LC3II quantification: n=7 wt sham, n=6 Raptor ko sham, n=5 wt C26 and Raptor C26).* ***B****. Same experiment of* ***A*** *in mTOR ko tumor-bearing mice. (p62 quantification: n=6 wt sham, n=4 wt C26, n= 12 mTOR ko sham, n= 10 mTOR ko C26; LC3II quantification: n=5 wt sham, n=4 mTOR ko sham, n= 8 wt and mTOR ko C26). Data presented as mean ± s.e.m. Two-way ANOVA with Tukey's multiple comparison post-hoc test was performed. *p<0.05, **p<0.01, ***p<0.001, ****p<0.0001.*

To understand if the increased LC3 lipidation during cachexia was due to an increased autophagic flux or a block in autophagy, we measured autophagic flux using colchicine. Colchicine leads to an accumulation of autophagic vacuoles through destabilization of the microtubule system and an impairment in autophagosome-lysosome fusion (104). Initially we analyzed by western blotting the different conditions only in muscles of wildtype mice and we found a significant increase in LC3 II and p62 protein after colchicine administration in C26 mice (Fig. 9A). This data suggests an activation of the autophagic flux during cancer cachexia. We performed the same experiment in Raptor ko mice and as can be seen in Fig. 9B we found an even further increase in LC3 II and p62 protein in tumor-bearing mice of ko animals compared to sham and wt mice. Indeed, comparing wt and Raptor ko mice we found that deletion of Raptor leads to a more pronounced induction of bulk autophagy during cancer cachexia than that observed in wildtype muscles (Fig. 9C).

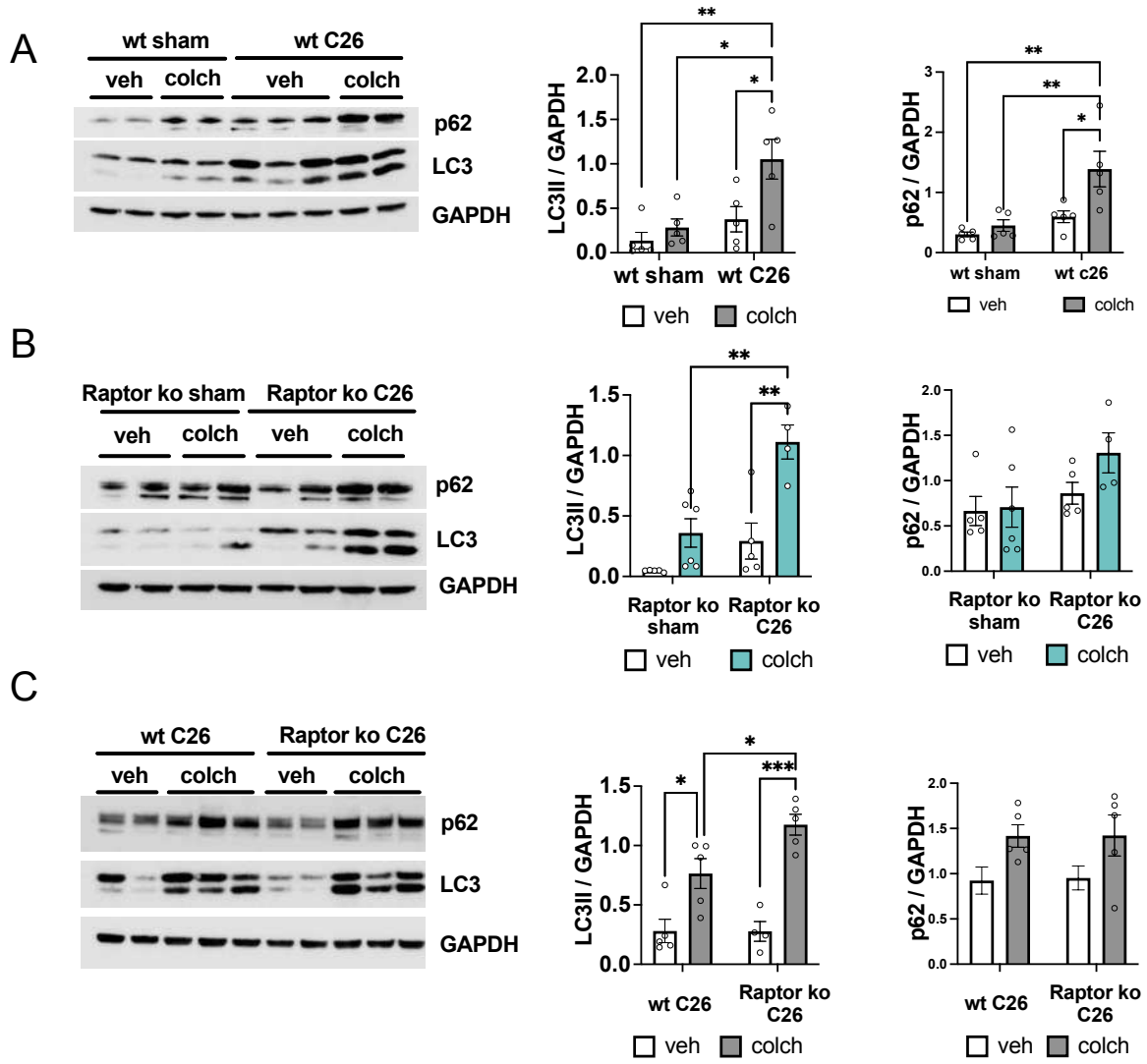

Figure 11. Raptor deletion leads to an increase in autophagic flux during cancer cachexia.

A. *Analysis of autophagic flux with colchicine treatment in wt mice during cancer cachexia. Representative LC3 and p62 western blots: quantification of LC3 lipidated form (LC3II) and p62 protein in wt sham and C26 animals, treated with colchicine or vehicle (n=5 each group).* ***B****. Same experiment of* ***A*** *in Raptor ko mice (n=5 Raptor ko sham and C26 vehicle, n= Raptor ko sham colchicine, n=4 Raptor ko C26 colchicine).* ***C****. Analysis of autophagic flux comparing wt and Raptor ko mice during cancer cachexia (n=5 wt C26 veh, wt C26 colch, Raptor ko C26 colch; n=4 Raptor ko C26 veh). Data presented as mean ± s.e.m. Two-way ANOVA with Tukey's multiple comparison post-hoc test was performed. *p<0.05, **p<0.01, ***p<0.001.*

Next, we wanted to determine if also mitophagy, a selective degradation of mitochondria by autophagy, is affected by cancer cachexia. A qualitative analysis of mitochondria through Succinate Dehydrogenase (SDH) staining does not reveal alterations in these organelles in Raptor ko mice (Fig. 10A). To measure mitophagic flux we used the mito-Keima probe in

isolated fibers from flexor digitorum brevis (FDB) muscles (Fig. 10B) (105). Mito-Keima probe exhibits both pH-dependent excitation and resistance to lysosomal proteases. These properties allow qualitative assessment of mitophagic flux, indeed the pH-dependent fluorescent properties of Keima allow rapid determination as to whether the protein is in the mitochondria (pH 8.0, green excitation) or the lysosome (pH 4.5, red excitation).

As shown in the quantification of mito-Keima (Fig. 10C), we observed an increase of mitochondria inside the lysosome and thus in mitophagic flux in Raptor ko mice during cachexia compared to normal condition.

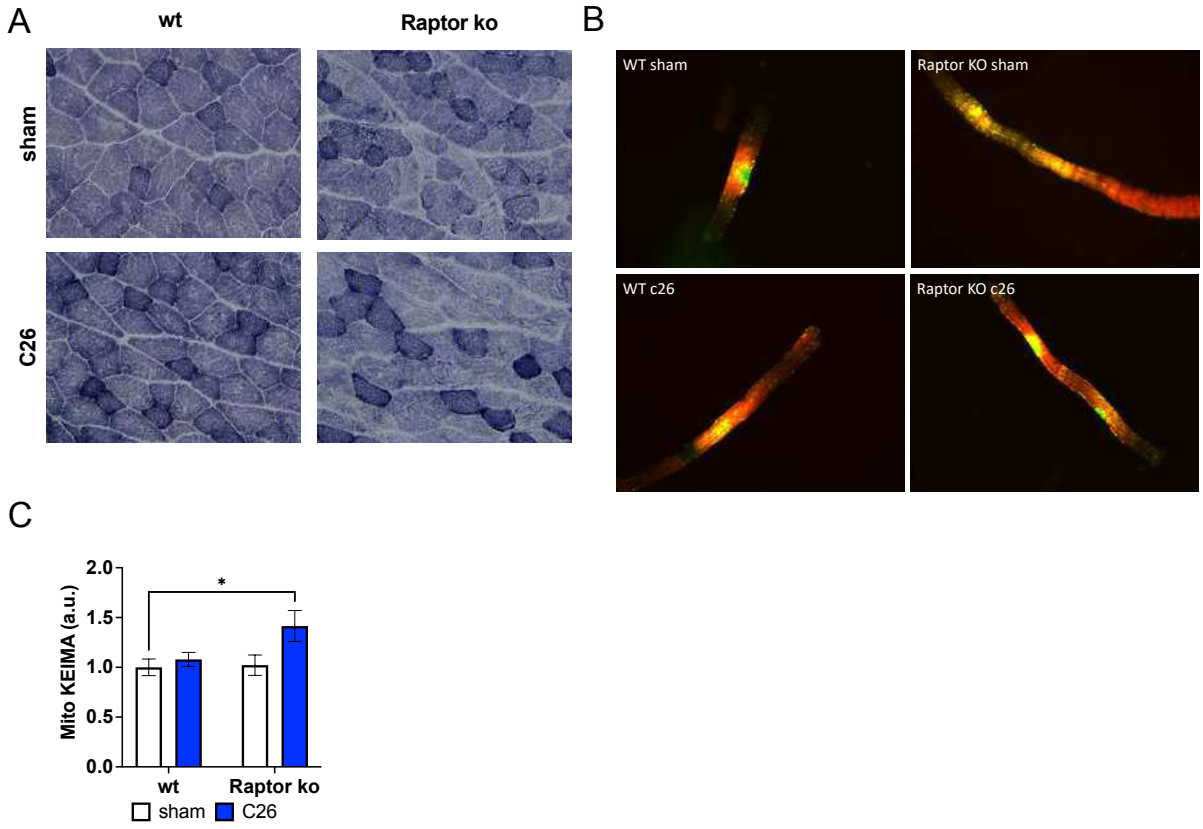

Figure 12. Mitophagy is increased in Raptor ko tumor-bearing mice.

A. *Representative images of SDH staining in Raptor ko C26 mice and controls.* ***B****. Fluorescence images of mito-Keima probe in FDB single fibers.* ***C****. Mito KEIMA measurements in FDB muscle of Raptor ko tumor-bearing mice and controls (n=5 muscles each group). Data presented as mean ± s.e.m. Two-way ANOVA with Tukey's multiple comparison post-hoc test was performed. *p<0.05.*

4.5. Loss of mTOR or Raptor does not alter skeletal muscle innervation during cancer cachexia

We have previously reported that mTORC1 signaling in muscle fibers is closely linked to the maintenance of neuromuscular junction. Furthermore, it was reported that cancer cachexia is accompanied by the appearance of denervated fibers (106). To understand if fiber denervation is differentially affected in mouse lacking Raptor or mTOR, we analyzed the levels and distribution of the denervation marker Neural Cell Adhesion Molecule 1 (NCAM-1). We confirmed the finding that cachexia is accompanied by an increase in Ncam1 transcript (Fig. 11A). In healthy fibers NCAM-1 is present at the sarcolemma around NMJ plaque while it spreads along all the fiber upon denervation. As can be seen in the representative images and in the quantification of the immunofluorescence (Fig. 11B), the NCAM-1 protein level, as the transcript one, is slightly increased during cancer cachexia but it is not affected by loss of mTOR or Raptor in C26 tumor-bearing mice. Even when we examined the transcriptional regulation of other genes linked to fiber denervation, i.e. Runx1 (107), MuSK (108), Myogenin (109) and AchRγ (110), we observed a trend to increase in knockout animals during cachexia (Fig. 11C).

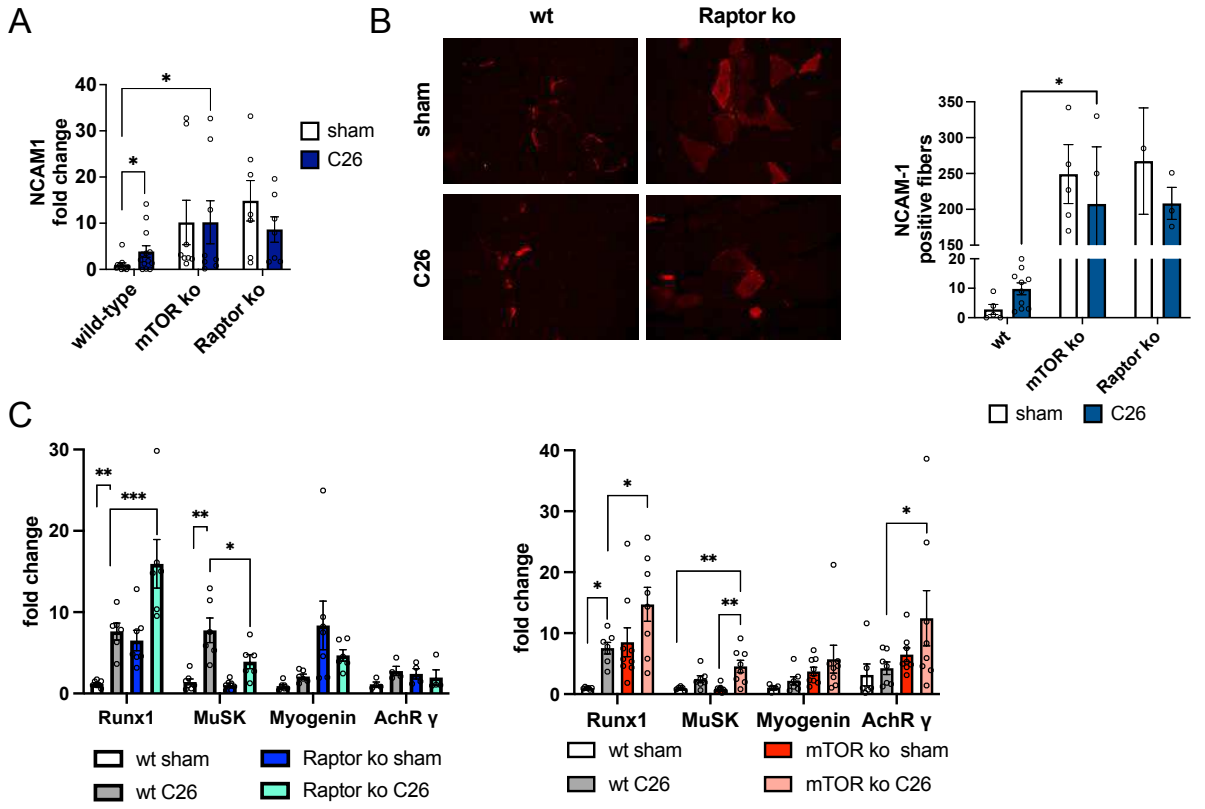

Figure 13. Analysis of NMJ markers in Raptor ko and mTOR ko mice during cancer cachexia.

***A**. Analysis of Ncam1 gene at transcriptional level by qRT-PCR (n= 12 wt sham, wt C26; n=8 mTOR ko sham and C26; n= 7 Raptor ko sham and C26). **B**. Representative images of NCAM-1 staining in gastrocnemius muscle and related quantification of total number of positive fibers per muscle in mTOR ko C26 and Raptor ko C26 animals and controls (n=5 wt sham, n=10 wt C26, n=10 mTOR ko sham, n=6 mTOR ko C26, n= 3 Raptor ko sham and C26). **C**. Analysis of NMJ markers by qRT-PCR technique in mTOR ko and Raptor ko tumor-bearing mice (Raptor ko graph: n=7 wt and Raptor sham, n=6 wt and Raptor C26; mTOR ko graph: n=6 wt sham, n=7 wt C26, n=9 mTOR ko sham, n=8 mTOR ko C26). Data presented as mean ± s.e.m. Two-way ANOVA with Tukey's multiple comparison post-hoc test was performed. *p<0.05, **p<0.01, ***p<0.001.*

4.6. Muscle-specific Akt activation is sufficient to rescue skeletal muscle mass in tumor-bearing mice.

As cancer cachexia is associated with reduced Akt-mTORC1 signaling, we wondered if reactivation of this signaling pathway would be sufficient to counteract cancer-related muscle wasting. To determine this, we used a mouse model in which we can inducibly activate Akt only in skeletal muscle. A constitutively active, myristoylated form of Akt is expressed in skeletal muscle and fused to an estrogen receptor domain making it unstable and leading to its rapid degradation. Administration of tamoxifen stabilizes and activates Akt, leading to a rapid muscle growth in healthy, normal muscle (59). To determine the effect of Akt activation on body weight and muscle wasting during cachexia, we implanted C26 cells and started administrating tamoxifen when mice lose 10-15% of body weight. As can be seen in Figure 12A, Akt mice express the myristoylated form of Akt at 75KDa and the endogenous one at 55KDa. The elevated level of phosphorylation of Akt and of the main targets of mTORC1, S6 and 4E-BP1, demonstrate the strong activation of the Akt-mTORC1 signaling in Akt mice. Surprisingly, Akt activation specifically in skeletal muscle for 5 days can partially rescue body weight loss during cancer cachexia (Fig. 12B). This change is due to a total rescue in the lean mass (Fig. 12C). Indeed, when we looked at skeletal muscle, both gastrocnemius and tibialis anterior muscles, showed a complete rescue in muscle atrophy (Fig. 12D).

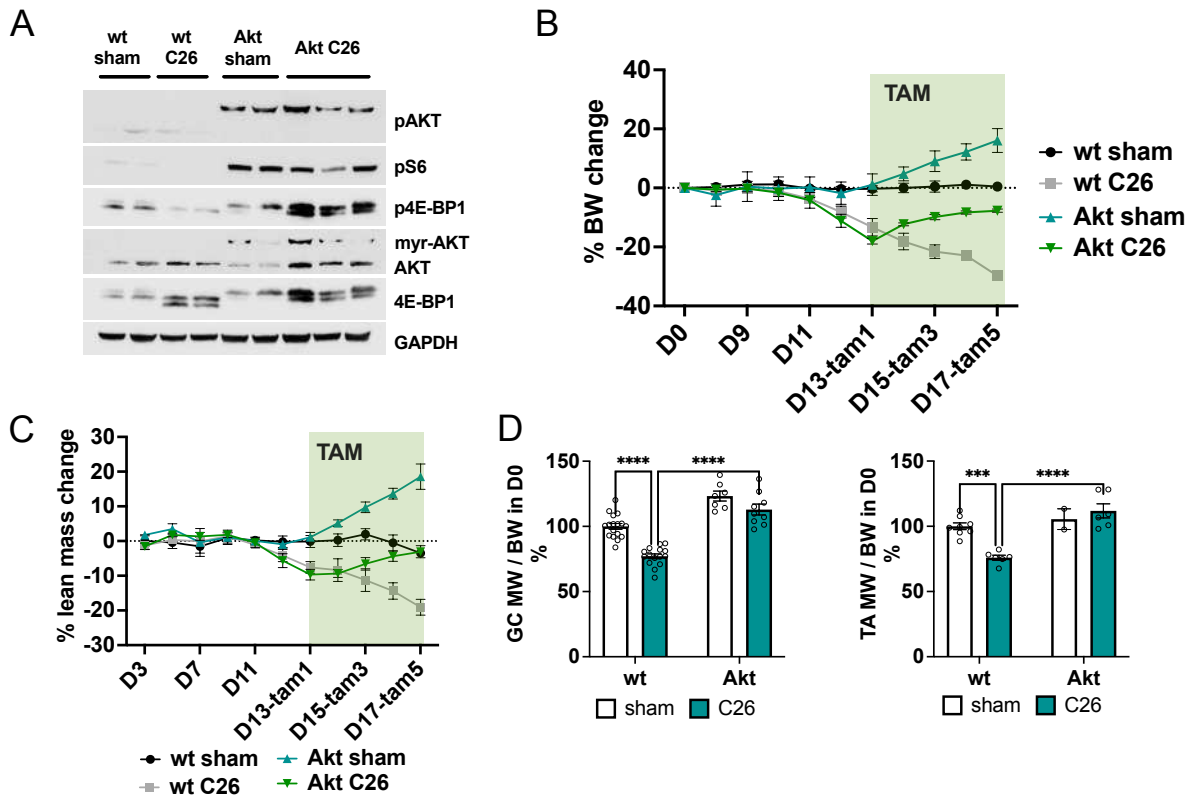

Figure 14. Activation of Akt-mTORC1 signaling restores body weight loss.

A. *Expression levels of phosphorylated AKT-ER (Ser473); total endogenous AKT (55KDa) and myrAKT-ER (75KDa) in sham and tumor-bearing Akt and wt mice; western blot analysis of mTOR signaling in Akt C26 mice and shams.* ***B.*** *Representation of body weight progression in wt and Akt mice with or without inoculation of C26: when mice lose about 10-12% of body weight, tamoxifen is administered daily for 5 days to activate Akt (n=7 each group)* ***C.*** *Measurement of lean mass during cancer cachexia and its restoration after Akt activation (n=7 each group).* ***D.*** *% of GC and TA weight in Akt tumor-bearing mice and controls. Data shown as expression relative to wt sham (GC: n=17 wt sham, n=15 wt C26, n=7 Akt sham, n=9 Akt C26; TA: n=8 wt sham, n=6 wt C26 and Akt C26, n=2 Akt sham). Data presented as mean ± s.e.m. Two-way ANOVA with Tukey's multiple comparison post-hoc test was performed. ***p<0.001, ****p<0.0001.*

Basic histological analysis of Akt C26 muscles revealed hypertrophic fibers without the presence of myopathic features (Fig. 13A). Then we looked at the glycogen content in these muscles since it is known that Akt activation in muscles leads to a strong increase in glycogen synthesis. As can be seen from PAS staining and quantification, the reduced amount of glycogen seen in cachectic muscles is restored after Akt activation (Fig. 13B).

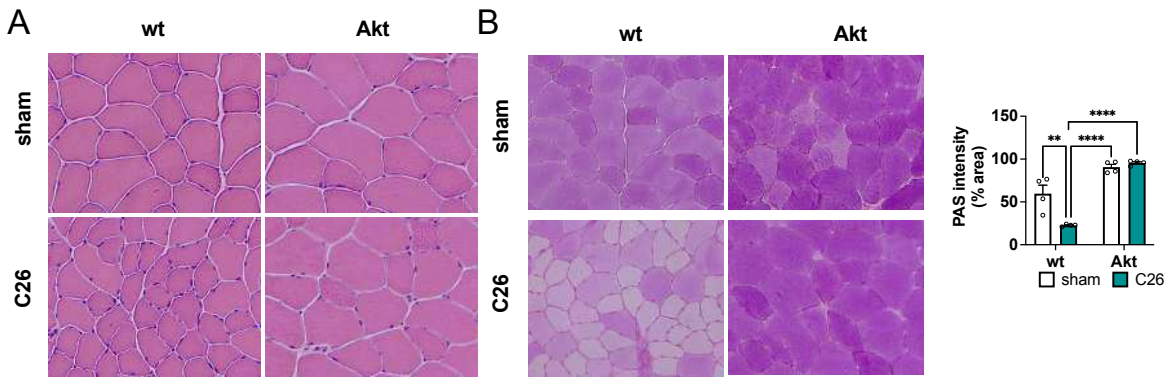

Figure 15. Analysis of muscle histology in Akt tumor-bearing mice.

A. *Representative images of H&E staining in GC muscle of Akt C26 mice and controls.* ***B.*** *Representative images of PAS staining and quantification of PAS intensity area in TA of Akt C26 mice and controls (n=4 each group). Data presented as mean ± s.e.m. Two-way ANOVA with Tukey's multiple comparison post-hoc test was performed. **p<0.01, ****p<0.0001.*

4.7. Akt overexpressing mice show a restoration of muscle function and denervation markers

To determine if Akt tumor-bearing mice undergo a functional hypertrophy, we measured muscle force of gastrocnemius muscle. The absolute force of these mice is completely restored to normal condition and even the normalized force does not show anymore the significant reduction present in cachectic mice (Fig. 14 A and B).

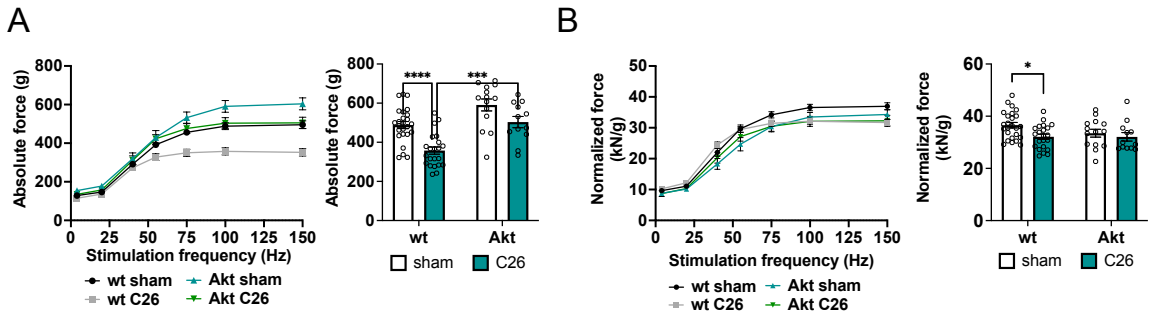

Figure 16. Akt activation in tumor-bearing mice restores muscle function.

A. *Force-frequency graph of absolute gastrocnemius muscle force in vivo in Akt C26 mice; quantification of tetanic force at 100Hz.* ***B.*** *Graph and tetanus force quantification of normalized force for gastrocnemius weight (n=25 muscles, n=13 mice for wt sham; n=22 muscles, n=12 mice for wt C26; n=14 muscles, n=12 mice Akt sham; n=12 muscles, n=6 mice Akt C26). Data presented as mean ± s.e.m. Two-way ANOVA with Tukey's multiple comparison post-hoc test was performed. *p<0.05, ***p<0.001, ****p<0.0001.*

Considering the restored muscle force, we wondered if the neuromuscular junction presents an amelioration after Akt activation during cancer cachexia. Since cachexia leads to an increase in denervation markers, we examined NMJ markers of denervation in Akt overexpressing mice. Interestingly, NCAM-1 positive fibers are not present anymore in Akt C26 muscles and denervation markers analyzed by qRT-PCR are restored to normal level (Fig. 15A and B).

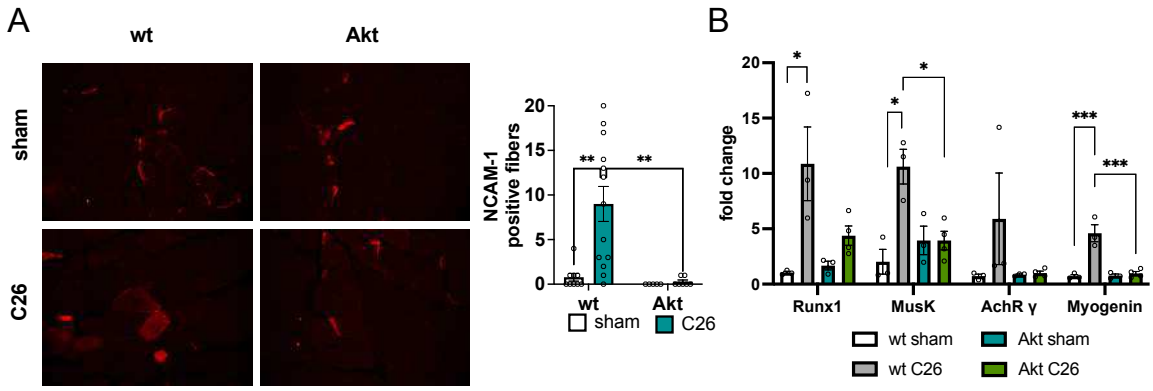

Figure 17. Restoration of denervation markers in Akt tumor-bearing mice.

A. *Representative images of NCAM-1 staining in gastrocnemius muscle and related quantification of total number of positive fibers per muscle in Akt C26 mice and controls (n=9 wt sham, n=13 wt C26, n=5 Akt sham, n=7 Akt C26).* ***B.*** *Analysis of NMJ markers at transcriptional level in Akt C26 mice and controls (n=3 wt sham, wt C26, Akt sham, n=4 Akt C26). Data presented as mean ± s.e.m. Two-way ANOVA with Tukey's multiple comparison post-hoc test was performed. *p<0.05, **p<0.01, ***p<0.001.*

4.8. Muscle-specific Akt activation does not affect tumor or spleen mass.

Next, we investigated if muscle-specific Akt activation affects tumor growth or other systemic parameters. As can be seen from Fig.16A tumor weight is comparable between Akt and wt mice. Moreover, the C26 colon carcinoma model is usually characterized by an increase in spleen mass, indeed wt C26 mice present an increase in spleen weight of about 50% compared to sham. Also, Akt tumor-bearing mice showed the same increase in spleen mass as wt (Fig. 16B).

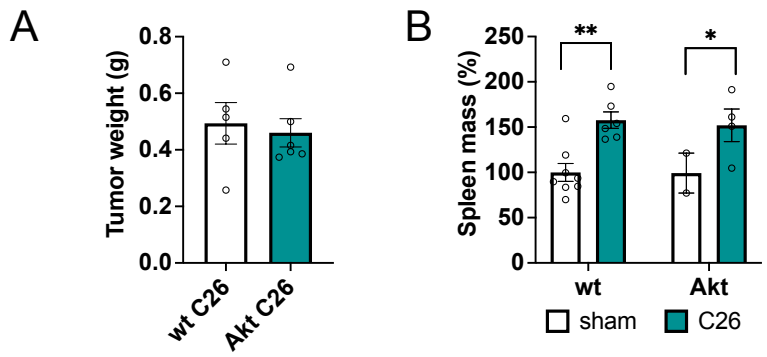

Figure 18. Tumor and spleen weight in Akt tumor-bearing mice.

A. *Absolute tumor weight in wt and Akt tumor-bearing mice (n=5 wt C26, n=6 Akt C26).* ***B. %*** *Spleen mass in Akt and wt tumor-bearing mice, data shown as expression relative to wt sham (n=8 wt sham, n=6 wt C26, n=2 Akt sham, n=6 Akt C26). Data presented as mean ± s.e.m. Two-way ANOVA with Tukey's multiple comparison post-hoc test was performed. *p<0.05, **p<0.01, ***p<0.001.*

4.9. Activation of Akt rescues skeletal muscle transcriptome

To determine the molecular mechanism behind this Akt-dependent rescue of muscle wasting in an unbiased way, we performed RNA sequencing analysis of wildtype, Raptor ko, mTOR ko and Akt overexpressing mice, both with and without inoculation of C26 cells. To obtain a systematic overview, we performed principal component analysis (Fig. 17A). Under control conditions, the different transgenic mice did not segregate along the first two components. However, we observed that the C26 cell inoculation induced distinct expression profiles in Raptor ko, mTOR ko and wildtype mice. Interestingly, activation of Akt in tumor-bearing mice is sufficient to completely normalize the gene expression profile as seen by the principal component analysis. To identify statistically significant genes that are regulated during cachexia and behave differently between wt and Akt mice, we performed a two-way ANOVA analysis (genotype, treatment). Next, we visualized the z-score normalized expression values using a hierarchical clustering (Fig. 17B) of genes (n=160) that showed a significant interaction (p value<0.001) and we detected several distinct clusters (n=6).

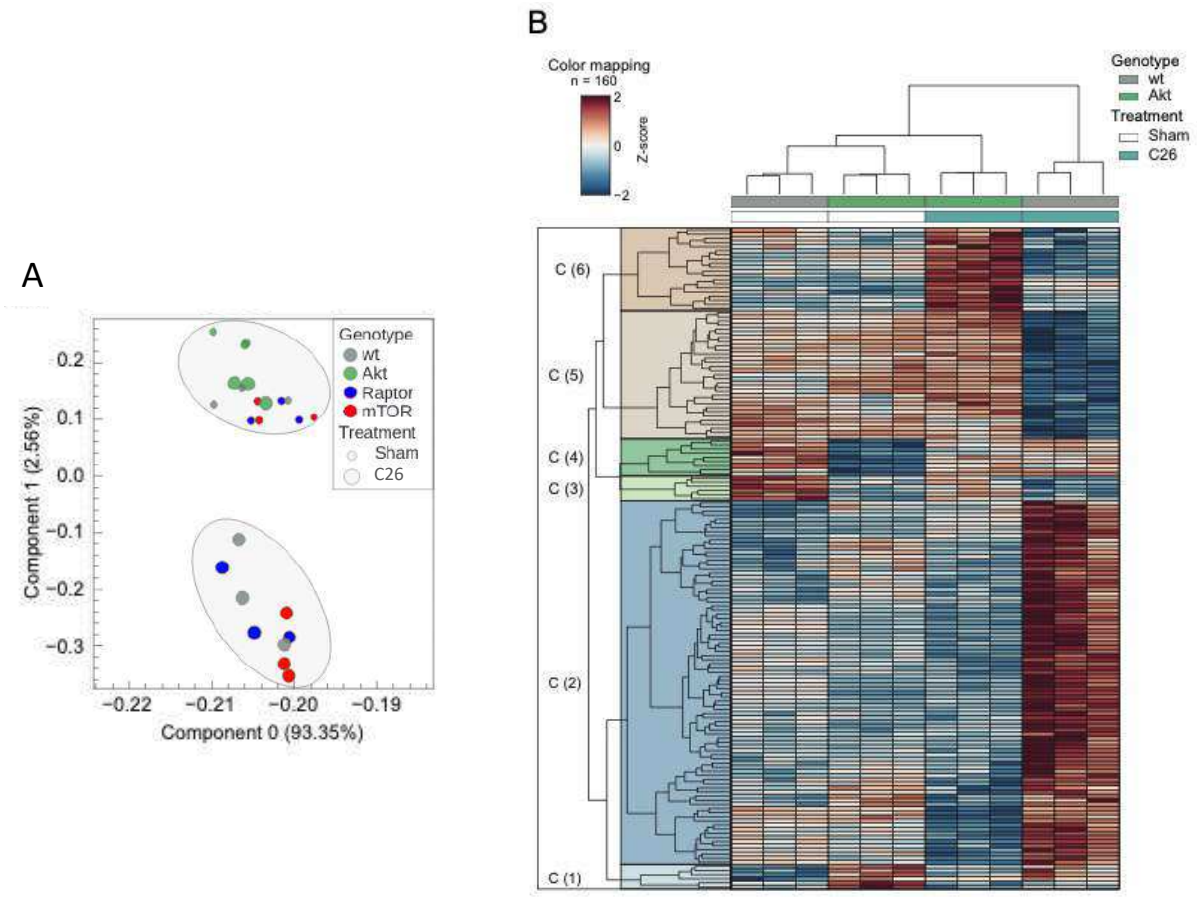

Figure 19. Activation of Akt recovers muscle transcriptome.

A. *Principal component analysis of RNAseq data of transgenic mice (Raptor ko, mTOR ko, Akt and wt) in control (sham) or post C26 inoculation (n = 3 animals per group)* ***B.*** *Subset of genes after two-way ANOVA comparing wt and Akt animals. Genes with interaction p-value < 0.001 are shown using Euclidean distance and the complete method.*

4.10. Differentially expressed genes revealed a normalization in the autophagy and ubiquitin proteasome systems in Akt tumor-bearing mice.

Gene ontology analysis made with Metascape (111) of differentially expressed genes (DEG) belonging to cluster 2 and 1 (96 genes), which are upregulated during cachexia and restored to normal level in Akt C26 mice, highlighted pathways involved in protein degradation processes, such as autophagy and ubiquitin proteasome system (UPS) (Fig. 18A). The heatmaps in figure 18B and C show some DEG belonging to autophagy (n=6) and UPS (n=13) respectively that are normalized in Akt C26 mice compared to wt C26.

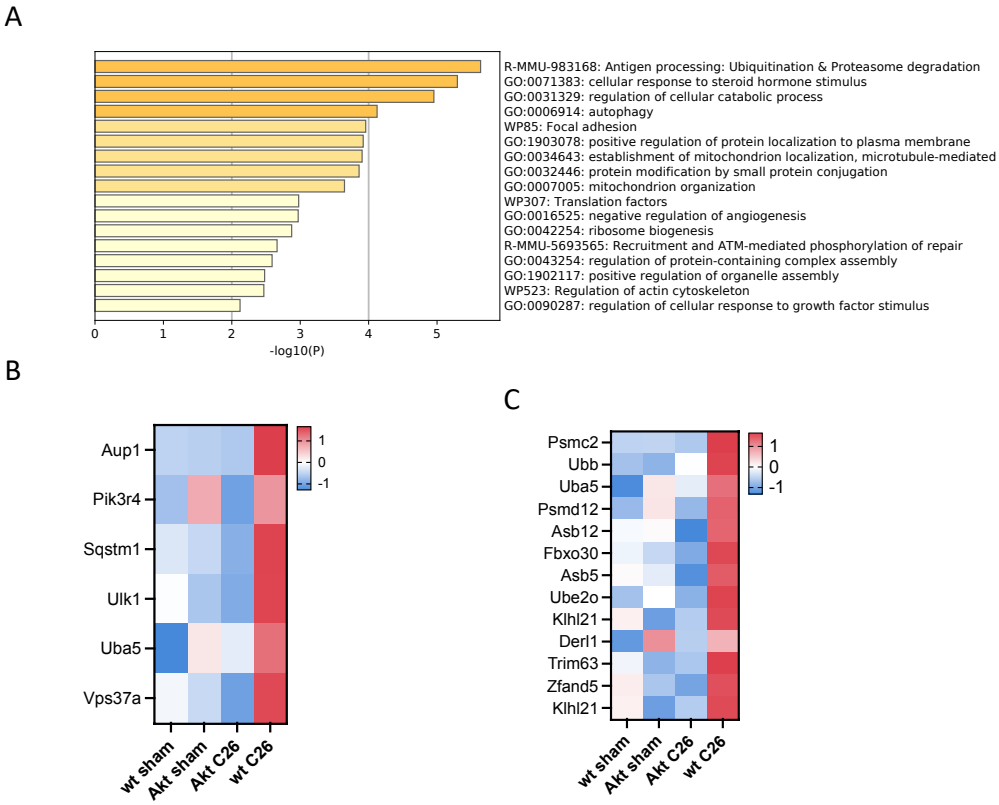

Figure 20. Gene ontology analysis of muscle transcriptome revealed normalization in the autophagy and UPS in Akt tumor-bearing mice.

A. *Metascape gene ontology analysis of DEG upregulated in wt C26 mice and restored in Akt tumor-bearing mice (n=96 genes).* ***B****. Heat map of Z-score value of genes belonging to the autophagy system (n=6).* ***C.*** *Heat map of Z-score value of genes belonging to the UPS (n=13).*

By RT-qPCR, we confirmed the inhibitory effect of Akt on the cachexia-induced upregulation of some of the well-known genes involved in these catabolic pathways (Fig.19).

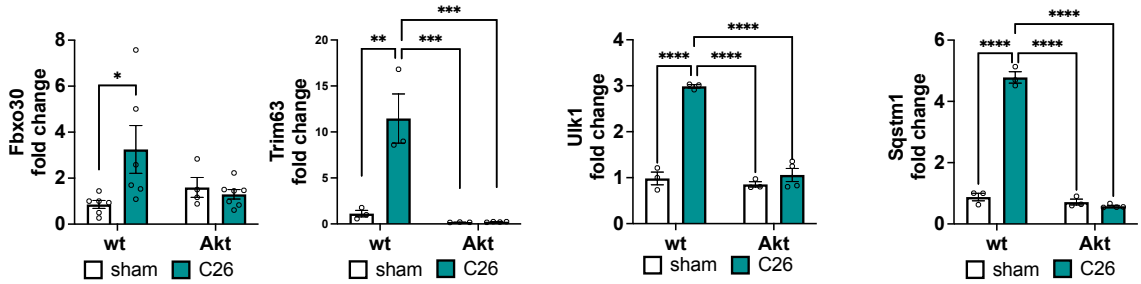

Figure 21. Akt activation reverts muscle transcriptome during cancer cachexia.

RT-qPCR analysis of genes for ubiquitin-proteasome (Trim63 (Murf1), Fbxo30 (Musa)) and autophagy-lysosome system (Sqstm1 (p62), Ulk1) in Akt C26 mice (n=3 wt sham, wt C26, Akt sham,

*n=4 Akt C26 for Trim63, Ulk1 and Sqstm1; n=5 wt sham, n=6 wt C26, n=4 Akt sham, n=7 Akt C26 for Fboxo30). Data presented as mean ± s.e.m. Two-way ANOVA with Tukey's multiple comparison post-hoc test was performed. *p<0.05, **p<0.01, ***p<0.001, ****p<0.0001.*

To investigate if transcriptional regulation results in altered activity of the degradative processes, we first evaluated level of LC3 lipidation and total p62 abundance. We observed a strong reduction in LC3 lipidation and a trend for reduction in p62 after Akt activation, suggesting a reduction in autophagy in these muscles (Fig. 20A). Next, we performed a western blotting analysis for lys48 ubiquitination to get an indication on the activity of ubiquitin-proteasome pathway. In line with the data of the RNA sequencing, we observed a significative reduction of protein ubiquitination in tumor-bearing mice after Akt activation (Fig. 20B).

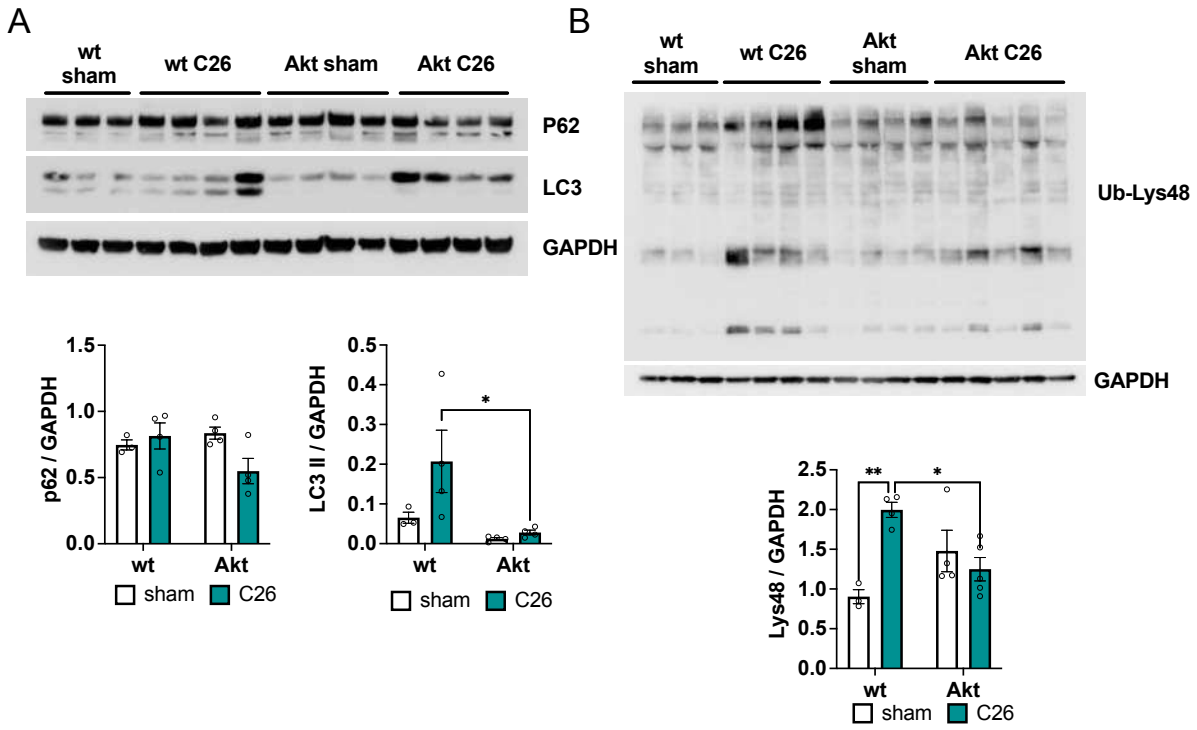

Figure 22. Protein expression of autophagy and UPS markers.

A. *Protein expression of autophagy markers, LC3 and p62, is restored after Akt activation during cancer cachexia (n=3 wt sham, n=4 wt C26, Akt sham and C26)* ***B.*** *Western blot analysis of Lys48 ubiquitinated proteins and related quantification (n=3 wt sham, n=4 wt C26, Akt sham and C26). Data presented as mean±s.e.m. Two-way ANOVA with Tukey's multiple comparison post-hoc test was performed. *p<0.05, **p<0.01.*

Activation of Akt however, does not only block the increase in protein degradation, but also affects protein translational process. Indeed, also the increase in the translational repressor 4E-BP1 in muscles from tumor-bearing animals is completely prevented at both the mRNA and protein level after Akt activation (Fig. 21A and B).

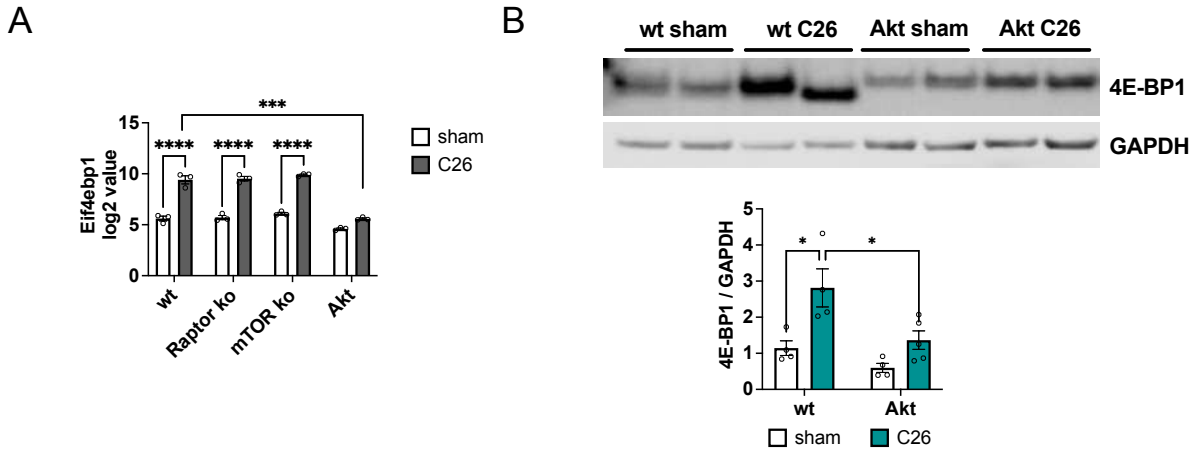

Figure 23. Akt activation rescues the increase in the translational repressor 4E-BP1.

A. *4E-BP1 expression in RNAseq analysis (n=3 per group) and* ***(B)*** *protein level in Akt C26 mice and controls (n=4 wt sham, wt C26, Akt sham; n=5 Akt C26).* *Data presented as mean±s.e.m. Two-way ANOVA with Tukey's multiple comparison test was performed. *p<0.05, ***p<0.001, ****p<0.0001.*

4.11. CIBERSORTx analysis suggests a decrease inflammatory state in muscle of Akt tumor-bearing mice.

CIBERSORTx uses an *in silico* analysis to accurately infer cell type abundance and cell-type-specific gene expression from RNA profiles of intact tissues. This method allows the transcriptomes of individual cell type to be digitally "purified" from bulk RNA admixtures without physical isolation (97). Taking advantage of CIBERSORTx and of a comprehensive temporal atlas of muscle regeneration in adult mice we could infer the abundance of inflammatory cell population and myogenic cell types from whole muscle transcriptomic analysis (98). From the stacked bar chart can be appreciated how wt, Raptor ko, mTOR ko present the same amount of cell fraction during cancer cachexia, instead Akt tumor-bearing mice show a different cell type abundance (Fig. 22).

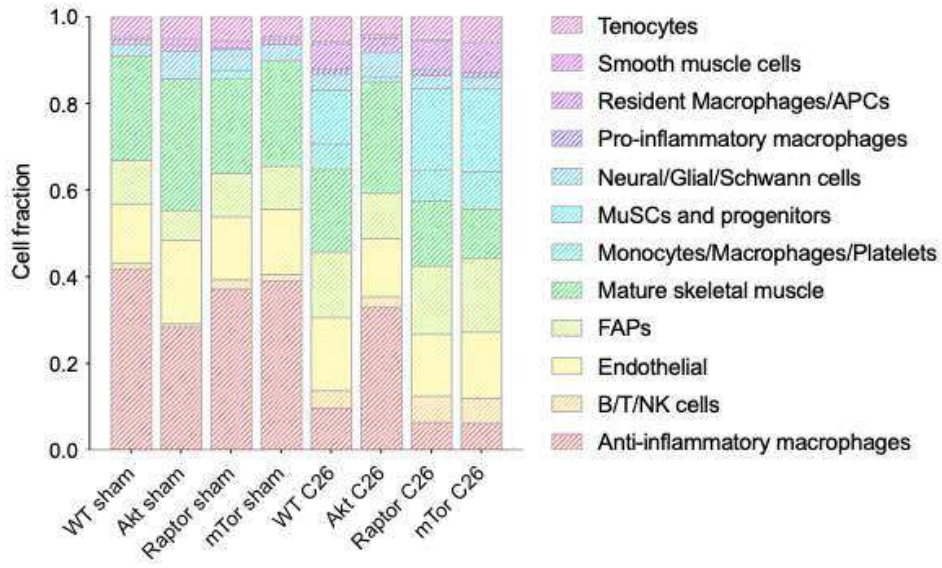

Figure 24. RNA deconvolution analysis with CIBERSORTx estimates member cell types in skeletal muscle.

The stacked bar chart shows the cell fraction of myogenic and inflammatory cell populations inferred by RNA deconvolution analysis using CIBERSORTx and muscle scRNA sequencing data from the Cosgrove lab (n=3 per group).

As can be seen in Figure 23, muscles of Akt tumor-bearing mice present a significant decrease in monocytes/macrophages/platelets cell population and an increase in anti-inflammatory macrophages compared to all the other C26 mouse models. Even other inflammatory cell population, such as resident macrophages and lymphocytes present a trend to decrease in Akt C26 mice. This analysis suggests that together with a normalization in the gene expression, muscles of Akt mice present a reduced inflammatory state during cancer cachexia.

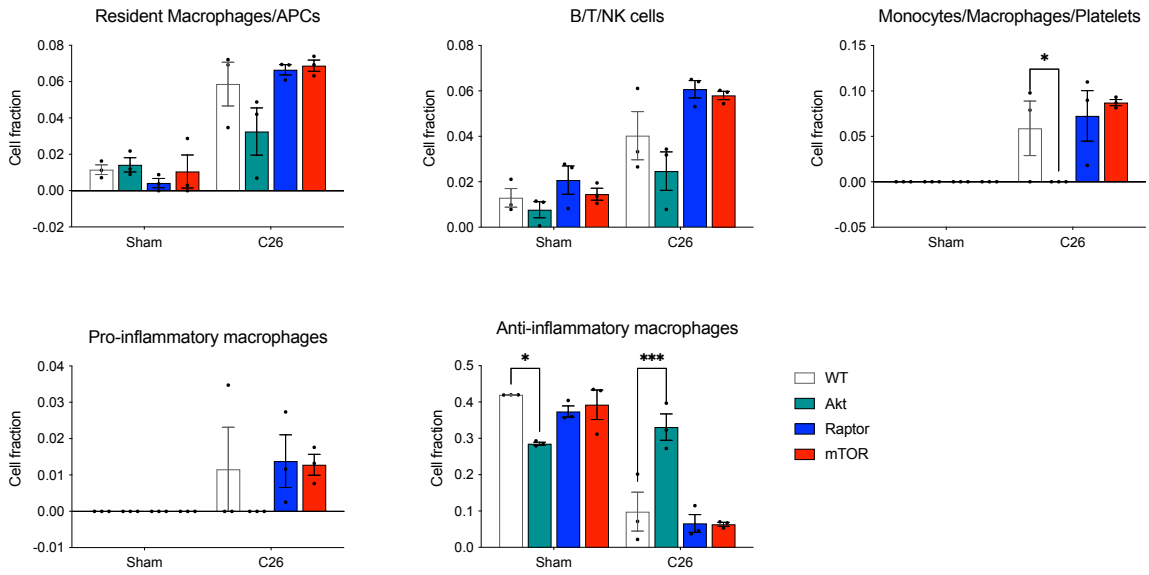

Figure 25. Inflammatory cell populations are differently expressed in Akt tumor-bearing mice.

Graphs of single cell population from CIBERSORTx analysis that are altered in Akt tumor-bearing mice.

5. DISCUSSION AND CONCLUSION

While cancer-dependent muscle wasting is a well-known problem in many, if not most, types of cancer, the underlying mechanisms are still not well described. This lack of mechanistic insight makes it very hard to anticipate when cachexia will start, how strong it will affect muscle physiology, and how it will influence the results of cancer treatment.

This project is focused on one of the main regulators of adult skeletal muscle mass, the Akt-mTORC1 pathway, during cancer-associated skeletal muscle wasting. Indeed, the use of mTOR inhibitors for anticancer treatments are approved for various advanced cancers but their effects during conditions of associated muscle wasting suggest an aggravation of this pathology. A retrospective study analyzed the consequences of long-term treatment with rapalogs and observed a decreased in skeletal muscle area (89). Another study showed a group of patients with advanced pancreatic neuroendocrine tumors treated with everolimus had an increased loss in body weight compared to the placebo group (112). Similar to these results, patients with metastatic renal cell cancer, which were treated with mTOR inhibitors, showed a significant exacerbation in muscle wasting (2). For these reasons we wanted to evaluate how modulation of the Akt-mTORC1 activity during cancer affects skeletal muscle homeostasis.

We found that loss of either mTOR or Raptor, mTORC1 scaffold protein, from skeletal muscle does not increase muscle wasting. However, it led to an increase in autophagy during cachexia. Importantly, while loss of mTORC1 signaling did not lead to an increased muscle wasting, activation of Akt-mTORC1 in skeletal muscle is sufficient to completely revert the loss in mass and force in cachectic animals. This rescue is characterized by a general normalization of the transcriptome, completely blunting the induction of many atrophy-related genes and reversing the increase in protein ubiquitination and autophagy seen in cachectic muscles.

Taken together, our data suggest that inhibition of mTOR during cachexia can negatively affect autophagy, however, its activation can completely restore muscle mass and function offering an interesting therapeutic target for cancer cachexia.

mTORC1 signaling affects autophagy during cachexia

In this study we evaluated if mTORC1 signaling is affected by cancer cachexia, and if reducing it further has deleterious effects on muscle wasting. While not all studies observed a decrease in mTORC1 signaling during cachexia (35), our results are in line with the majority of reports showing a general decrease in mTORC1 signaling (69,70). Some of the discrepancies observed in literature can be explained by the intrinsically high diurnal variability of this signaling

pathway, making it very sensitive to aspects like food intake and intrinsic circadian timing (113), something not always easy to control for in cachectic animals. The reduced mTOR signaling seen in tumor-bearing mice could be explained by the effects of proinflammatory cytokines, such as TNFα and IL-β, on the IGF-1 pathway. Indeed these cytokines leads to the inhibition of IRS-1 and effectively blunt the activation of downstream effector pathways, including PI3-K and Akt (114,115).

While we do not observe an increase in muscle wasting after loss of mTORC1 signaling, we do find an even further increase in autophagic and mitophagic flux. It is likely that the timeframe of the muscle wasting (4-6 days) is too short to lead to major muscle defects, but it is tempting to assume that prolonging autophagy induction over time can eventually lead to a block in autophagy and the appearance of a muscle pathology, as reported previously (90). A similar observation was made in muscle-specific Raptor ko mice after denervation. Indeed, also in this condition, autophagic flux was increased more than in wildtype mice, leading to a more pronounced loss in muscle mass, which was most evident after 28 days (61). The increase in autophagic flux in Raptor ko mice during cachexia can be interpreted in two ways; i) the induction of autophagy during cachexia is independent of mTORC1 ii) the reduction in mTORC1 is responsible for the induction of autophagy during cachexia, but the more pronounced reduction in mTORC1 signaling after genetic loss-of-function leads to an even further increase in autophagic flux through the same signaling pathway. While we cannot give a definite answer, it has been shown that knockdown of Raptor reduces signaling to downstream mediators, yet does not eliminate their sensitivity to nutrient levels (116), leaving open the possibility that this increased autophagic flux is mTORC1-independent.

A newly described feature of cancer-dependent muscle wasting is the fact that cachexia is accompanied by the appearance of fiber denervation (106). In this study the authors showed that reduced BMP signaling during cancer cachexia is a major factor leading to fiber denervation, as treatment with the BMP activator tilorone is sufficient to reduce muscle wasting and NMJ dysfunction. Interestingly, we and others have recently shown that one of the main roles of mTORC1 signaling in muscle fibers is the maintenance of the NMJ (90,117). Considering that a significant part of the trophic effect of BMP signaling in skeletal muscle goes through its regulation of mTORC1 signaling (118), it is tempting to assume that also during cancer cachexia the loss in fiber innervation is partially through a reduction in mTORC1 signaling in muscle fibers. Indeed, we did not find any significant increase in denervated fibers in tumor-bearing Raptor or mTOR ko mice.

Activation of Akt-mTORC1 signaling completely reverts cancer cachexia

A major finding in this study is the fact that activation of Akt for a few days is sufficient to completely restore muscle mass and force in already cachectic animals. This finding is of great importance, as it has been shown that the rescue of muscle mass is sufficient to improve survival, without affecting tumor growth (84). Modulating the levels of certain cytokines has been shown to be beneficial for muscle growth during cachexia. Antibodies which reduce either activin/myostatin (84), FN14 (119), or GDF15 (120,121) in the circulation have either prevented or reversed the muscle wasting seen during cachexia. While these results have shown the importance of preventing/reversing cachexia on overall survival, the intracellular signaling pathways involved are not well defined. Interestingly, activin, FN14, and GDF15, are all known to reduce the activation of the Akt-mTORC1 pathway (84,122,123), suggesting that preventing this inhibition is an important aspect of improving muscle wasting. Indeed, our results clearly show that muscle wasting can be completely reversed by short-term activation of Akt signaling. Notably, activation of muscle-specific Akt does not lead to an alteration in systemic parameters, such as tumor or spleen mass.

Somewhat unexpected, this reversal of cachexia is also accompanied by a very robust alteration of the muscle transcriptome. As observed also by others, we find more upregulated genes than down regulated genes in cachectic muscles (124,125), without major differences between tumor-bearing wildtype and Raptor/mTOR ko mice. An important part of these upregulated genes code for proteins involved in protein degradation. Interestingly, activation of Akt is able to completely abrogate the upregulation a most of these genes. This block in transcription of genes linked to protein degradation can be partially due to the strong inhibitory effect of Akt on FoxO transcription factors (126). FoxO transcription factors regulate an extensive network of genes linked to both the ubiquitin-proteasome and autophagy-lysosome system (41). Another support for a reduced activity of FoxO after Akt activation is the fact that the increase in the translational repressor 4E-BP1 during cachexia is completely blocked by Akt activation, giving mechanistic insight to the muscle growth observed in these animals. This important role for FoxO-dependent transcription during cancer cachexia was also suggested by studies overexpressing a dominant-negative plasmid for FoxO (124). Indeed, this overexpression leads to a complete block in muscle atrophy and loss in muscle force in tumor-bearing mice. The fact that we do not find a major change in transcriptome after Akt activation is in line with previous results (87), and again suggests that Akt is able to prevent the pathological increase

in transcription which accompanies the progression of cancer cachexia. Also, evaluation of the expression of other FoxO target genes, confirms the inhibition of FoxO activity after Akt activation in cachectic muscles (Suppl. Fig. 6F).

It has been demonstrated that Akt activation induces compensatory hypertrophy after hind limb suspension and can prevent denervation-induced muscle atrophy through mTOR pathway (1). It is likely to suppose that the beneficial effects observed in Akt tumor-bearing mice are mediated by mTOR considering that we do not only see a block in muscle wasting but also muscle hypertrophy.

Moreover, CIBERSORT$_x$ analysis suggests a decreased inflammatory state in muscles of Akt tumor-bearing mice which possibly explains the overall recovery in muscle transcriptome.

Cancer cachexia is a condition associated with altered metabolism and insulin resistant. The hyperinsulinemia state caused by the Cori Cycle between tumor and liver and by inflammatory cytokines cause glucose intolerance and insulin resistance during cancer cachexia (127,128). This insulin insensitivity leads to a decrease in the PI3K/Akt pathway contributing to muscle wasting that occurs during cancer. Skeletal muscle tissue accounts for the 30-35% of the total glucose uptake and this insulin-mediated glucose uptake is induced through Akt activation, predominantly Akt isoform 2 (129,130). Considering that Akt kinase plays a prominent role mediating the metabolic effects of insulin, muscle-specific Akt1 overexpression influences glucose metabolism also during cancer cachexia. Akt tumor-bearing mice show an increased muscle glycogen content compared to controls, most likely increasing glycogen synthesis through inhibition of GSK3-β. More experiments are needed to determine how Akt overexpression influences insulin resistance and glucose tolerance during cancer cachexia, but preliminary results show that cancer-induced hypoglycemia is restored to normal level after Akt overactivation (data not shown), suggesting a positive effect on glucose metabolism.

It is tempting to speculate that also in more severe situations, like during chemotherapy or refractory cachexia, Akt maintains the capacity to stimulate muscle growth. It has been suggested that cachectic patients maintain anabolic capacity (132,133), and we have previously shown that also in other pathological conditions, like muscular dystrophy or aging (62,92), activation of Akt is able to stimulate muscle growth. While it is not straight forward to imagine a systemic drug delivery which activates Akt only in skeletal muscles, the activation of muscle Akt can be considered an important marker in predicting the efficiency of nutritional and exercise interventions.

Taken together, we show in this thesis that Akt-mTORC1 signaling plays an important role during cancer-dependent muscle wasting. Loss of mTORC1 signaling is sufficient to further increase autophagic flux, which can potentially over time, lead to debilitating effects on muscle mass and function. On the contrary, activation of this pathway in skeletal muscle is sufficient to completely rescue muscle wasting, opening interesting new therapeutic avenues for this debilitating aspect of many different cancers.

SUPPLEMENTARY FIGURES

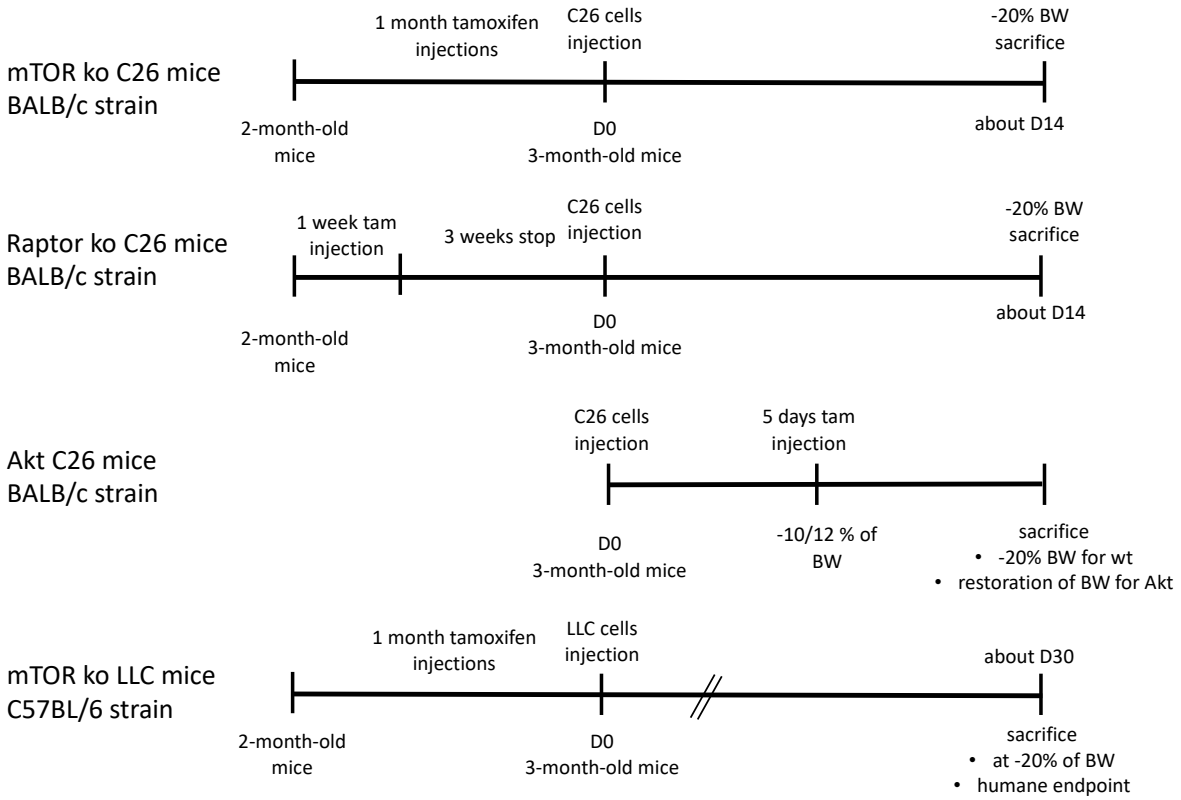

Supplementary Figure 1. Timeline representation of mice treatments

Timeline representation of mice treatments for mTOR ko, Raptor ko and Akt overexpressing C26 tumor-bearing mice. Timeline of mTOR ko LLC mice.

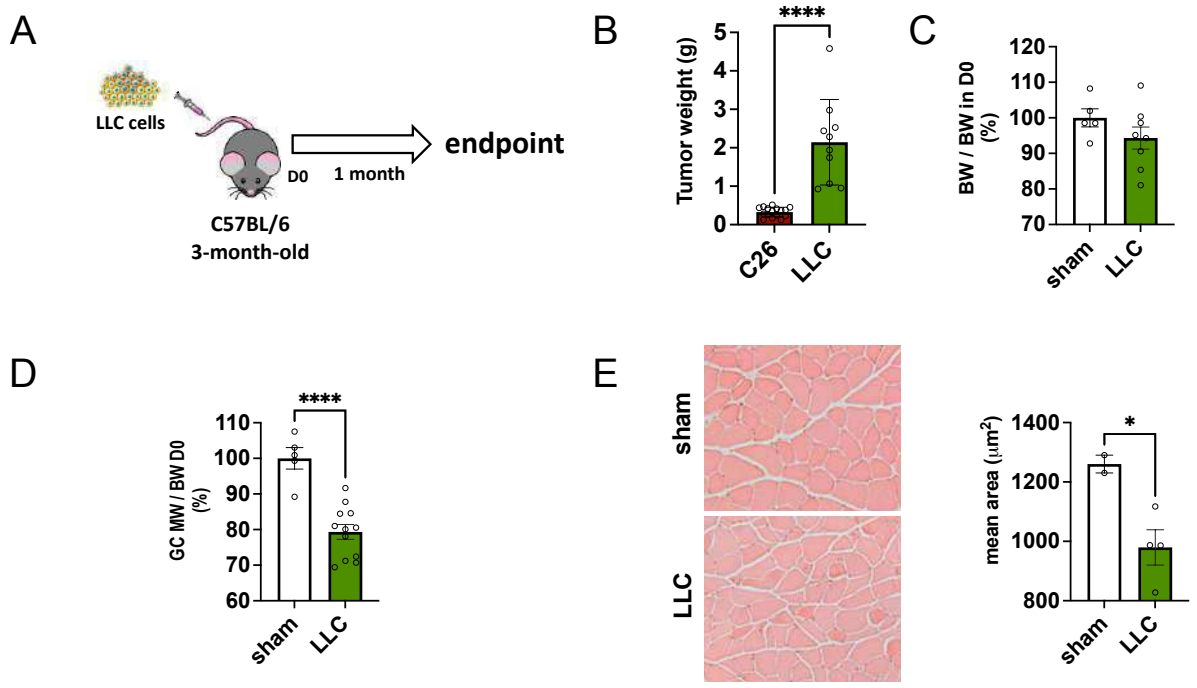

Supplementary Figure 2. Characterization of Lewis Lung carcinoma as cancer cachexia mouse model.

A. *Schematic representation of Lewis Lung carcinoma (LLC) experiment in C57BL/6 mice.* ***B.*** *Tumor weight graph shwoing the differences between C26 and LLC mouse model (n=16 C26, n=10 LLC).* ***C.*** *% of final body weight respect to D0 in LLC and sham mice (n=5 sham, n=8 LLC)* ***D.*** *Quantification of gastrocnemius (GC) muscle weight in LLC mice and controls (n=5 sham, n=12 LLC)* ***E.*** *Representative images of H&E staining and average cross-sectional area in GC muscles of LLC and control mice (n=2 sham, n=4 LLC). Data presented as mean ± s.e.m. Unpaired two-tailed student's t test. *p<0.05; ****p<0.0001.*

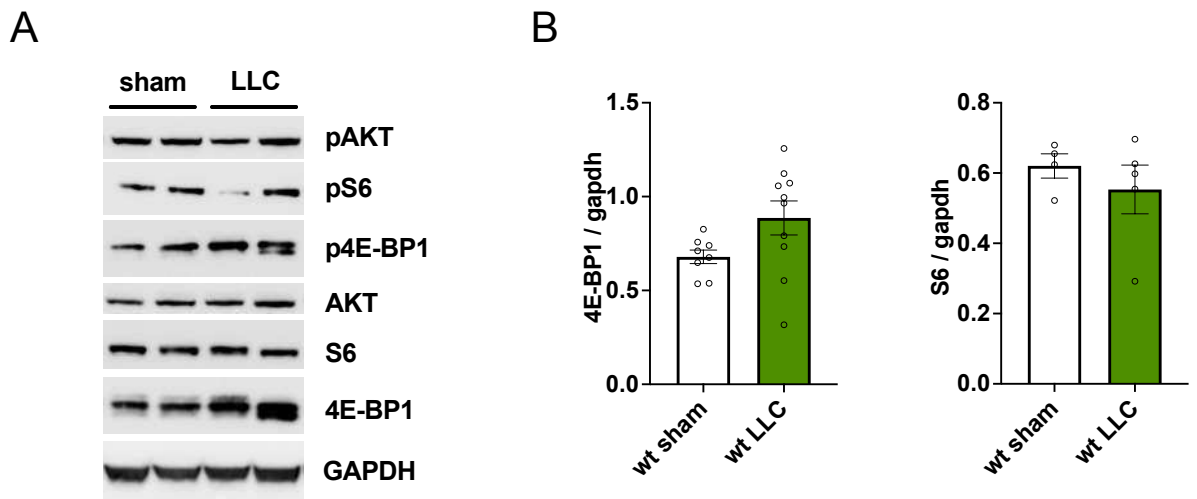

Supplementary Figure 3. Analysis of mTOR signaling showed a slight decrease in mTOR signaling.

A. *Western blotting representation of Akt-mTOR signaling in mTOR ko LLC mice and controls.* ***B.*** *Quantification of 4E-BP1 and S6 protein level from western blotting analysis (4E-BP1 quantification: n=8 sham, n=10 LLC; S6 quantification: n=4 sham, n=5 LLC). Data presented as mean ± s.e.m.*

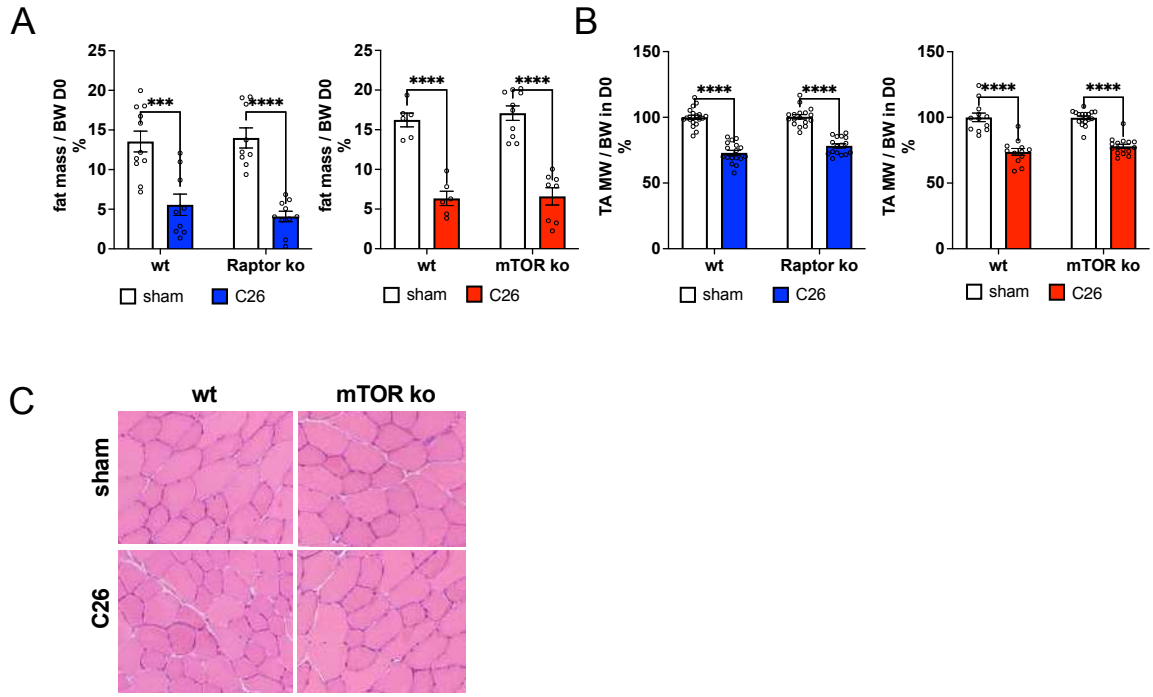

Supplementary Figure 4. Fat and muscle analysis in Raptor ko and mTOR ko C26 mice.

A. *Analysis of fat mass using EchoMRI in Raptor ko and mTOR ko tumor-bearing mice. Data presented as percentage of fat mass respect to body weight in D0 (n=11 wt sham, n=9 wt C26, n= 9 Raptor ko sham, n= 10 Raptor ko C26).* ***B.*** *Graphs of TA muscle weight in Raptor ko and mTOR ko tumor-bearing mice. Data presented as percentage of muscle weight respect to body weight in D0 (n=17 each group).* ***C.*** *H&E representative image of mTOR ko tumor-bearing mice and controls. Data presented as mean±s.e.m. Two-way ANOVA with Tukey's multiple comparison test was performed. ****p<0.0001*

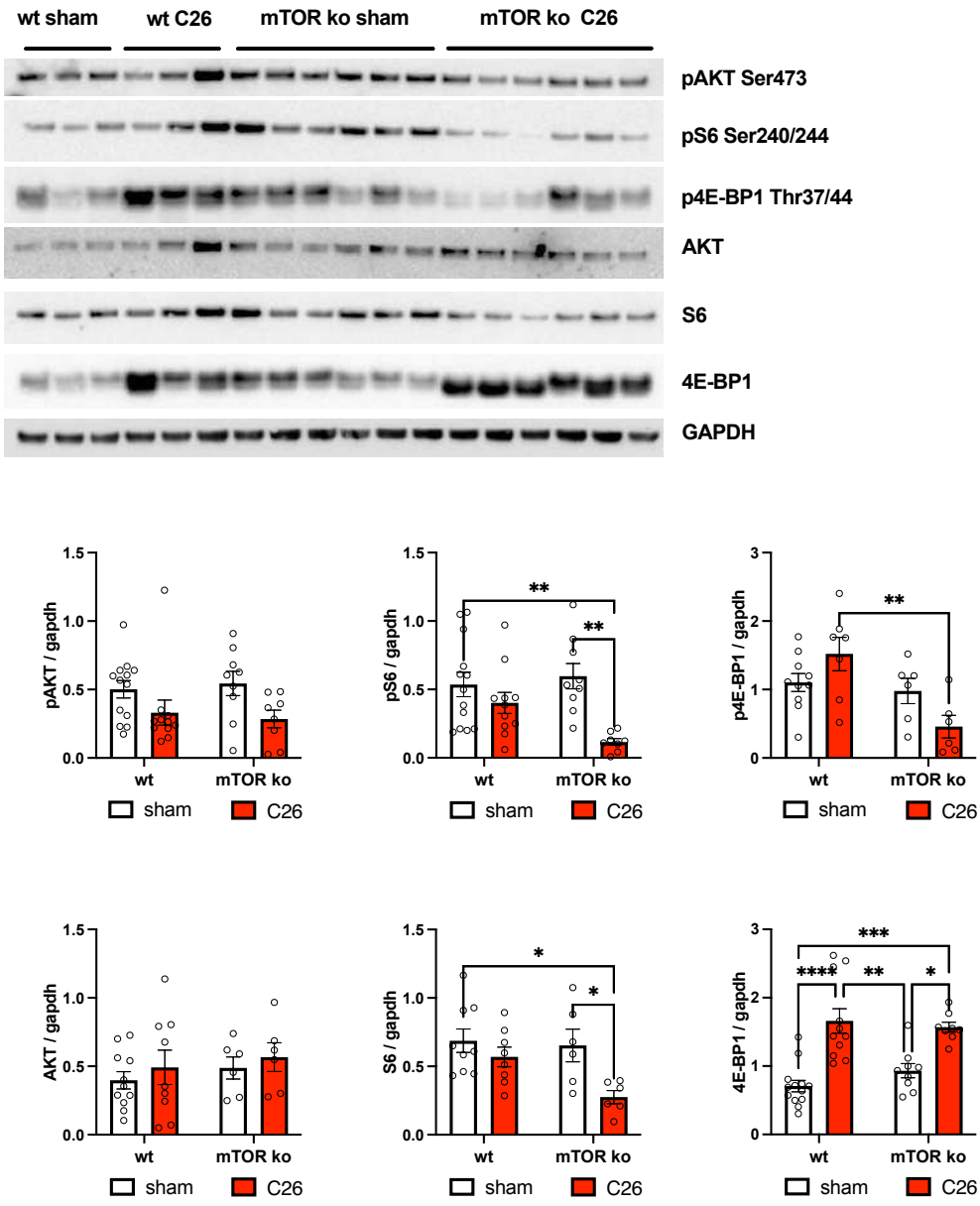

Supplementary Figure 5. Akt-mTOR signaling western blotting analysis in mTOR ko C26 mice. *Representative images of western blotting analysis of Akt-mTOR signaling in mTOR ko tumor-bearing mice and related quantification (n=9 each group). Data presented as mean±s.e.m. Two-way ANOVA with Tukey's multiple comparison test was performed. *<0.05, **<0.01, ***<0.01 ****p<0.0001.*

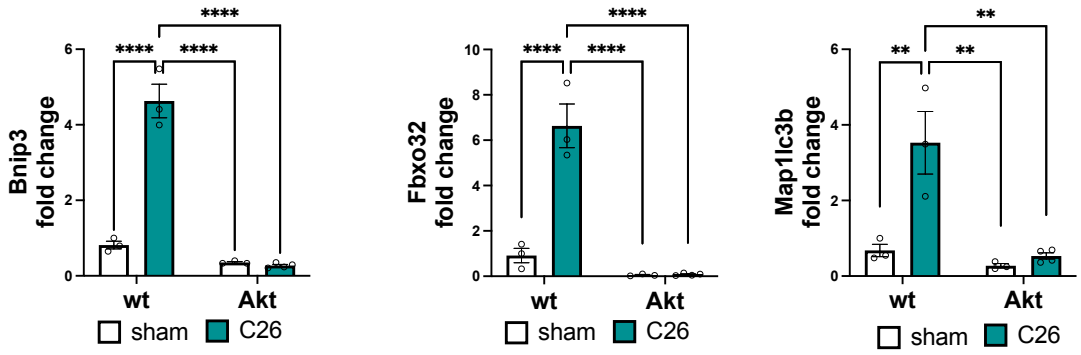

Supplementary Figure 6. Expression of FoxO-dependent genes are blunted in Akt tumor-bearing mice.

*RT-qPCR of FoxO-dependent genes: Bnip3, Fbxo32 (Atrogin-1) and Map1lc3b (LC3) in Akt C26 mice (n=3 wt sham, wt C26, Akt sham, n=4 Akt C26). Data presented as mean±s.e.m. Two-way ANOVA with Tukey's multiple comparison test was performed. **<0.01, ****p<0.0001.*

REFERENCES

1. Bodine SC, Stitt TN, Gonzalez M, Kline WO, Stover GL, Bauerlein R, et al. Akt/mTOR pathway is a crucial regulator of skeletal muscle hypertrophy and can prevent muscle atrophy in vivo. Nat Cell Biol. 2001 Nov;3(11):1014–9.

2. Antoun S, Birdsell L, Sawyer MB, Venner P, Escudier B, Baracos VE. Association of Skeletal Muscle Wasting With Treatment With Sorafenib in Patients With Advanced Renal Cell Carcinoma: Results From a Placebo-Controlled Study. JCO. 2010 Feb 20;28(6):1054–60.

3. Fearon K, Strasser F, Anker SD, Bosaeus I, Fainsinger RL, Jatoi A, et al. Definition and classification of cancer cachexia: an international consensus. The Lancet Oncology. 2011 May;12(5):489–95.

4. Argilés JM, Busquets S, Stemmler B, López-Soriano FJ. Cancer cachexia: understanding the molecular basis. Nat Rev Cancer. 2014 Nov;14(11):754–62.

5. Baracos VE, Martin L, Korc M, Guttridge DC, Fearon KCH. Cancer-associated cachexia. Nat Rev Dis Primers. 2018 Jun 7;4(1):17105.

6. Weber BZC, Arabaci DH, Kir S. Metabolic Reprogramming in Adipose Tissue During Cancer Cachexia. Front Oncol. 2022;12:848394.

7. Schmidt SF, Rohm M, Herzig S, Berriel Diaz M. Cancer Cachexia: More Than Skeletal Muscle Wasting. Trends in Cancer. 2018 Dec;4(12):849–60.

8. Argiles JM, Lopez-Soriano FJ, Busquets S. Counteracting inflammation: a promising therapy in cachexia. Crit Rev Oncog. 2012;17(3):253–62.

9. Coussens LM, Werb Z. Inflammation and cancer. Nature. 2002 Dec 19;420(6917):860–7.

10. Mantovani G, Macciò A, Mura L, Massa E, Mudu MC, Mulas C, et al. Serum levels of leptin and proinflammatory cytokines in patients with advanced-stage cancer at different sites. J Mol Med (Berl). 2000;78(10):554–61.

11. Patel HJ, Patel BM. TNF-α and cancer cachexia: Molecular insights and clinical implications. Life Sci. 2017 Feb 1;170:56–63.

12. Moses AGW, Maingay J, Sangster K, Fearon KCH, Ross JA. Pro-inflammatory cytokine release by peripheral blood mononuclear cells from patients with advanced pancreatic cancer: relationship to acute phase response and survival. Oncol Rep. 2009 Apr;21(4):1091–5.

13. Bonetto A, Aydogdu T, Kunzevitzky N, Guttridge DC, Khuri S, Koniaris LG, et al. STAT3 activation in skeletal muscle links muscle wasting and the acute phase response in cancer cachexia. PLoS One. 2011;6(7):e22538.

14. Fonseca GWP da, Farkas J, Dora E, von Haehling S, Lainscak M. Cancer Cachexia and Related Metabolic Dysfunction. Int J Mol Sci. 2020 Mar 27;21(7):E2321.

15. Janssen I, Heymsfield SB, Wang ZM, Ross R. Skeletal muscle mass and distribution in 468 men and women aged 18-88 yr. J Appl Physiol (1985). 2000 Jul;89(1):81–8.

16. Scott W, Stevens J, Binder–Macleod SA. Human Skeletal Muscle Fiber Type Classifications. Physical Therapy. 2001 Nov 1;81(11):1810–6.

17. Schiaffino S, Reggiani C. Fiber types in mammalian skeletal muscles. Physiol Rev. 2011 Oct;91(4):1447–531.

18. Bonaldo P, Sandri M. Cellular and molecular mechanisms of muscle atrophy. Disease Models & Mechanisms. 2013 Jan 1;6(1):25–39.

19. Fearon KCH, Glass DJ, Guttridge DC. Cancer Cachexia: Mediators, Signaling, and Metabolic Pathways. Cell Metabolism. 2012 Aug;16(2):153–66.

20. Bonaldo P, Sandri M. Cellular and molecular mechanisms of muscle atrophy. Dis Model Mech. 2013 Jan;6(1):25–39.

21. Nakamura S, Yoshimori T. New insights into autophagosome-lysosome fusion. J Cell Sci. 2017 Apr 1;130(7):1209–16.

22. Jiang P, Mizushima N. LC3- and p62-based biochemical methods for the analysis of autophagy progression in mammalian cells. Methods. 2015 Mar 15;75:13–8.

23. Jung CH, Ro SH, Cao J, Otto NM, Kim DH. mTOR regulation of autophagy. FEBS Lett. 2010 Apr 2;584(7):1287–95.

24. Egan DF, Shackelford DB, Mihaylova MM, Gelino S, Kohnz RA, Mair W, et al. Phosphorylation of ULK1 (hATG1) by AMP-activated protein kinase connects energy sensing to mitophagy. Science. 2011 Jan 28;331(6016):456–61.

25. Arico S, Petiot A, Bauvy C, Dubbelhuis PF, Meijer AJ, Codogno P, et al. The tumor suppressor PTEN positively regulates macroautophagy by inhibiting the phosphatidylinositol 3-kinase/protein kinase B pathway. J Biol Chem. 2001 Sep 21;276(38):35243–6.

26. He C, Klionsky DJ. Regulation Mechanisms and Signaling Pathways of Autophagy. Annu Rev Genet. 2009;43:67–93.

27. Mammucari C, Milan G, Romanello V, Masiero E, Rudolf R, Del Piccolo P, et al. FoxO3 controls autophagy in skeletal muscle in vivo. Cell Metab. 2007 Dec;6(6):458–71.

28. Sandri M. Autophagy in skeletal muscle. FEBS Letters. 2010;584(7):1411–6.

29. Masiero E, Agatea L, Mammucari C, Blaauw B, Loro E, Komatsu M, et al. Autophagy is required to maintain muscle mass. Cell Metab. 2009 Dec;10(6):507–15.

30. Aversa Z, Pin F, Lucia S, Penna F, Verzaro R, Fazi M, et al. Autophagy is induced in the skeletal muscle of cachectic cancer patients. Sci Rep. 2016 Sep;6(1):30340.

31. Penna F, Costamagna D, Pin F, Camperi A, Fanzani A, Chiarpotto EM, et al. Autophagic degradation contributes to muscle wasting in cancer cachexia. Am J Pathol. 2013 Apr;182(4):1367–78.

32. Penna F, Ballarò R, Martinez-Cristobal P, Sala D, Sebastian D, Busquets S, et al. Autophagy Exacerbates Muscle Wasting in Cancer Cachexia and Impairs Mitochondrial Function. Journal of Molecular Biology. 2019 Jul;431(15):2674–86.

33. Autocrine activin A signalling in ovarian cancer cells regulates secretion of interleukin 6, autophagy, and cachexia - PubMed [Internet]. [cited 2022 Jul 20]. Available from: https://pubmed.ncbi.nlm.nih.gov/31436048/

34. Pettersen K, Andersen S, Degen S, Tadini V, Grosjean J, Hatakeyama S, et al. Cancer cachexia associates with a systemic autophagy-inducing activity mimicked by cancer cell-derived IL-6 trans-signaling. Sci Rep. 2017 May 17;7(1):2046.

35. Pigna E, Berardi E, Aulino P, Rizzuto E, Zampieri S, Carraro U, et al. Aerobic Exercise and Pharmacological Treatments Counteract Cachexia by Modulating Autophagy in Colon Cancer. Sci Rep. 2016 May 31;6:26991.

36. Chen D, Dou QP. The ubiquitin-proteasome system as a prospective molecular target for cancer treatment and prevention. Curr Protein Pept Sci. 2010 Sep;11(6):459–70.

37. Tenno T, Fujiwara K, Tochio H, Iwai K, Morita EH, Hayashi H, et al. Structural basis for distinct roles of Lys63- and Lys48-linked polyubiquitin chains. Genes Cells. 2004 Oct;9(10):865–75.

38. Bodine SC, Latres E, Baumhueter S, Lai VK, Nunez L, Clarke BA, et al. Identification of ubiquitin ligases required for skeletal muscle atrophy. Science. 2001 Nov 23;294(5547):1704–8.

39. Gomes MD, Lecker SH, Jagoe RT, Navon A, Goldberg AL. Atrogin-1, a muscle-specific F-box protein highly expressed during muscle atrophy. Proc Natl Acad Sci U S A. 2001 Dec 4;98(25):14440–5.

40. Lecker SH, Jagoe RT, Gilbert A, Gomes M, Baracos V, Bailey J, et al. Multiple types of skeletal muscle atrophy involve a common program of changes in gene expression. FASEB J. 2004 Jan;18(1):39–51.

41. Milan G, Romanello V, Pescatore F, Armani A, Paik JH, Frasson L, et al. Regulation of autophagy and the ubiquitin–proteasome system by the FoxO transcriptional network during muscle atrophy. Nat Commun. 2015 Apr 10;6(1):6670.

42. Reed SA, Sandesara PB, Senf SM, Judge AR. Inhibition of FoxO transcriptional activity prevents muscle fiber atrophy during cachexia and induces hypertrophy. FASEB J. 2012 Mar;26(3):987–1000.

43. Parajuli P, Kumar S, Loumaye A, Singh P, Eragamreddy S, Nguyen TL, et al. Twist1 Activation in Muscle Progenitor Cells Causes Muscle Loss Akin to Cancer Cachexia. Dev Cell. 2018 Jun 18;45(6):712-725.e6.

44. Rhoads MG, Kandarian SC, Pacelli F, Doglietto GB, Bossola M. Expression of NF-kappaB and IkappaB proteins in skeletal muscle of gastric cancer patients. Eur J Cancer. 2010 Jan;46(1):191–7.

45. McClung JM, Judge AR, Powers SK, Yan Z. p38 MAPK links oxidative stress to autophagy-related gene expression in cachectic muscle wasting. Am J Physiol Cell Physiol. 2010 Mar;298(3):C542-549.

46. Moore-Carrasco R, Busquets S, Almendro V, Palanki M, López-Soriano FJ, Argilés JM. The AP-1/NF-kappaB double inhibitor SP100030 can revert muscle wasting during experimental cancer cachexia. Int J Oncol. 2007 May;30(5):1239–45.

47. Zhang L, Tang H, Kou Y, Li R, Zheng Y, Wang Q, et al. MG132-mediated inhibition of the ubiquitin-proteasome pathway ameliorates cancer cachexia. J Cancer Res Clin Oncol. 2013 Jul;139(7):1105–15.

48. Shi J, Luo L, Eash J, Ibebunjo C, Glass DJ. The SCF-Fbxo40 complex induces IRS1 ubiquitination in skeletal muscle, limiting IGF1 signaling. Dev Cell. 2011 Nov 15;21(5):835–47.

49. Sun YS, Ye ZY, Qian ZY, Xu XD, Hu JF. Expression of TRAF6 and ubiquitin mRNA in skeletal muscle of gastric cancer patients. J Exp Clin Cancer Res. 2012 Sep 26;31:81.

50. Paul PK, Gupta SK, Bhatnagar S, Panguluri SK, Darnay BG, Choi Y, et al. Targeted ablation of TRAF6 inhibits skeletal muscle wasting in mice. J Cell Biol. 2010 Dec 27;191(7):1395–411.

51. Bossola M, Muscaritoli M, Costelli P, Bellantone R, Pacelli F, Busquets S, et al. Increased muscle ubiquitin mRNA levels in gastric cancer patients. Am J Physiol Regul Integr Comp Physiol. 2001 May;280(5):R1518-1523.

52. DeJong CHC, Busquets S, Moses AGW, Schrauwen P, Ross JA, Argiles JM, et al. Systemic inflammation correlates with increased expression of skeletal muscle ubiquitin but not uncoupling proteins in cancer cachexia. Oncol Rep. 2005 Jul;14(1):257–63.

53. Jagoe RT, Redfern CPF, Roberts RG, Gibson GJ, Goodship THJ. Skeletal muscle mRNA levels for cathepsin B, but not components of the ubiquitin-proteasome pathway, are increased in patients with lung cancer referred for thoracotomy. Clin Sci (Lond). 2002 Mar;102(3):353–61.

54. Op den Kamp CM, Langen RC, Minnaard R, Kelders MC, Snepvangers FJ, Hesselink MK, et al. Pre-cachexia in patients with stages I-III non-small cell lung cancer: systemic inflammation and functional impairment without activation of skeletal muscle ubiquitin proteasome system. Lung Cancer. 2012 Apr;76(1):112–7.

55. Dolly A, Lecomte T, Tabchouri N, Caulet M, Michot N, Anon B, et al. Pectoralis major muscle atrophy is associated with mitochondrial energy wasting in cachectic patients with gastrointestinal cancer. Journal of Cachexia, Sarcopenia and Muscle. 2022;13(3):1837–49.

56. Mavalli MD, DiGirolamo DJ, Fan Y, Riddle RC, Campbell KS, van Groen T, et al. Distinct growth hormone receptor signaling modes regulate skeletal muscle development and insulin sensitivity in mice. J Clin Invest. 2010 Nov;120(11):4007–20.

57. Musarò A, McCullagh K, Paul A, Houghton L, Dobrowolny G, Molinaro M, et al. Localized Igf-1 transgene expression sustains hypertrophy and regeneration in senescent skeletal muscle. Nat Genet. 2001 Feb;27(2):195–200.

58. Murgia M, Serrano AL, Calabria E, Pallafacchina G, Lomo T, Schiaffino S. Ras is involved in nerve-activity-dependent regulation of muscle genes. Nat Cell Biol. 2000 Mar;2(3):142–7.

59. Blaauw B, Canato M, Agatea L, Toniolo L, Mammucari C, Masiero E, et al. Inducible activation of Akt increases skeletal muscle mass and force without satellite cell activation. The FASEB Journal. 2009 Aug 6;23(11):3896–905.

60. Castets P, Lin S, Rion N, Di Fulvio S, Romanino K, Guridi M, et al. Sustained Activation of mTORC1 in Skeletal Muscle Inhibits Constitutive and Starvation-Induced Autophagy

and Causes a Severe, Late-Onset Myopathy. Cell Metabolism. 2013 May 7;17(5):731–44.

61. Castets P, Rion N, Théodore M, Falcetta D, Lin S, Reischl M, et al. mTORC1 and PKB/Akt control the muscle response to denervation by regulating autophagy and HDAC4. Nat Commun. 2019 Jul 18;10(1):3187.

62. Sandri M, Barberi L, Bijlsma AY, Blaauw B, Dyar KA, Milan G, et al. Signalling pathways regulating muscle mass in ageing skeletal muscle. The role of the IGF1-Akt-mTOR-FoxO pathway. Biogerontology. 2013 Jun;14(3):303–23.

63. Bentzinger CF, Romanino K, Cloëtta D, Lin S, Mascarenhas JB, Oliveri F, et al. Skeletal muscle-specific ablation of raptor, but not of rictor, causes metabolic changes and results in muscle dystrophy. Cell Metab. 2008 Nov;8(5):411–24.

64. Risson V, Mazelin L, Roceri M, Sanchez H, Moncollin V, Corneloup C, et al. Muscle inactivation of mTOR causes metabolic and dystrophin defects leading to severe myopathy. The Journal of Cell Biology. 2009 Dec 14;187(6):859–74.

65. Schmitt TL, Martignoni ME, Bachmann J, Fechtner K, Friess H, Kinscherf R, et al. Activity of the Akt-dependent anabolic and catabolic pathways in muscle and liver samples in cancer-related cachexia. J Mol Med. 2007 Jun 1;85(6):647–54.

66. Stephens NA, Skipworth RJE, Gallagher IJ, Greig CA, Guttridge DC, Ross JA, et al. Evaluating potential biomarkers of cachexia and survival in skeletal muscle of upper gastrointestinal cancer patients. Journal of Cachexia, Sarcopenia and Muscle. 2015;6(1):53–61.

67. White JP, Baynes JW, Welle SL, Kostek MC, Matesic LE, Sato S, et al. The regulation of skeletal muscle protein turnover during the progression of cancer cachexia in the Apc(Min/+) mouse. PLoS One. 2011;6(9):e24650.

68. White JP, Puppa MJ, Gao S, Sato S, Welle SL, Carson JA. Muscle mTORC1 suppression by IL-6 during cancer cachexia: a role for AMPK. Am J Physiol Endocrinol Metab. 2013 May 15;304(10):E1042-1052.

69. Puppa MJ, Gao S, Narsale AA, Carson JA. Skeletal muscle glycoprotein 130's role in Lewis lung carcinoma-induced cachexia. FASEB J. 2014 Feb;28(2):998–1009.

70. Puppa MJ, White JP, Velázquez KT, Baltgalvis KA, Sato S, Baynes JW, et al. The effect of exercise on IL-6-induced cachexia in the ApcMin/+ mouse. J Cachexia Sarcopenia Muscle. 2012 Jun;3(2):117–37.

71. Morinaga M, Sako N, Isobe M, Lee-Hotta S, Sugiura H, Kametaka S. Aerobic Exercise Ameliorates Cancer Cachexia-Induced Muscle Wasting through Adiponectin Signaling. International Journal of Molecular Sciences. 2021 Jan;22(6):3110.

72. Chen X, Wu Y, Yang T, Wei M, Wang Y, Deng X, et al. Salidroside alleviates cachexia symptoms in mouse models of cancer cachexia via activating mTOR signalling. J Cachexia Sarcopenia Muscle. 2016 May;7(2):225–32.

73. Penna F, Bonetto A, Muscaritoli M, Costamagna D, Minero VG, Bonelli G, et al. Muscle atrophy in experimental cancer cachexia: is the IGF-1 signaling pathway involved? Int J Cancer. 2010 Oct 1;127(7):1706–17.

74. Hatakeyama S, Summermatter S, Jourdain M, Melly S, Minetti GC, Lach-Trifilieff E. ActRII blockade protects mice from cancer cachexia and prolongs survival in the presence of anti-cancer treatments. Skelet Muscle. 2016;6:26.

75. Talbert EE, Yang J, Mace TA, Farren MR, Farris AB, Young GS, et al. Dual Inhibition of MEK and PI3K/Akt Rescues Cancer Cachexia through both Tumor-Extrinsic and -Intrinsic Activities. Molecular Cancer Therapeutics. 2017 Feb 2;16(2):344–56.

76. Sartori R, Milan G, Patron M, Mammucari C, Blaauw B, Abraham R, et al. Smad2 and 3 transcription factors control muscle mass in adulthood. Am J Physiol, Cell Physiol. 2009 Jun;296(6):C1248-1257.

77. Zimmers TA, Davies MV, Koniaris LG, Haynes P, Esquela AF, Tomkinson KN, et al. Induction of cachexia in mice by systemically administered myostatin. Science. 2002 May 24;296(5572):1486–8.

78. Bogdanovich S, Krag TOB, Barton ER, Morris LD, Whittemore LA, Ahima RS, et al. Functional improvement of dystrophic muscle by myostatin blockade. Nature. 2002 Nov 28;420(6914):418–21.

79. Amthor H, Macharia R, Navarrete R, Schuelke M, Brown SC, Otto A, et al. Lack of myostatin results in excessive muscle growth but impaired force generation. Proc Natl Acad Sci U S A. 2007 Feb 6;104(6):1835–40.

80. Trendelenburg AU, Meyer A, Rohner D, Boyle J, Hatakeyama S, Glass DJ. Myostatin reduces Akt/TORC1/p70S6K signaling, inhibiting myoblast differentiation and myotube size. Am J Physiol Cell Physiol. 2009 Jun;296(6):C1258-1270.

81. Aversa Z, Bonetto A, Penna F, Costelli P, Di Rienzo G, Lacitignola A, et al. Changes in myostatin signaling in non-weight-losing cancer patients. Ann Surg Oncol. 2012 Apr;19(4):1350–6.

82. Trendelenburg AU, Meyer A, Jacobi C, Feige JN, Glass DJ. TAK-1/p38/nNFκB signaling inhibits myoblast differentiation by increasing levels of Activin A. Skelet Muscle. 2012 Feb 7;2(1):3.

83. Leto G, Incorvaia L, Badalamenti G, Tumminello FM, Gebbia N, Flandina C, et al. Activin A circulating levels in patients with bone metastasis from breast or prostate cancer. Clin Exp Metastasis. 2006;23(2):117–22.

84. Zhou X, Wang JL, Lu J, Song Y, Kwak KS, Jiao Q, et al. Reversal of cancer cachexia and muscle wasting by ActRIIB antagonism leads to prolonged survival. Cell. 2010 Aug 20;142(4):531–43.

85. Benny Klimek ME, Aydogdu T, Link MJ, Pons M, Koniaris LG, Zimmers TA. Acute inhibition of myostatin-family proteins preserves skeletal muscle in mouse models of cancer cachexia. Biochem Biophys Res Commun. 2010 Jan 15;391(3):1548–54.

86. Sandri M. Protein breakdown in muscle wasting: Role of autophagy-lysosome and ubiquitin-proteasome. Int J Biochem Cell Biol. 2013 Oct;45(10):2121–9.

87. Pereira MG, Dyar KA, Nogara L, Solagna F, Marabita M, Baraldo M, et al. Comparative Analysis of Muscle Hypertrophy Models Reveals Divergent Gene Transcription Profiles

and Points to Translational Regulation of Muscle Growth through Increased mTOR Signaling. Front Physiol. 2017;8:968.

88. Schiaffino S, Reggiani C, Akimoto T, Blaauw B. Molecular Mechanisms of Skeletal Muscle Hypertrophy. J Neuromuscul Dis. 2021;8(2):169–83.

89. Gyawali B, Shimokata T, Honda K, Kondoh C, Hayashi N, Yoshino Y, et al. Muscle wasting associated with the long-term use of mTOR inhibitors. Mol Clin Oncol. 2016 Nov;5(5):641–6.

90. Baraldo M, Geremia A, Pirazzini M, Nogara L, Solagna F, Türk C, et al. Skeletal muscle mTORC1 regulates neuromuscular junction stability. Journal of Cachexia, Sarcopenia and Muscle. 2020 Feb;11(1):208–25.

91. Schuler M, Ali F, Metzger E, Chambon P, Metzger D. Temporally controlled targeted somatic mutagenesis in skeletal muscles of the mouse. genesis. 2005 Apr 1;41(4):165–70.

92. Blaauw B, Mammucari C, Toniolo L, Agatea L, Abraham R, Sandri M, et al. Akt activation prevents the force drop induced by eccentric contractions in dystrophin-deficient skeletal muscle. Hum Mol Genet. 2008 Dec 1;17(23):3686–96.

93. Solagna F, Nogara L, Dyar KA, Greulich F, Mir AA, Türk C, et al. Exercise-dependent increases in protein synthesis are accompanied by chromatin modifications and increased MRTF-SRF signalling. Acta Physiologica. n/a(n/a):e13496.

94. Mw P. A new mathematical model for relative quantification in real-time RT-PCR. Nucleic acids research [Internet]. 2001 May 1 [cited 2022 Aug 1];29(9). Available from: https://pubmed.ncbi.nlm.nih.gov/11328886/

95. Schindelin J, Arganda-Carreras I, Frise E, Kaynig V, Longair M, Pietzsch T, et al. Fiji: an open-source platform for biological-image analysis. Nat Methods. 2012 Jul;9(7):676–82.

96. Civiletto G, Dogan SA, Cerutti R, Fagiolari G, Moggio M, Lamperti C, et al. Rapamycin rescues mitochondrial myopathy via coordinated activation of autophagy and lysosomal biogenesis. EMBO Mol Med. 2018 Nov;10(11):e8799.

97. Newman AM, Steen CB, Liu CL, Gentles AJ, Chaudhuri AA, Scherer F, et al. Determining cell type abundance and expression from bulk tissues with digital cytometry. Nat Biotechnol. 2019 Jul;37(7):773–82.

98. De Micheli AJ, Laurilliard EJ, Heinke CL, Ravichandran H, Fraczek P, Soueid-Baumgarten S, et al. Single-Cell Analysis of the Muscle Stem Cell Hierarchy Identifies Heterotypic Communication Signals Involved in Skeletal Muscle Regeneration. Cell Reports. 2020 Mar;30(10):3583-3595.e5.

99. Tyanova S, Temu T, Sinitcyn P, Carlson A, Hein MY, Geiger T, et al. The Perseus computational platform for comprehensive analysis of (prote)omics data. Nat Methods. 2016 Sep;13(9):731–40.

100. Tusher VG, Tibshirani R, Chu G. Significance analysis of microarrays applied to the ionizing radiation response. Proceedings of the National Academy of Sciences. 2001 Apr 24;98(9):5116–21.

101. Nolte H, MacVicar TD, Tellkamp F, Krüger M. Instant Clue: A Software Suite for Interactive Data Visualization and Analysis. Sci Rep. 2018 Aug 23;8(1):12648.

102. Ballarò R, Costelli P, Penna F. Animal models for cancer cachexia. Current Opinion in Supportive & Palliative Care. 2016 Dec;10(4):281–7.

103. Schiaffino S, Reggiani C, Akimoto T, Blaauw B. Molecular Mechanisms of Skeletal Muscle Hypertrophy. J Neuromuscul Dis. 8(2):169–83.

104. Ju JS, Varadhachary AS, Miller SE, Weihl CC. Quantitation of "autophagic flux" in mature skeletal muscle. Autophagy. 2010 Oct;6(7):929–35.

105. Sun N, Yun J, Liu J, Malide D, Liu C, Rovira II, et al. Measuring in vivo mitophagy. Mol Cell. 2015 Nov 19;60(4):685–96.

106. Sartori R, Hagg A, Zampieri S, Armani A, Winbanks CE, Viana LR, et al. Perturbed BMP signaling and denervation promote muscle wasting in cancer cachexia. Sci Transl Med. 2021 Aug 4;13(605):eaay9592.

107. Zhu X, Yeadon JE, Burden SJ. AML1 is expressed in skeletal muscle and is regulated by innervation. Mol Cell Biol. 1994 Dec;14(12):8051–7.

108. Burden SJ, Yumoto N, Zhang W. The Role of MuSK in Synapse Formation and Neuromuscular Disease. Cold Spring Harb Perspect Biol [Internet]. 2013 May [cited 2018 May 30];5(5). Available from: https://www.ncbi.nlm.nih.gov/pmc/articles/PMC3632064/

109. Macpherson PCD, Wang X, Goldman D. Myogenin regulates denervation-dependent muscle atrophy in mouse soleus muscle. Journal of Cellular Biochemistry. 112(8):2149–59.

110. Gu Y, Hall ZW. Characterization of acetylcholine receptor subunits in developing and in denervated mammalian muscle. J Biol Chem. 1988 Sep 15;263(26):12878–85.

111. Zhou Y, Zhou B, Pache L, Chang M, Khodabakhshi AH, Tanaseichuk O, et al. Metascape provides a biologist-oriented resource for the analysis of systems-level datasets. Nat Commun. 2019 Apr 3;10(1):1523.

112. Yao JC, Shah MH, Ito T, Bohas CL, Wolin EM, Van Cutsem E, et al. Everolimus for advanced pancreatic neuroendocrine tumors. N Engl J Med. 2011 Feb 10;364(6):514–23.

113. Crosby P, Hamnett R, Putker M, Hoyle NP, Reed M, Karam CJ, et al. Insulin/IGF-1 Drives PERIOD Synthesis to Entrain Circadian Rhythms with Feeding Time. Cell. 2019 May 2;177(4):896-909.e20.

114. Shen WH, Zhou JH, Broussard SR, Freund GG, Dantzer R, Kelley KW. Proinflammatory cytokines block growth of breast cancer cells by impairing signals from a growth factor receptor. Cancer Res. 2002 Aug 15;62(16):4746–56.

115. O'Connor JC, McCusker RH, Strle K, Johnson RW, Dantzer R, Kelley KW. Regulation of IGF-I function by proinflammatory cytokines: at the interface of immunology and endocrinology. Cell Immunol. 2008 Apr;252(1–2):91–110.

116. Kim DH, Sarbassov DD, Ali SM, King JE, Latek RR, Erdjument-Bromage H, et al. mTOR Interacts with Raptor to Form a Nutrient-Sensitive Complex that Signals to the Cell Growth Machinery. Cell. 2002 Jul;110(2):163–75.

117. Castets P, Ham DJ, Rüegg MA. The TOR Pathway at the Neuromuscular Junction: More Than a Metabolic Player? Front Mol Neurosci. 2020;13:162.

118. Winbanks CE, Chen JL, Qian H, Liu Y, Bernardo BC, Beyer C, et al. The bone morphogenetic protein axis is a positive regulator of skeletal muscle mass. The Journal of Cell Biology. 2013 Oct 28;203(2):345–57.

119. Johnston AJ, Murphy KT, Jenkinson L, Laine D, Emmrich K, Faou P, et al. Targeting of Fn14 Prevents Cancer-Induced Cachexia and Prolongs Survival. Cell. 2015 Sep 10;162(6):1365–78.

120. Lerner L, Tao J, Liu Q, Nicoletti R, Feng B, Krieger B, et al. MAP3K11/GDF15 axis is a critical driver of cancer cachexia. J Cachexia Sarcopenia Muscle. 2016 Sep;7(4):467–82.

121. Suriben R, Chen M, Higbee J, Oeffinger J, Ventura R, Li B, et al. Antibody-mediated inhibition of GDF15-GFRAL activity reverses cancer cachexia in mice. Nat Med. 2020 Aug;26(8):1264–70.

122. Dogra C, Changotra H, Wedhas N, Qin X, Wergedal JE, Kumar A. TNF-Related Weak inducer of Apoptosis (TWEAK) is a potent skeletal muscle-wasting cytokine. FASEB J. 2007 Jun;21(8):1857–69.

123. Wang X, Chrysovergis K, Kosak J, Kissling G, Streicker M, Moser G, et al. hNAG-1 increases lifespan by regulating energy metabolism and insulin/IGF-1/mTOR signaling. Aging (Albany NY). 2014 Aug;6(8):690–704.

124. Judge SM, Wu CL, Beharry AW, Roberts BM, Ferreira LF, Kandarian SC, et al. Genome-wide identification of FoxO-dependent gene networks in skeletal muscle during C26 cancer cachexia. BMC Cancer. 2014 Dec 24;14(1):997.

125. Talbert EE, Cuitiño MC, Ladner KJ, Rajasekerea PV, Siebert M, Shakya R, et al. Modeling Human Cancer-induced Cachexia. Cell Rep. 2019 Aug 6;28(6):1612-1622.e4.

126. Sandri M, Sandri C, Gilbert A, Skurk C, Calabria E, Picard A, et al. Foxo transcription factors induce the atrophy-related ubiquitin ligase atrogin-1 and cause skeletal muscle atrophy. Cell. 2004 Apr 30;117(3):399–412.

127. Masi T, Patel BM. Altered glucose metabolism and insulin resistance in cancer-induced cachexia: a sweet poison. Pharmacol Rep. 2021 Feb;73(1):17–30.

128. Asp ML, Tian M, Wendel AA, Belury MA. Evidence for the contribution of insulin resistance to the development of cachexia in tumor-bearing mice. International Journal of Cancer. 2010;126(3):756–63.

129. Jaiswal N, Gavin MG, Quinn WJ, Luongo TS, Gelfer RG, Baur JA, et al. The role of skeletal muscle Akt in the regulation of muscle mass and glucose homeostasis. Molecular Metabolism. 2019 Oct;28:1–13.

130. Garofalo RS, Orena SJ, Rafidi K, Torchia AJ, Stock JL, Hildebrandt AL, et al. Severe diabetes, age-dependent loss of adipose tissue, and mild growth deficiency in mice lacking Akt2/PKB beta. J Clin Invest. 2003 Jul;112(2):197–208.

131. Raun SH, Knudsen JR, Han X, Jensen TE, Sylow L. Cancer causes dysfunctional insulin signaling and glucose transport in a muscle-type-specific manner. FASEB J. 2022 Mar;36(3):e22211.

132. Engelen MPKJ, Safar AM, Bartter T, Koeman F, Deutz NEP. High anabolic potential of essential amino acid mixtures in advanced nonsmall cell lung cancer. Ann Oncol. 2015 Sep;26(9):1960–6.

133. Prado CM, Sawyer MB, Ghosh S, Lieffers JR, Esfandiari N, Antoun S, et al. Central tenet of cancer cachexia therapy: do patients with advanced cancer have exploitable anabolic potential? Am J Clin Nutr. 2013 Oct;98(4):1012–9.